SURFACE TO SUBSURFACE CORRELATION OF THE SHUBLIK FORMATION: IMPLICATIONS FOR TRIASSIC PALEOCEANOGRAPHY AND SOURCE ROCK ACCUMULATION

By

Eric M. Hutton

RECOMMENDED:

Dr. Paul McCarthy

Dr. Catherine Hanks

Dr. Michael Whalen, Advisory Committee Chair

Dr. Paul McCarthy, Chair
Department of Geology and Geophysics

APPROVED:

Dr. Paul Layer, Dean
College of Natural Science and Mathematics

Dr. John Eichelberger, Dean of the Graduate School

4/22/14

Date

# SURFACE TO SUBSURFACE CORRELATION OF THE SHUBLIK FORMATION: IMPLICATIONS FOR TRIASSIC PALEOCEANOGRAPHY AND SOURCE ROCK ACCUMULATION

A

THESIS

Presented to the Faculty

of the University of Alaska Fairbanks

in Partial Fulfillment of the Requirements

for the Degree of

MASTER OF SCIENCE

By

Eric M. Hutton, B.S.

Fairbanks, Alaska

May 2014

# ABSTRACT

The Middle to Late Triassic Shublik Formation in northern Alaska is the dominant source rock for Prudhoe Bay, the largest conventional hydrocarbon accumulation in North America, and is being studied as an unconventional reservoir because of recent shale oil exploitation in North America. This heterogeneous shale unit in the subsurface of northern Alaska provides insight on the evolution of upwelling systems during relative sea level change over geologic time. The accumulation, dilution, and more importantly preservation of organic matter are linked to relative changes in sea level, shelf bathymetry and paleoredox conditions. Multiple well correlations and isochore maps indicate thickness trends were influenced by topographical features and relative sea level during the Middle–Upper Triassic in northern Alaska. Sedimentary features, primary production, $C_{org}$ preservation and oxygen concentrations were controlled by the upwelling-influenced position of the oxygen minimum zone during fluctuations in relative sea level. The Shublik Formation is a world class resource play with $C_{org}$ concentrations up to 10 wt. % within the predominantly carbonate mudstone to wackestone transgressive systems tracts. Previous sequence stratigraphic interpretations of Middle–Upper Triassic deposits in northern Alaska indicate three, 3$^{rd}$ order depositional sequences. Evaluation of the closely spaced samples and general trends in lithology has led to a revised sequence stratigraphic architecture that includes an additional fourth depositional sequence in comparison to previous interpretations.

# TABLE OF CONTENTS

Page

Page

Page

# LIST OF FIGURES

Page

Page

Page

# LIST OF APPENDICES

Page



## SUPPLEMENTAL FILE

# ACKNOWLEGEMENTS

There are many organizations that contributed aid and individuals that provided guidance for the completion of this project. First and foremost I'd like to thank Dr. Michael Whalen and Dr. Richard Koehler for their patience and continued support during my graduate studies and the completion of this project. I would like to extend my utmost gratitude to the U.S. Fish and Wildlife Service, specifically Mr. Richard Voss for granting access into the Arctic National Wildlife Refuge (ANWR). I'd also like to thank both the United States Geological Survey (USGS), including David Houseknecht, Katherine Whidden and Julie Dumoulin, and the Alaska Division of Geological and Geophysical Surveys (DGGS), including Marwan Wartes, and Bob Swenson for helicopter and field support in ANWR. My thesis project was partially funded by the University of Alaska Fairbanks Department of Geology and Geophysics (UAF) including teaching support. An internship and school support was awarded from Great Bear Petroleum. Internship and field support was awarded from Repsol. Awards were offered from the American Association of Petroleum Geologists (AAPG) Grants in Aid, BP Exploration-Alaska, and The Arctic Institute of North America (AINA) for rock analyses. I'd also like to thank Dr. Ken Severin, Dr. Maciej G. Śliwiński and Dr. Karen Spaleta of the Advanced Instrumentation Laboratory (AIL) at UAF for providing laboratory guidance, thoughtful advice and other various insights. I'd also like to commend the UAF Geology and Geophysics Department faculty and graduate students for their unyielding dedication to geology and the furthering of our science.

# CHAPTER 1: INTRODUCTION

The Shublik Formation (Fm.) is the primary source rock for the giant Prudhoe Bay oil field (Tailleur, 1964; Magoon & Claypool, 1983; Bird & Molenaar, 1987; Magoon & Bird, 1988; Bird, 1994; Kupecz, 1995) and is currently being evaluated as a potential shale resource play (e.g. Peters *et al.*, 2006; Decker, 2011). Fueled by the petroleum industry's increased focus on shale-dominated reservoirs (Ratcliffe *et al*., 2006; Ratcliffe *et al*., 2012) the purpose of this study is to understand the distribution and preservation of organic carbon ($C_{org}$) within the Shublik Fm. Additionally, the increased prospectivity of shale resource plays has emphasized the need to further develop the stratigraphic framework of the Shublik Fm. to predict the location and abundance of economically viable plays across northern Alaska.

During the summer of 2012 scientists from the University of Alaska Fairbanks (UAF), the U.S. Geology Survey (USGS) and the Alaska Division of Geological and Geophysical Surveys (DGGS) conducted field work in the Arctic National Wildlife Refuge (ANWR). The purpose of the fieldwork was to sample and evaluate the outcrop exposure of the Shublik Fm. at Fire Creek in northern Alaska, and correlate the exposure with nearby well data in order to better understand the characteristic gamma-ray log signature in the subsurface (Fig. 1). The correlation builds upon previous sequence stratigraphic correlations by Kupecz (1995), Robison *et al*., (1996), Hulm (1999), Parrish *et al*. (2001b) and Kelly *et al*. (2007) to create a high-frequency sequence stratigraphic framework of the Shublik Fm. throughout the region.

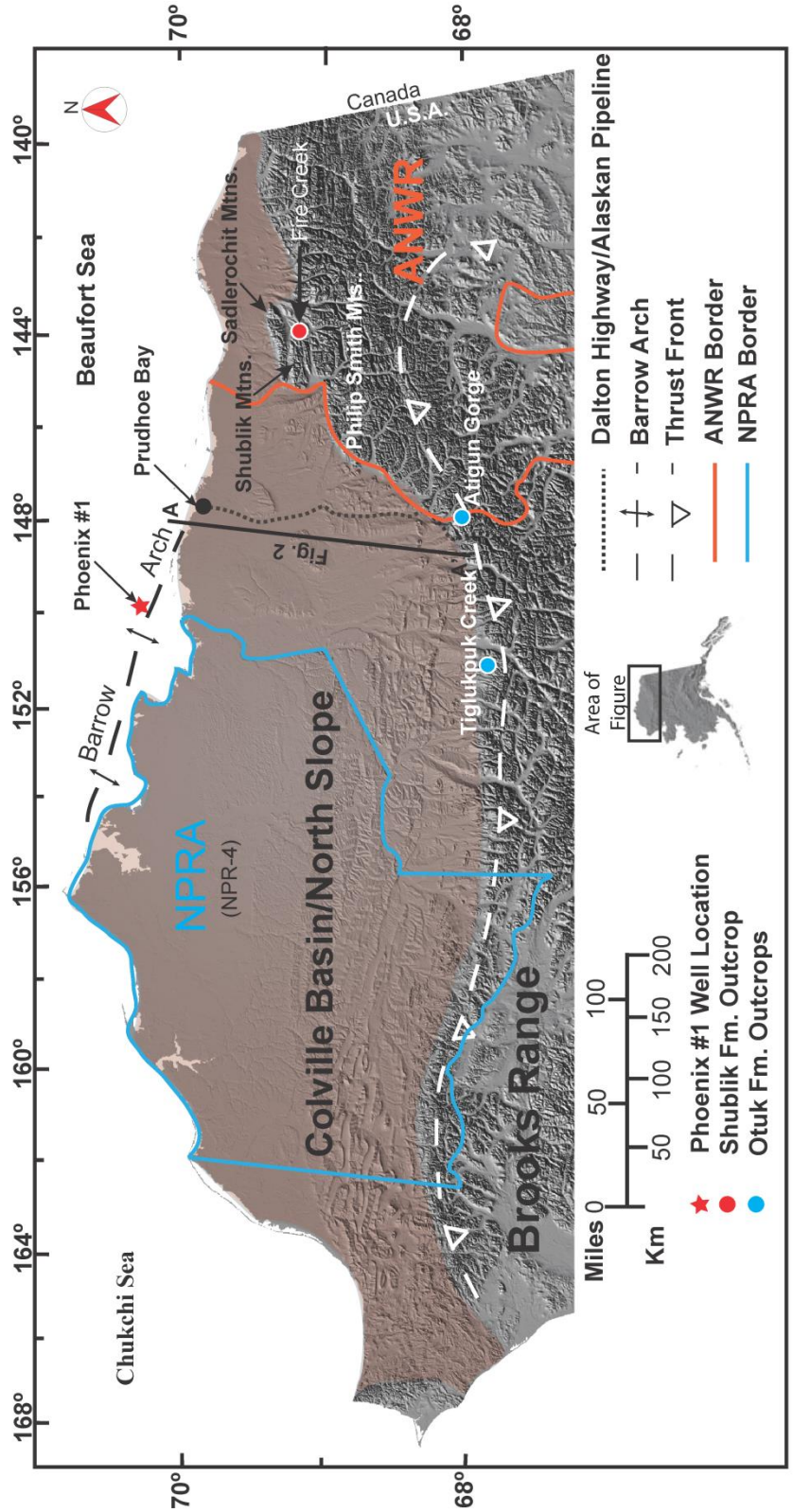


**Fig. 1** Digital Elevation Model (DEM) image of northern Alaska (Riehle *et al.*, 1997). Outlines of the National Petroleum Reserve (NPRA, NPR-4) and Arctic National Wildlife Preserve (ANWR) are indicated. Brown shaded area indicates the general location of the Colville Basin/North Slope of northern Alaska. Red circle indicates the Fire Creek outcrop exposure, the primary type-section outcrop of the Shublik Fm. and the blue circles are where the distal equivalent Otuk Fm. exposures are located. The Phoenix #1 well penetration contains the only full-section core of the Shublik Fm. publicly available.

The increased use of horizontal drilling completion programs utilized in the exploitation of modern unconventional hydrocarbon accumulations requires high-resolution stratigraphic interpretations (Ratcliffe *et al.*, 2012). Thus, to better predict organic-rich zones, high-frequency trace element proxy data can be used to model paleoceanographic controls that mediate the primary production, dilution and preservation of $C_{org}$. The use of elemental data in regional stratigraphic correlations is a relatively new technique that provides researchers with detailed information for evaluating changing paleoceanographic conditions (e.g. Pearce *et al*., 2005; Ratcliffe *et al*., 2006; Wright & Ratcliffe, 2010; Hildred *et al*., 2010; Ratcliffe *et al*., 2012). Specific trace elements become enriched within the sediments due to the oxidation state in the shallow subsurface or at the sediment−water interface. Trends in trace element enrichment (i.e. uranium or molybdenum) within the stratigraphic section can be used to map and predict the deposition of organic-rich facies where trace element concentrations correlate to a high degree with $C_{org}$ enrichment ($R^2$ >0.8) (Ratcliffe *et al*., 2012). Because trace elements are linked to oxidation state and are preserved within the organic-rich, fine-grained sediments, they can be used to identify zones of oxic vs. anoxic bottom water conditions (Tribovillard *et al*., 2006).

In Kelly *et al*. (2007), an inorganic geochemical dataset utilizing a select suite of elemental data including the Rare Earth Elements (Ce, Dy, Er, Gd, and Yb), and select trace and major element enrichments and ratios (Mn, P, V and Ca/Mn) (see Briet & Wanty, 1991; Sholokovitz *et al*., 1994; Quinby-Hunt & Wilde, 1996; Shields & Stille, 2001) is used for regional correlations and paleoredox indicators. This study utilizes a

different set of trace and major elemental enrichment proxies, from the Kelly *et al.* (2007) dataset, in order to recognize trends of primary productivity, paleoredox conditions, and detrital proxies. This research attempts to interpret depositional controls on $C_{org}$ enrichment and preservation through recognition of multiple trace element indicators coupled with thin-section petrography for a high-resolution investigation of depositional cycles within the Shublik Fm.

Furthermore, this study uses sequence stratigraphy, chemostratigraphy, lithostratigraphy, and thin-section petrography to re-evaluate the sequence stratigraphic architecture at the Fire Creek outcrop in the Arctic National Wildlife Refuge (ANWR). High-frequency microfacies and geochemical analyses were performed in an attempt to understand the distribution of $C_{org}$ within individual depositional cycles. Evaluation of the closely spaced samples and general trends in lithology has led to a revised sequence stratigraphic architecture that includes an additional sequence in comparison to previous interpretations (Kelly *et al*., 2007). The sequences are then correlated westward into the subsurface Middle−Upper Triassic deposits of northern Alaska. Field-based observations are integrated with elemental data, thin-section petrography and outcrop spectral gamma-ray (SGR) data to identify facies stacking patterns and to correlate and tie the outcrop data to petrophysical log data from nearby industry wells. Lateral facies variations are then explored utilizing isochore maps and cross-sections derived from well data correlated with outcrop exposures. Results from this project assist in identifying biotic and sedimentologic variations within the heterogeneous rock formation and interpret where the organic-rich facies were preferentially deposited.

# CHAPTER 2: GEOLOGIC SETTING AND BACKGROUND

## 2.1 Geologic Setting

Geologic investigations of post-Carboniferous rocks in northern Alaska began in the early 1900s, and in 1923, they were coupled with petroleum assessments of the Naval Petroleum Reserve No. 4 (now the National Petroleum Reserve Alaska; Gryc, 1988) (Fig. 1). Zones of interest included the Lower Triassic Ivishak Fm. and the Late Triassic Sag River Sandstone, both prolific hydrocarbon reservoirs. The lithologically heterogeneous, organic-rich Middle–Upper Triassic Shublik Fm. is stratigraphically located between the Ivishak Fm. and the Sag River Sandstone and is the focus of this thesis. The Shublik Fm. is exposed in the northeastern Brooks Range (ANWR) and dips into the subsurface of the North Slope of Alaska to the west (Fig. 1).

The North Slope of Alaska has been explored and studied by many geoscientists over the last ~100 years. In particular, stratigraphic and structural evaluations to assess resource potential have dominated geologic research and the following summary is based on Moore *et al*. (1994). Northern Alaska is comprised of three main physiographic provinces: the Brooks Range, the Arctic Foothills and the Arctic Coastal Plain (Fig. 2). The Arctic Foothills and the Arctic Coastal Plain comprise the North Slope of Alaska. The North Slope is underlain by the Colville Basin, a foreland basin of Cretaceous and Tertiary age, and lies north of the east-west trending fold-and-thrust belt of the central Brooks Range.

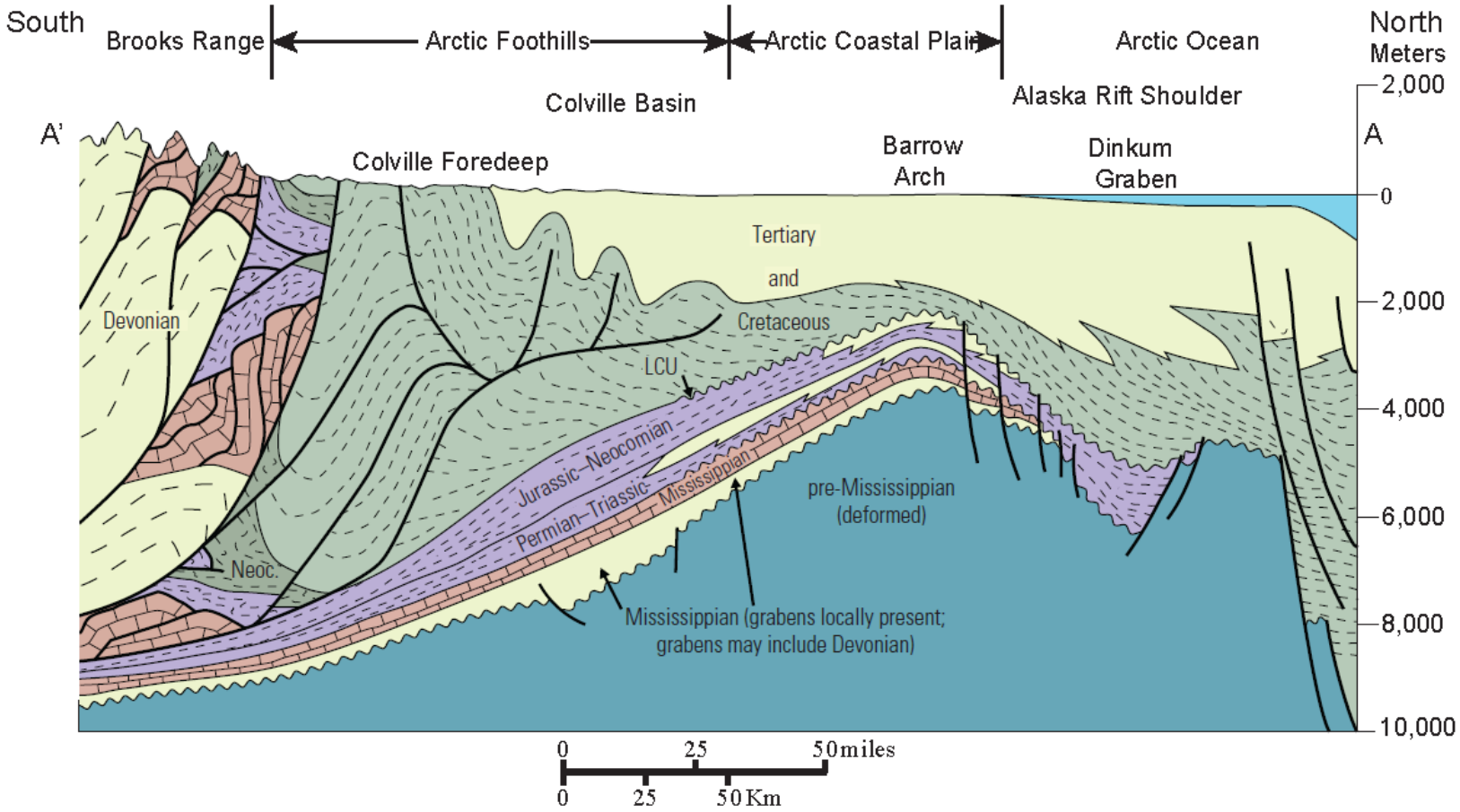


**Fig. 2** Generalized cross section of northern Alaska. Stratigraphic and structural elements from the Brooks Range to the northern margin of the Alaska rift shoulder are pictured. The Arctic Coastal Plain and Arctic Foothills comprise the North Slope of Alaska (modified from Bird & Bader, 1987 and Houseknecht *et al*., 2012b).

The Brooks Range formed during three episodes of deformation from Late Jurassic to the present, contains the continental divide, and is the northwestern extent of the North American Cordillera.

Paleozoic through Cenozoic sedimentary and metasedimentary deposits of northern Alaska are subdivided into four tectonostratigraphic mega-sequences named the Franklinian, Ellesmerian, Beaufortian and Brookian (Fig. 3).The lowermost, the Franklinian mega-sequence, is composed of a diverse assemblage of Upper Cambrian–pre-Mississippian rocks that were strongly deformed before the deposition of Mississippian sediments. The overlying Carboniferous–Triassic Ellesmerian mega-sequence consists of marine carbonate rocks and marine–non-marine siliciclastic rocks deposited on a south-facing passive continental margin and includes deposition of the Shublik Formation. The Lower Jurassic–Lower Cretaceous Beaufortian mega-sequence consists of syn-rift deposits and is a stratigraphically complex, mud-dominated sequence (Houseknecht & Bird, 2004). Uplift and erosion along the rift margin occurred during the opening of the Canada Basin and created the Lower Cretaceous Unconformity (LCU), which is geographically coincident with the Barrow Arch (Fig. 1). The overlying Brookian mega-sequence consists of mid-Cretaceous−Cenozoic sedimentary deposits of the Colville Basin, which are largely derived from the Brooks Range (Fig. 1 and 2).

The marine carbonate and non-marine siliciclastic rocks of the Ellesmerian mega-sequence rest unconformably on pre-Mississippian rocks throughout the North Slope and represent about 150 Ma (pre-Mississippian through Triassic) years of sedimentation.

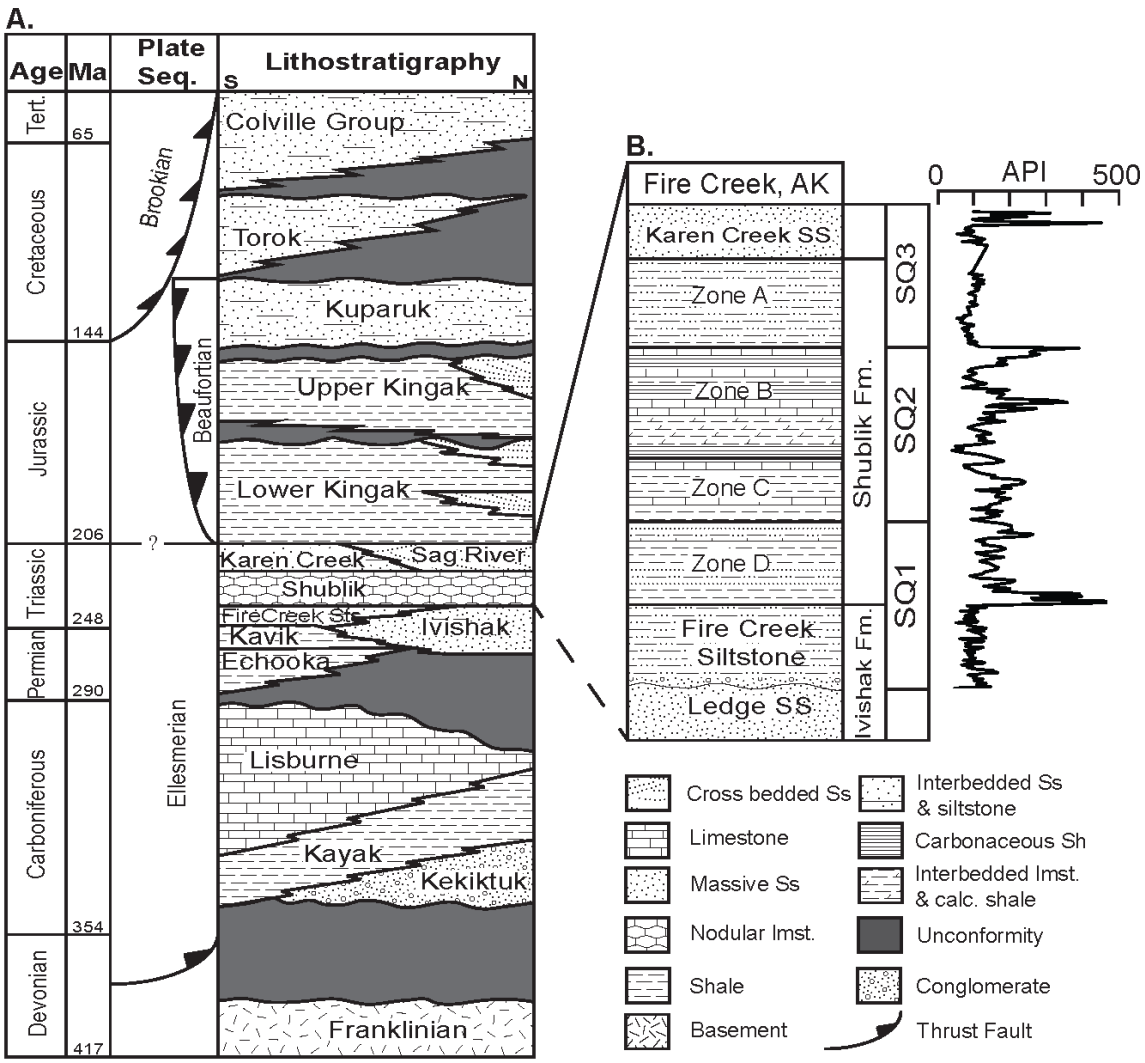


**Fig. 3 (A)** Simplified stratigraphy of northern Alaska (modified from Hubbard *et al*., 1987). Period boundary ages from The Geological Society of America (2012) **(B)** Simplified outcrop stratigraphy of Triassic successions in the northeastern Brooks Range, Fire Creek, AK. Zones are based on well log picks in the Prudhoe Bay Unit Common Database and subsurface core descriptions from the Prudhoe Bay Unit and NPRA (Kupecz, 1995;Hulm, 1999) Spectral gamma-ray measurements from the outcrop exposure at Fire Creek were converted to API and are displayed on a 0−500 API scale (modified from Kelly, 2004; Kelly *et al*., 2007).

Ellesmerian mega-sequence rocks are exposed within a series of thrust-fault bounded, stacked allocthons that comprise several smaller mountain ranges including the Sadlerochit Mountains, Shublik Mountains and the Philip Smith Mountains in ANWR

(Fig. 1). On the eastern edge of the Shublik Mts., the Ivishak Fm., the Shublik Fm., the overlying Karen Creek Sandstone and Jurassic Kingak Shale are exposed in outcrop along Fire Creek. The outcrop exposure of the Shublik Fm. at Fire Creek is considered the type section and is the only exposure where a relatively undeformed full section is exposed.

### 2.2 Sequence Stratigraphy

The application of sequence stratigraphic analysis to document local changes in paleogeography and the controls governing sedimentologic processes is widely used to enhance petroleum exploration and production (Catuneanu *et al*., 2009). Facies stacking patterns and geometric relationships between packages of strata provide the necessary building blocks to model the sequence stratigraphic framework. The facies relationships and stratal architectures defined within sequence stratigraphic models can be different between petroleum systems. A generalized overview of sequence stratigraphic concepts is provided to help define the relationships recognized and interpreted within this study.

"A depositional sequence is defined as a relatively conformable succession of genetically related strata bounded by unconformities or their correlative conformities" (Mitchum *et al*., 1977). The sequence described by Mitchum *et al*. (1977) can be subdivided into genetically related strata that contain no internal unconformities and are composed of parasequences or sets of parasequences arranged in systems tracts. Van Wagoner *et al*. (1988) referred to parasequences as facies stacked into genetic units bounded above and below by marine flooding surfaces and the vertically stacked

sedimentary cycles can be interpreted as parasequence sets. A sedimentary cycle within a lithostratigraphic section implies a specific order of repetition where a lithological unit repeats within the stratigraphic profile. Cyclicity is a common occurrence within sedimentary successions including siliciclastic deposits and carbonate successions such as platforms, reefs and slope to basinal environments (Read, 1985; Mitchum & Van Wagoner, 1991). A shallowing upward, meter-scale cycle bounded by marine flooding surfaces is one scale of stratigraphic cycle or parasequence that tends to be systematically stacked into larger-scale successions called parasequence sets (Goldhammer *et al*., 1990). The stacking patterns of the parasequence sets can be used to interpret larger scale sequences, their systems tracts and longer term sea level fluctuations (Osleger & Read, 1991). Thus, the identification of genetic units and bounding surfaces that can be readily defined allows for sequence stratigraphic interpretations to be made and this approach is implemented within this study (Catuneanu *et al*., 2009).

### 2.2.1 Middle–Upper Triassic Sequence Stratigraphy

The Middle–Late Triassic Shublik Fm. has a maximum thickness of ~175 m (Bird, 1982) and records long term (~30–35 million years) upwelling along a shallow marine shelf environment (Dingus, 1984; Parrish, 1987; Parrish *et al*., 2001 a&b; Kelly *et al*., 2007). The formation was previously mapped and described by Leffingwell (1919), Detterman (1970a), Detterman *et al*., (1975), and Tourtelot & Tailleur (1971) and is a useful marker horizon because of its highly organic-rich zones, abundant faunal remains and easily recognizable gamma-ray log characteristics (Chapman *et al*., 1964; Tailleur,

1964; Tourtelot & Tailleur, 1971; Detterman *et al*., 1975; Jones & Speers, 1976; Dingus, 1984; Kupecz, 1995).

Recent literature notes the cyclic nature of the Shublik Fm. based on analysis of lithofacies architecture, sequence stratigraphy and geochemistry (Isaacs *et al*., 1995; Hulm, 1999; Parrish *et al*., 2001 a&b; Kelly, 2004; Kelly *et al*., 2007). The Shublik Fm. is typically composed of nine different rock types: claystone, organic-rich shale, bioclastic wackestone and packstone, sandstone, nodular and pebbly phosphorite, and phosphatic and glauconitic sandstone (Detterman, 1970a; Tourtelot & Tailleur, 1971; Parrish, 1987; Kupecz, 1995; Hulm, 1999; Parrish *et al*., 2001 a&b). Meter-scale stratal stacking patterns within the Shublik Fm. were interpreted by Kelly (2004) and Kelly *et al*. (2007) based on facies associations. This high-frequency is indicative of depositional parasequence sets, according to the Van Wagoner *et al*. (1988) classification scheme. The parasequences and parasequence sets record sea-level changes on a low-angle passive continental margin influenced by transgressive and regressive cycles during the Middle−Upper Triassic (Parrish *et al*., 2001 a&b). Interest in the source rock potential of the Shublik Fm. has led to several sequence stratigraphic interpretations which incorporate petrophysical logs, geochemical data, core and outcrop correlations including Kupecz (1995), Robison *et al*. (1996), Hulm (1999), Parrish *et al*. (2001 a&b), Kelly (2004), and Kelly *et al*. (2007).

The Shublik Fm. was divided into four regionally traceable zones (A, B, C and D, from top to bottom) using gamma-ray petrophysical log data (Fig. 3a), for the Prudhoe Bay Unit Common Database (e.g., Kupecz, 1995; Hulm, 1999). The Shublik Fm. and its

subsurface bounding units were described in a sequence stratigraphic framework by Hulm (1999) who built upon stratigraphic interpretations by Kupecz (1995) and Robinson *et al.* (1996). Hulm (1999) interpreted the facies architecture, depositional setting, and sequence stratigraphy of the Eileen sandstone, Shublik Fm., and Sag River Sandstone. His study documents two complete (3rd order) depositional sequences and a portion of a third within the Middle–Upper Triassic in northern Alaska including: 1) sequence one comprised of the Eileen sandstone (uppermost Ivishak Fm., Fire Creek Siltstone equivalent), Zone D (lowermost Shublik Fm.) and Zone C**;** 2) sequence two comprised of Zone B and Zone A respectively, and; 3) sequence three comprised solely of an interpreted lowstand systems tract in the Sag River Sandstone (Hulm, 1999) (supplemental file).

Kelly (2004) and Kelly *et al*. (2007) incorporated interpretations from Hulm's (1999) NPRA and Prudhoe Bay subsurface data to correlate the outcrop exposure at Fire Creek with the offshore Tenneco Phoenix #1 well north of the Barrow Arch (Fig. 1). Kelly *et al.* (2007) built upon previous work by Hulm (1999), Parrish (1987) and Parrish *et al.* (2001a) describing fourteen lithofacies within the Shublik Fm., Fire Creek Siltstone (further abbreviated FCS), Karen Creek Sandstone (distal equivalent of the Sag River Sandstone) and Otuk Fm. (distal equivalent of the Ivishak and Shublik Formations) based on lithology, sedimentary and diagenetic features, and biota (see Kelly *et al*., 2007, Table 2 and references therin). Kelly *et al*. (2007) used lithostratigraphy, ichnofabric and geochemical data from the Fire Creek outcrop to identify facies stacking patterns within the Shublik Fm. and interpreted three (3rd order) depositional sequences including: 1)

sequence one comprised of the FCS and Zone D**;** 2) sequence two comprised of Zone C and Zone B respectively, and 3) sequence three incorporated Zone A and the Karen Creek Sandstone as a complete depositional sequence (supplemental file).

Kelly *et al*. (2007) built their sequence stratigraphic model based on the grouping of fourteen lithofacies into nine different facies associations. Kelly *et al*. (2007) created a sea level curve for their study which implies three potential rises in sea level during the Middle–Upper Triassic and postulates a fourth potential rise in sea level during the Carnian (Fig. 4). In Kelly *et al*.'s (2007) model, facies associations are based on

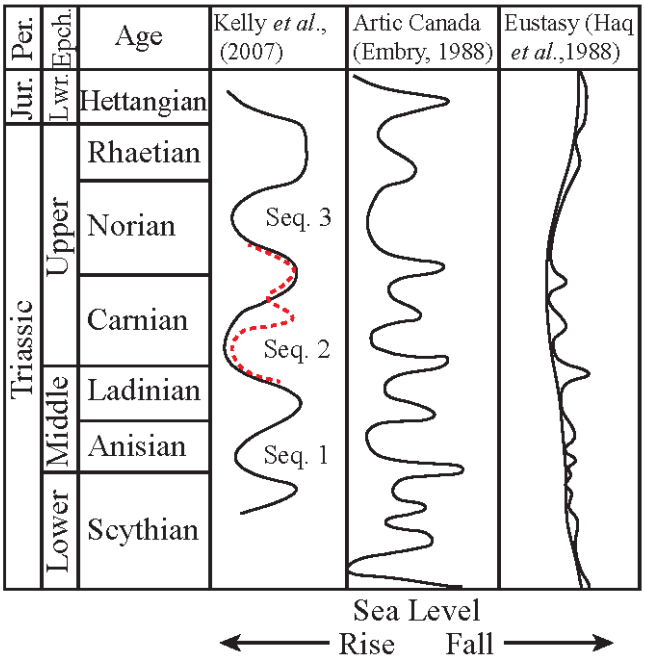


**Fig. 4** Sea level curves for the Triassic. Kelly *et al*., (2007) documents a possible second rise in sea level (red dashed line) during the Carnian which agrees with Embry (1988) and Haq *et al.*, (1988) The additional sequence proposed within this study agrees with proposed curve by Kelly *et al*., (2007) (modified from Kelly *et al*., 2007; Embry, 1988; Haq *et al*., 1988).

stratal stacking patterns including retrogradational, progradational and aggradational events that imply transgression, regression, or still-stand respectively, and are related to relative changes in sea level (Mitchum & Van Wagoner, 1991). Kelly *et al*. (2007) broke out the facies associations into six proximal settings within the Shublik Fm. and three distal settings within the partially equivalent Otuk Fm. The six proximal facies associations include: 1) siliciclastic retrogradational (FCS); 2) siliciclastic, phosphatic progradational (FCS and Zone D); 3) mixed siliciclastic, carbonate, phosphatic retrogradational (Zone C); 4) carbonate, phosphatic progradational (upper Zone C and Zone B); 5) siliciclastic, phosphatic retrogradational (lower Zone A) and; 6) siliciclastic, carbonate, phosphatic progradational (upper Zone A and Karen Creek Sandstone) (supplemental file). Kelly *et al*. (2007) correlated the FCS and the Shublik Fm. at Fire Creek with the distally equivalent lower three members of the Otuk Fm. at Tiglukpuk Creek and Atigun Gorge. These units are located in the central Brooks Range foothills which lay in allochthonous structural positions of the northern foothills of the central Brooks Range (Fig. 1). The distal deposits of the Otuk Fm. were broken into three associations including: 1) siliciclastic, siliceous retrogradational; 2) siliciclastic, siliceous progradational and 3) carbonate progradational facies associations (see Figs. 8-10 in Kelly *et al.*, 2007).

Sequence to parasequence scale cyclicity was observed within the Shublik Fm. at the Fire Creek outcrop and is documented within this study. Recognition of these depositional patterns within the cycles has allowed for interpretation of sequence stratigraphic architecture and correlation between proximal and distal deposits. The

sequences are interpreted to be third-order (1-10 Ma duration) according to the classification scheme of Vail *et al.* (1977). The Hulm (1999) and Kelly *et al*. (2007) interpretations of depositional sequences are based on the identification of transgressive (TST) and highstand systems tracts (HST) and each contains three sequences. However, the sequence boundary locations conflict relative to the zonal divisions (Zone A-D) within each study (supplemental file). This thesis attempts to resolve the discrepancies in sequence stratigraphic architecture and nomenclature by providing detailed interpretations of outcrop features, chemostratigraphy, thin-section petrography and petrophysical well correlations to evolve the current interpretation.

### 2.2.2 Current Sequence Stratigraphic Architecture

A detailed measured section of Middle−Upper Triassic deposits was documented by Kelly *et al*. (2007) at the Fire Creek exposure from the base of the FCS (0 m) to the top of the Karen Creek Sandstone (176 m). Sequence one (53.5 m thick) consists of the FCS which is overlain by a thick succession of phosphatic, fine-grained, non-calcareous sandstone of the lower Shublik Fm. (Kelly *et al*., 2007) (supplemental file). The thin conglomerate at the base of the FCS is interpreted as representing the reworking of lowstand foreshore tidal and/or deltaic channel sediments during initial rise of sea level (Posamentier & Allen, 1999; Kelly *et al*., 2007). The sequence boundary between the Ledge Sandstone and Eileen Sandstone members of the Ivishak Fm. is considered a type one sequence boundary recognized by a regional unconformity (Hulm, 1999). Kelly *et al*. (2007) document the FCS as belonging to the siliciclastic retrogradational facies association comprised of pebbly medium–fine-grained argillaceous quartz sandstones

interbedded with parallel-laminated siltstones and sandstones characterized by burrows, bioturbation, tabular cross-bedding and hummocky cross-stratification (HCS). Interbedded HCS and parallel-laminated sandstones are documented by Kelly *et al*. (2007) within sequence one, and they note how these sedimentary structures resulted from episodic storm deposition and storm relaxation or fairweather shelf deposition, respectively. These thin argillaceous sandstones are grain supported and composed of subrounded–rounded, fine–medium- grained quartz sand with rare muscovite grains, in a silt and minor clay matrix, with local calcite cement (Kelly, 2004; Kelly *et al*., 2007). At the Fire Creek exposure the FCS is characterized by back-stepping depositional cycles with successively more distal facies up-section interpreted as retrogradationally stacked parasequences. Kelly *et al*. (2007) document the fining-upward nature within the FCS and interpret a maximum flooding surface (mfs) (as defined by Mitchum & Van Wagoner, 1991) at 26 m within the section where the cycles progressively fine upward then and are overlain by coarsening-upward more proximal facies. The retrogradational stacking pattern of the parasequences, capped by a mfs supports the interpretation that this represents the TST of sequence one.

Abruptly overlying the FCS is a massive (27 m thick), fine–medium-grained, medium bedded (10−15cm), non-calcareous, well-sorted, phosphatic nodular sandstone with interbedded fine-grained siltstones (5−20 cm) (Fig. 5). Detterman *et al*. (1975) and Parrish *et al*. (2001a) note a phosphatic hard ground capping sequence one, which was later interpreted as a sequence boundary by Kelly (2004) and Kelly *et al*. (2007). The massive interbedded sandstone unit is comprised of two progradational stacked

parasequences displaying local tabular cross-bedding and HCS deposited within an inner shelf environment (Kelly *et al*., 2007). Each parasequence is capped by phosphatic nodular sandstone beds and together they comprise the HST of sequence one. The parasequences were deposited as part of the siliciclastic, phosphatic progradational facies association (Kelly *et al*., 2007) including a lower parasequence from 32−39 m and a thick


**Fig. 5** Outcrop photograph of HST of SQ1 (Kelly *et al*., 2007). **(A)** Two parasequences (PS1-PS2) are outlined from 32−39 m and 39−53.5 m, figures B-D locations indicated by yellow star **(B)** Meter scale coarsening upward depositional cycles contain evidence of HCS and winnowed phosphorite. **(C)** HCS interbedded with fine grained siltstones and winnowed phosphorite deposits. **(D)** Winnowed phosphorites deposit and oil staining on the outcrop.

upper parasequence from 39−53.5 m (Fig. 5). The increase in grain size coincides with less shale dilution and an overall coarsening-upward nature within the HST and indicates a progradatonal stacking pattern within the first parasequence (32–39 m) of sequence one. The second parasequence (45–53.5 m) is marked by an increase in fine-grained siltstone beds at the base with another more massive coarsening-upward section containing thin-to-thick bedded sandstones towards the top of the sequence. Individual depositional events within the HST of sequence one are comprised of finer grained siltstones or phosphatic siltstones overlain by coarser grained silty sandstones–nodular phosphatic sandstones (Kelly *et al*., 2007). Depositional cycles within the HST of sequence one are capped by massive phosphatic nodular sandstone beds (~0.5 m thick) interbedded with pebbly phosphorite lag deposits (Fig. 5c-d). These fine-grained sandstones are dominated by HCS and are interbedded with laminated siltstones influenced by episodic storm processes.

Kelly *et al*. (2007) interpreted a second sequence conformably overlying sequence one (66.5 m in thickness) from 53.5 m (stratigraphic top of sequence one) to 120 m (supplemental file). Sequence two at the Fire Creek outcrop consists of phosphatic argillaceous fissile organic siltstones–mudstones at the base (Fig. 6) overlain by phosphatic argillaceous to bioclastic packstone–wackestone that shoal upwards into a bioclastic packstone cap. Kelly *et al*. (2007) document three parasequences within the uppermost Zone C and B (supplemental file). The base of sequence two is located above the phosphatic hardground capping sequence one and is located 53.5 m above the base of the FCS. The lower part of sequence two consists of sharp-based, fining-upward

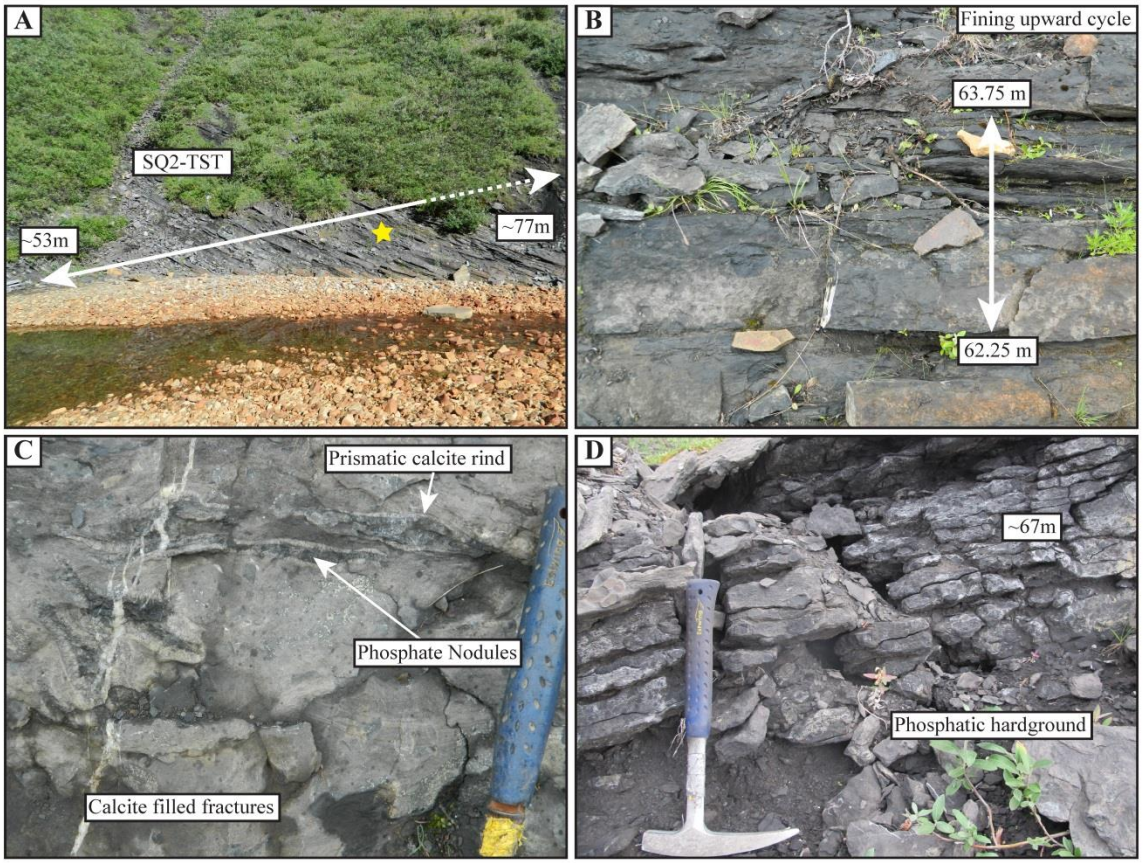


**Fig. 6** Outcrop photograph of TST of SQ2 (Kelly *et al*., 2007). **(A)** The lower portion of the TST is outlined from 53.5−66 m. **(B)** Meter scale fining upward depositional cycles. **(C)** Elongate phosphatic nodules surrounded by prismatic calcite. **(D)** Thinly bedded nodular phosphatic wackestone with abundant phosphate filling shell molds and within burrows near the mfs at 77 m (Kelly *et al*., 2007).

phosphatic argillaceous nodular wackestone–packstone facies interbedded with nodular siltstones (Fig. 6) that fine into argillaceous nodular phosphatic mudstones with abundant phosphate nodules (Kelly *et al*., 2007). The argillaceous phosphatic mudstones are laminated, fissile and poorly cemented. The phosphatic argillaceous nodular packstone–wackestone beds thicken at ~61 m and then fine upwards indicating more distal facies deposition (Kelly *et al*., 2007).

The phosphatic argillaceous nodular mudstone–packstone facies of sequence two were deposited in a moderate energy environment subjected to transgressive reworking of inner shelf sediments (Kelly *et al*., 2007). There is a positive shift in the gamma-ray profile and phosphate enrichment at 77 m which is interpreted as a phosphatic hardground and represents the mfs of sequence two (Kelly *et al*., 2007). The strata beneath the mfs are interpreted as a mixed siliciclastic, carbonate phosphatic retrogradational shelf facies association (Kelly *et al*., 2007) and are interpreted as the TST of sequence two (Fig. 7). The mfs at 77 m is overlain by cyclically deposited phosphatic carbonates (~17 m thick) that form a massive cliff face at the Fire Creek outcrop (Fig. 8). The overall coarsening-upward stacked ramp succession (Burchette & Wright, 1992; Kelly, 2004) is capped by coquinas (~2 m thick) within a carbonate mud matrix, interbedded with fine grained sandstones (10−15 cm beds). This package of carbonate and phosphatic sediments represents the phosphatic, carbonate progradational facies association (Kelly *et al*., 2007).

Kelly *et al*. (2007) attributed thinning of the limestone facies upsection from 94 m–120 m (Fig. 8) to an overall decrease in accommodation space during the carbonate and phosphatic progradational facies association, and thus interpreted the HST of sequence two within this interval. Kelly *et al*. (2007) interpreted flooding events at parasequence boundaries within sequence two which caused a decrease in carbonate production and resulted in thinning-upward phosphatic fine-grained siliciclastic and argillaceous limestone deposition overlying the interbedded coquinas at ~94 m (Fig. 8). Carbonate production followed as the shelf prograded and more optimal conditions for

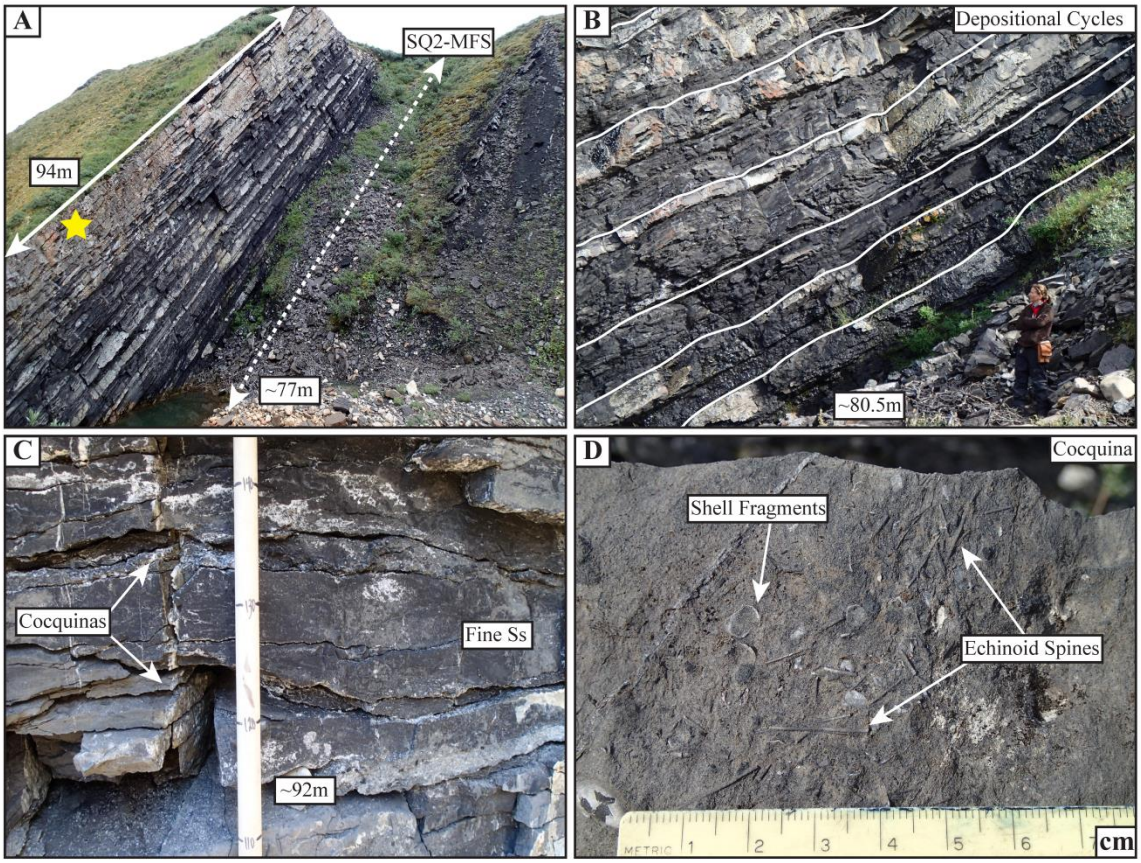


**Fig. 7** Outcrop photograph of coarse grained carbonates within SQ2 (Kelly *et al*., 2007). **(A)** Outcrop photo of the phosphatic, carbonate progradational facies association and approximate location of the mfs of sequence two. **(B)** Coarsening-upward cycles are documented within the phosphatic, carbonate progradational facies association **(C)** The massive unit is capped with interbedded coquinas and fine grained sandstones (location of 7C & 7D indicated by yellow star in 7A). **(D)** Coquinas contain disarticulated bivalve fragments, echinoid spines and gastropods within a calcareous matrix of thin shelled flat clams.

carbonate production were established. There is an abrupt change in lithology between Kelly *et al*.'s (2007) sequences two and three at 120 m (Fig. 8), from phosphatic bioclastic wackestone–packstones to thinly bedded, laminated mudstones and shales, which is interpreted as a regional flooding event.

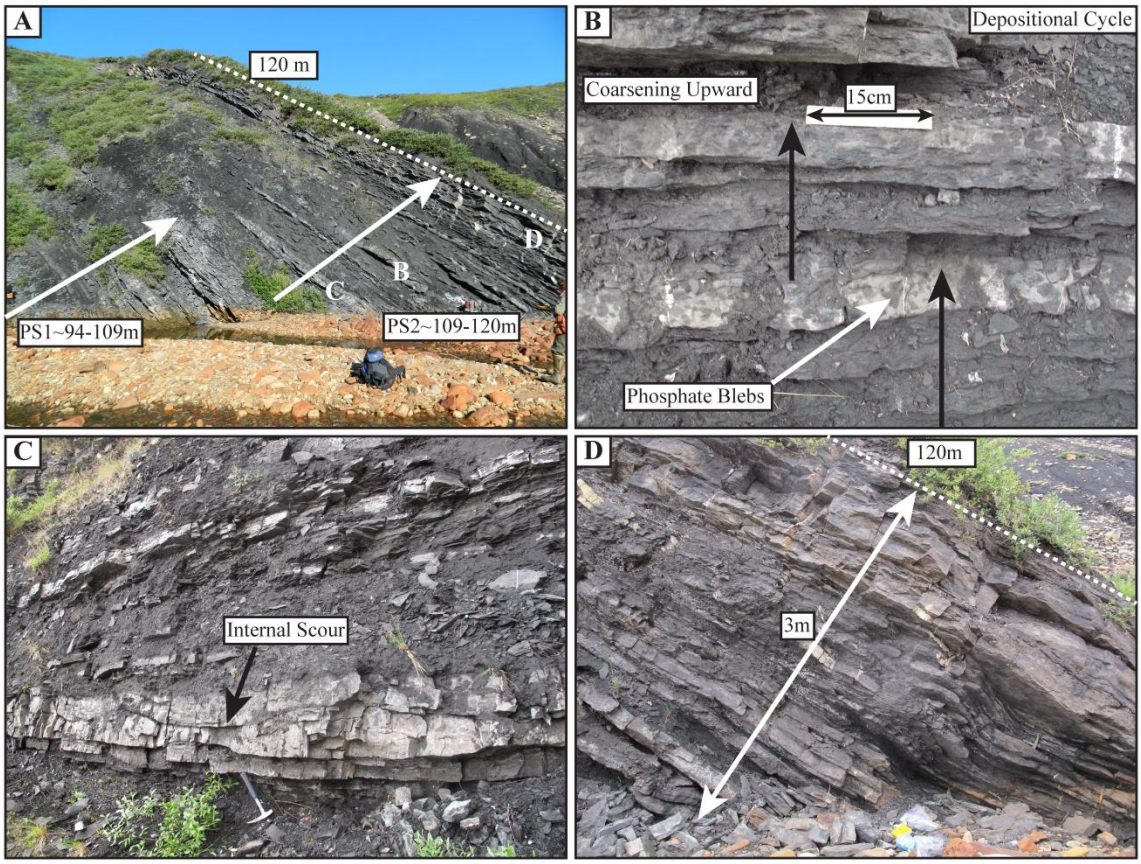


**Fig. 8 (A)** Outcrop photograph of upper SQ2. Two parasequences, PS1 and PS2 (94-109 m and 109-120 m), are outlined within Kelly *et al.*,'s (2007) upper sequence two. Outcrop photo locations of 8B-D indicated by white letters **(B)** Composite bed sets show a coarsening upward nature within PS1, ~25 cm thick **(C)** Multiple channel scours (largest ~1.5 m in width) **(D)** Thinly bedded wackestone to packstone facies within PS2 that coarsens upward to a massive packstone cap.

Kelly *et al*. (2007) note the presence of two condensed phosphorite beds located in the lower part of sequence three (lower Zone A) and place this section within the siliciclastic and phosphatic retrogradational facies association which is interpreted as the TST of sequence three. Due to the large section of covered interval within the TST and the small variations within the gamma-ray response the mfs is not accurately identified. There is a change in facies from laminated siltstones and shales to interbedded, thin,

argillaceous, phosphatic limestones, and shales at ~165 m. Overlying the interbedded siltstones and thin limestones, the phosphatic sandstone and medium sandstone deposits of the Karen Creek Sandstone cap sequence three (Kelly *et al*., 2007) (Fig. 9). The Karen Creek Sandstone, consisting of fine–medium-grained, burrowed sandstones represents the siliciclastic, carbonate, phosphatic progradational facies association and was thus interpreted as the HST of sequence three according to Kelly *et al*. (2007).

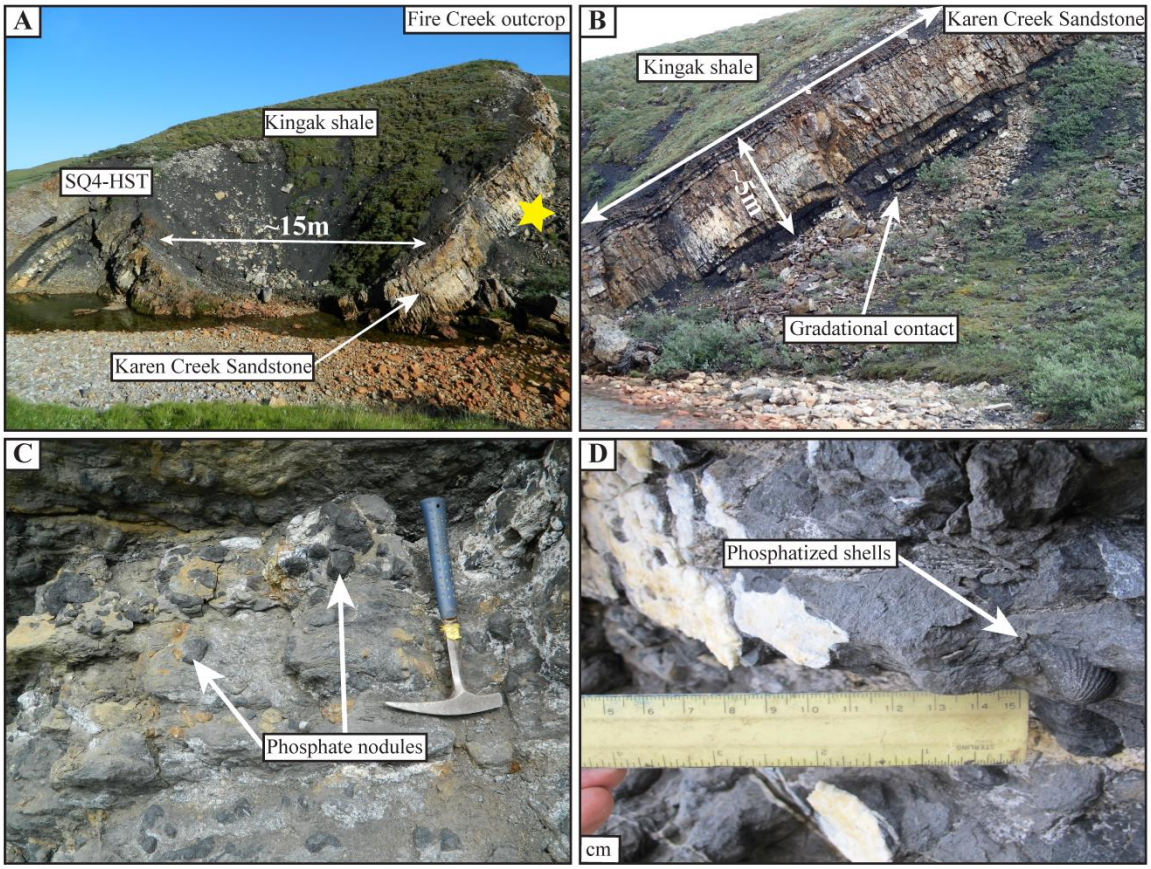


**Fig. 9** Outcrop photograph of upper SQ3. Upper Shublik Fm. and Karen Creek Sandstone (Kelly *et al*., 2007) are pictured. **(A)** Photograph of compressional folding within the Karen Creek Sandstone. Yellow star indicates photographic locations 9B-D. **(B)** The transition above the mfs (~126 m, below gradational contact) into the Karen Creek Sandstone. **(C)** Abundant phosphatized horizons within heavily burrowed strata. **(D)** Phosphatized bivalves and gastropods in a phosphatic calcareous matrix.

The uppermost sequence boundary within the Late Triassic in northeastern Alaska is located at the top of the Karen Creek Sandstone which is overlain by a thick succession of papery black shale comprising the Kingak Fm. (Hulm, 1999; Kelly *et al*., 2007) (Fig. 9).

## 2.3 Chemostratigraphy Background

The relatively new stratigraphic technique of chemostratigraphy utilizes geochemical proxy data to model paleoenvironmental conditions, thus tracking geologic events laterally and vertically within a potential basin (Ratcliffe *et al*., 2012). This study utilizes major and trace element geochemistry inconjunction with thin-section petrographic analyses to understand the primary controls on $C_{org}$ deposition. Since aqueous proxies are unavailable for the paleomarine in Arctic Alaska, sediment-based proxies were used to detect the presence of redox sensitive and relatively immobile trace metals preserved in the sediment record (Tribovillard *et al*., 2006; Algeo & Rowe, 2012). Trends in proxy data are used to identify periods of oxic, suboxic and anoxic (paleoredox) bottom water conditions, while major element concentrations are used to identify large shifts in carbonate and terrigenous deposition. Trace element measurements are used as proxies to document three different variables including: 1) paleoredox conditions (e.g. U, Mo, V and Ni); 2) productivity (e.g. Ni, Cu, Ba, Zn and P); and 3) terrigenous input (Al, $SiO_2$, K, Ti, Ti/Al and Cr). Utilization of certain redox sensitive trace element concentrations as proxies allows for the delineation of syn-depositional bottom water redox conditions (e.g. Calvert & Pedersen, 1993; Jones & Manning, 1994;

Calvert *et al*., 1996; Algeo & Maynard, 2008; Tribovillard *et al*., 2006; Tribovillard *et al*., 2012; Ratcliffe *et al*., 2012).

Inorganic whole-rock data extracted from heterolithic organic-rich formations can be used to create a regional chemostratigraphic correlation framework that identifies depositional changes due to shifts in paleobathymetry and environmental fluctuations. Shifts in the oxidation state at the sediment-water interface along with increased productivity are inferred from trace element concentrations. The value of these paleoenvironmental proxies is to differentiate preferential elemental uptake under low-oxygen and/or sulfidic water mass conditions at or just below the sediment-water interface. Cyclic changes in ocean-atmosphere circulation patterns influence the regional intensity of upwelling currents due to changes in Ekman transport. Seasonal or episodic high biologic productivity, related to an influx in nutrient-laden, oxygen-poor bottom waters, influences oxygen levels at the sediment-water interface (Fig. 10).

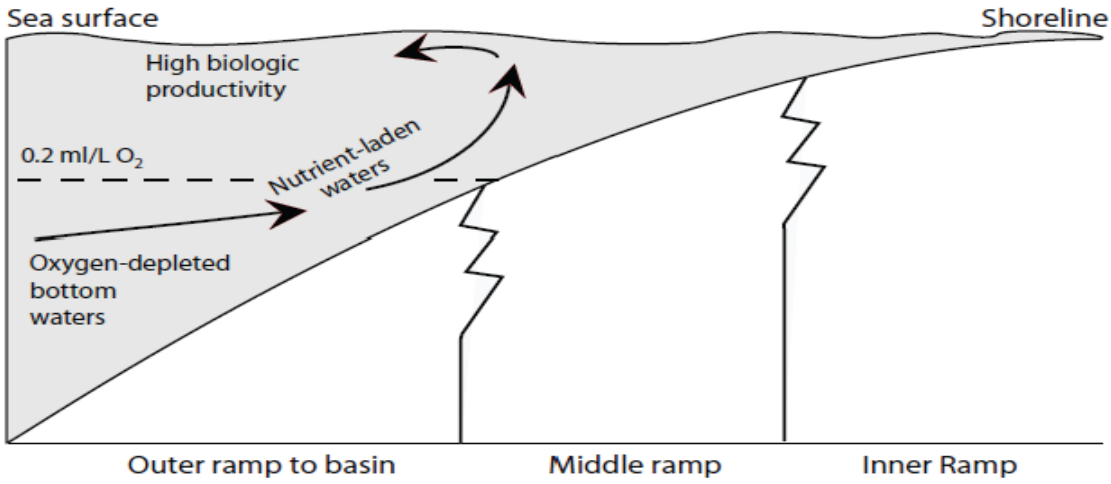


**Fig. 10** Schematic reconstruction of the continental shelf and vertical circulation perpendicular to the shoreline. Diagram illustrates upwelling currents relative to zones of high productivity and associated oxygen depleted bottom water conditions influenced by abundant organic matter detritus (modified from Parrish, 1982).

Upwelling currents provide deep water renewal of trace metals providing bioavailable micronutrients and increasing bioproductivity (Algeo & Maynard, 2008).

Cyclic changes in relative sea level as well as changes in the climate influence upwelling processes, biologic productivity and $C_{org}$ deposition and the position of oxygen depleted waters at the sediment-water interface. The relative position of sea level on the shelf margin will also influence the position or zone of depleted oxygen levels, this zone of oxygen deficient water at or near the sediment-water interface is subsequently referred to as the oxygen minimum zone (OMZ). Thus, upwelling and high bioproductivity conditions influence the enrichment of authigenic redox sensitive trace metals and provide information toward understanding $C_{org}$ preservation. The chemostratigraphic profile of redox-sensitive trace elements permits interpretation of temporal and vertical variation in paleoredox conditions (Ratcliffe *et al*., 2012) which can be applied regionally to understand their lateral extent through well correlations.

Detrital proxies indicate an influx of terrigenous input with increased Al, Si, K and Ti input from argillaceous sediments and an overall decrease in carbonate matrix. Because the composition of commonly used shale standards and the reference values of normalized elements widely used are not representative of sediments in the study area the proxies used in this study have not been subjected to Al-normalization. Uncorrelated variables subjected to normalization could enhance or distort the pre-existing relationships between trace element enrichment and terrigenous dilution (Van der Weijden, 2002).

## 2.4 Phosphatic Sediment Overview

The microfacies examined in this thesis contain variable amounts of phosphate (10-40% visual estimation). Thus, in order to correlate the abundance of phosphorus (P) mineralization in thin-sections to depositional setting, a basic interpretation of marine phosphogenesis must be completed. A comprehensive literature base concerning authigenic phosphorite deposition and varied interpretations on P burial mechanisms exists and is summarized below.

Sedimentary P from microbial breakdown of organic matter and recycling by redox-driven mechanisms constitutes the main driver of phosphogenesis near the sediment-water interface leading to development of pristine phosphatic nodules (Föllmi, 1996). P exists in many forms in marine waters including organic, inorganic and mineral phases that are subject to transformations in response to changing environments. Continental P is carried to deep ocean basins and in prevailing coastal upwelling conditions high levels of nutrients are found in association with nodular phosphorites and organic-rich facies (Föllmi, 1996), such as within the Triassic Shublik Fm.

The removal of P during sediment burial takes place through organic P in organic matter or skeletal debris, as inorganic P through adsorption on iron (Fe) and manganese (Mn) oxyhydroxides, or incorporation into authigenic phosphate-bearing minerals such as apatite, francolite and fluorapatite (Berner *et al*., 1993). The sequestration of P incorporated in the calcium-phosphate mineral apatite [$Ca_5(PO_4)_3$], in marine sediments, is thought to be the largest P sink that occurs over geologic time and it is precipitated as

micro- and macroscopic cements, peloids and nodules. Fe and Mn oxyhydroxides are significant carriers for solid inorganic P and are commonly found as coatings on particulates such as clays or organic materials. Continental weathering of inorganic P-bearing rocks is considered the major pre-anthropogenic source of P to enter the marine realm (Föllmi, 1996).

Recent studies (e.g. Goldhammer *et al*., 2010) have inferred that bacterial mediation provides the kinetic energy to remove calcium and P from marine waters. Goldhammer *et al*. (2010) found direct evidence that bacterial mediated poly-phosphate production occurred in coastal upwelling conditions with high nutrient levels and organic-rich sediments in the Benguela upwelling system off the coast of Namibia. Goldhammer *et al*. (2010) linked apatite growth to a biogenic compound called poly-P, found in organisms along with abundant calcium that provides a template for apatite precipitation. The study used inorganic radioactive $^{33}P$ to trace the pathway of apatite formation by introducing the compound into poly-phosphate producing bacteria. The study indicates apatite precipitation was enhanced under anoxic vs. oxic conditions, which contradicts studies in ancient and modern deposits where precipitation is limited under anoxic settings due to P recycling into the water column (Ingall & Jahnke, 1994; Ingall, 2010). Within anoxic pore waters, where large sulphide bacteria were present, the precipitated apatite contained abundant radioactive $^{33}P$ tracer. Within the control group, with no large sulphide bacteria, there was no authigenic apatite precipitation enhanced with the $^{33}P$ tracer. The study indicates that large sulphide bacteria play an instrumental

role in inorganic P precipitation into apatite under anoxic conditions that wouldn't occur without bio-mediation.

The phosphate-rich (20%, Detterman, 1970a) Middle –Upper Triassic Shublik Fm. is interpreted as having been deposited under upwelling conditions and contains a distinctive pattern of sedimentary lithofacies including glauconitic, phosphatic, organic-rich, and cherty sediments deposited from shoreface to basin, respectively (Parrish, 1987). These distinctive lithofacies, commonly associated with upwelling systems, have been documented within the Shublik Fm. and other paleoenvironments where upwelling processes influenced deposition (e.g. Baturin, 1982; Parrish, 1982, 1987, 2001 a&b; Thiede & Suess, 1983; Bodnar , 1984; Dingus, 1984; Notholt & Jarvis, 1990; Föllmi & Grimm, 1990; Föllmi *et al*., 1991; Hulm, 1999; Kelly *et al*., 2007). Similar suites of facies have been documented in ancient formations such as, the Miocene Monterey Fm. of California (Garrison & Douglas, 1981) and the Permian Phosphoria Fm. of southern Idaho, Wyoming and Utah (McKelvey *et al*. 1967; Hendrix & Byers, 2000).

In a sequence stratigraphic framework during transgressive events, at or near maximum flooding, slow sedimentation rates commonly result in condensed sections with high gamma-ray readings, organic-rich rocks and authigenic glauconite−phosphorite mineralization (Loutit *et al*., 1988). During transgression deposits can be cannibalized resulting in deposition of winnowed authigenic glauconitic-phosphate nodules (Föllmi, 1996). According to Föllmi (1996), the distribution, type of stratification, type of P mineralization, and the degree of P condensation allow for interpretation of the ecosystem or environment in which the deposit formed. In a sequence stratigraphic

context, phosphates are preferentially condensed along marine flooding surfaces and reworked during transgressions and transported to highstand or lowstand deposits (Föllmi, 1996). Thus, depositional facies within the Shublik Fm. that contain higher than normal P enrichment can be interpreted in a sequence stratigraphic context and used for correlation purposes and predicting preferable $C_{org}$-rich zones.

# CHAPTER 3: METHODS

## 3.1 Outcrop Investigation

For this study a portion of the Fire Creek section was measured with a Jacob's Staff and closely spaced samples were collected within the lower part of Kelly *et al*.'s (2007) sequence two from 53.5 m to 94 m (supplemental file). Samples were preferentially taken from the phosphatic, carbonate facies association in order to document geochemical and lithological changes within the high frequency, organic-rich, coarsening-upward depositional cycles. Documentation of depositional, biogenic, diagenetic and deformational structures, which included stratification associated with bedding and sedimentary structures, were used to identify vertical changes in lithological stacking patterns. Particular features such as hummocky cross-stratification, winnowed zones and graded bedding were instructive for interpretation of depositional processes. Hand samples were collected and used for thin-section, geochemical and facies analyses. Outcrop photographs were taken and subsequently used to document facies stacking patterns and sedimentary structures within the stratigraphic architecture.

This study utilized the Galloway (1989a) *genetic stratigraphic sequence model* to aid in further refinement of previous stratigraphic interpretations (c.f. Kupecz, 1995; Hulm, 1999; Parrish *et al*., 2001 a&b; Kelly *et al*., 2007). The Galloway (1989a) model proposed that genetic stratigraphic units are bound by hiatal surfaces, corresponding to maximum flooding within the basin. The model recognized the importance of separating systems tracts as distinct genetic units. In order to correctly describe facies relationships,

depositional patterns, and sequence stratigraphic interpretations (transgressive and highstand systems tracts) nomenclature from Van Wagoner *et al*. (1988) or the Exxon Research Group (ERG) was applied.

### 3.2 Petrography

Microfacies analysis was performed at the University of Alaska Fairbanks to document the depositional environment or facies transitions using standard carbonate lithofacies descriptions from Dunham (1962), Embry & Klovan (1971) and Flügel (2004). Grain type associations, fossil assemblages, bioturbation (ichnofabric evidence, see Droser & Bottjer, 1986), and graded bedding were characteristics used to distinguish four microfacies. Qualitative visual estimates of thin-section constituents were performed utilizing charts from Baccelle and Bosellini (1965). Diagenetic features such as stylolites, fractures, cement mineralogy and textures were used to interpret post-depositional history. The petrographic data was then incorporated into analysis of facies stacking patterns and integrated with elemental proxy data and $C_{org}$ concentrations to document variations in the depositional environment with respect to fluctuations in sea level.

### 3.3 Geochemical Analysis

Using analytical equipment at the Advanced Instrument Laboratory (AIL), at the University of Alaska Fairbanks, 35 closely spaced samples collected from the Fire Creek exposure were analyzed for trace element concentrations using XRF analyses (Appendix A-C). A total of 83 samples were analyzed for $C_{org}$ (wt. %) concentrations using a LECO C230 carbon analyzer (Appendix D). The Kelly (2004) dataset includes an additional 58

measurements for $C_{org}$ (wt. %) concentrations and 86 samples for inorganic geochemistry collected at regular intervals (~1m) throughout the Fire Creek exposure that were incorporated into this analysis.

Closely spaced (~25cm) samples from fresh, minimally weathered, rock exposure surfaces were preferentially selected for geochemical analyses of the Shublik Fm. at the Fire Creek outcrop. Samples were trimmed of any remnant weathering rinds and veins and then pulverized in an alumina-ceramic mortar at the USGS Crustal Geophysics and Geochemistry Science Center in Denver, Colorado. Rock powders were then mixed with a polyvinyl alcohol (PVA) binder in an agate mortar and pestle and pressed under 10 metric tons of pressure into 27 mm diameter, 5 mm thick pellets. Analytical equipment at the Advanced Instrument Laboratory (AIL), at the University of Alaska Fairbanks, were used to measured trace element concentrations using X-Ray Fluorescence mass spectrometry (XRF). Concentrations of 43 trace elements were determined using a WD-XRF. These analyses employed PANalytical PROTrace analytical standards and software. This study used specific trace element measurements from the Kelly (2004) geochemical dataset to supplement data generated from samples collected during recent field work (Appendix A).

### 3.4 Petrophysical Correlation

Petrophysical log data from 97 industry wells were used to conduct a regional correlation of the Shublik Fm. and related units. This project utilized formation top data to guide interpretation of relevant formation tops associated with the sequence

stratigraphic interpretations presented within this thesis. Specifically, the Ivishak Fm. and the Sag River Sandstone tops were used to define the relevant boundaries within the stratigraphic interpretation. Distinctive gamma-ray log patterns indicate changes in stratigraphic architecture, such as from proximal−distal depositional settings. Outcrop spectral gamma-ray (SGR data) documented within the Kelly (2004) dataset was used in the recognition of cycles, their stacking patterns and sequence stratigraphy and correlated to nearby industry wells. Distinctive, laterally persistent shifts in the gamma-ray profile were used to indicate transgressive and regressive patterns and major shifts in sedimentation. Well log data were used to interpret sequence boundaries, and using mean log thickness data from each well, isochore maps were constructed to identify trends in thickness. Thus, paleoenvironment was inferred within the Middle−Upper Triassic deposits in northern Alaska and correlated from the outcrop at Fire Creek to the west across northern Alaska (Fig. 11).

Finally, elemental data, in conjunction with SGR data, thin-section petrography and field-based observations are used to identify variations within the meter-scale depositional cyclicity of organic-rich and carbonate to phosphatic facies. These data are used in conjunction with sequence stratigraphic methods to document the accumulation and preservation of organic-rich sediments during the Triassic in northern Alaska. Using a stratigraphic profile of grain size, bioturbation, fossil assemblages and trace element concentrations a model is constructed to elucidate paleoredox and biological productivity conditions during deposition of the Shublik Fm. Core and log analyses are then compared to outcrop data to test surface–subsurface correlations and previously developed sequence

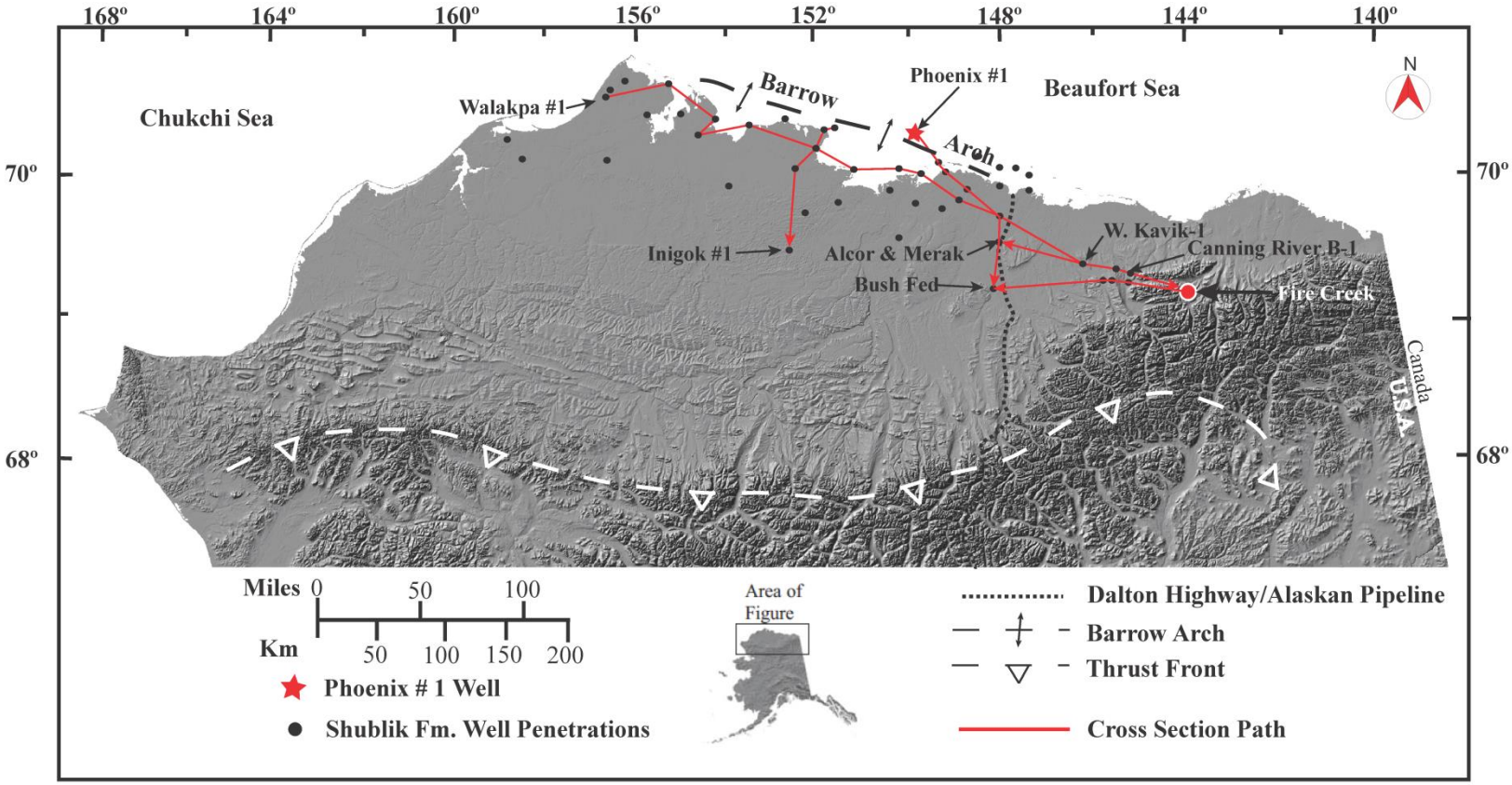


**Fig. 11** Digital Elevation Model **(**DEM) image of northern Alaska. The location of Fire Creek outcrop and wells used for petrophysical correlations and isochore maps are illustrated (modified from Moore, *et al*., 1994).

stratigraphic models (Hulm, 1999; Parrish *et al*., 2001a&b; Kelly, 2004; Kelly *et al*., 2007). Wire line log data is correlated with outcrop measurements and observations which allow interpretation of the lateral and vertical variations in depositional facies, thus delineating the high-resolution sequence stratigraphic framework.

# CHAPTER 4: OBSERVATIONS AND DATA

## 4.1 Fire Creek Outcrop Observations

For the purposes of this study a detailed measured section, closely spaced lithologic samples, and observations were only documented within the mixed siliciclastic, carbonate, phosphatic retrogradational shelf facies association and phosphatic, carbonate facies association within sequence two (Fig. 12). The base of Kelly *et al*.'s (2007) sequence two from 53.5 m to 67.5 m contains fining upward interbedded argillaceous siltstone and packstone–wackestone facies interpreted to be within the mixed siliciclastic, carbonate, phosphatic, retrogradational shelf facies association. Sedimentary features recognized include convolute bedding, prismatic calcite surrounding phosphatic and calcite nodules, calcite filled fractures, and thin clay seams (Fig. 6). Overlying these sediments is a 13.5 meter interval covered with abundant vegetation where outcrop observations were difficult and interpretations could not be drawn. Immediately overlying the covered interval is 13.5 meters of thinly laminated phosphatic mudstones to siltstones that grade into black phosphatic bioclastic organic wackestone–packstones within 9 depositional cycles (Fig. 7) capped by ~ 2 meters of coquinas.

Above the coquina facies there is a prominent transition in depositional environment located at 94 m (Fig.12) within the Fire Creep outcrop exposure. This surface is demarcated by a shift from coarse-grained coquina beds interbedded with fine grained calcareous sandstones to organic-rich mudstones with up to 4 wt. % $C_{org}$.

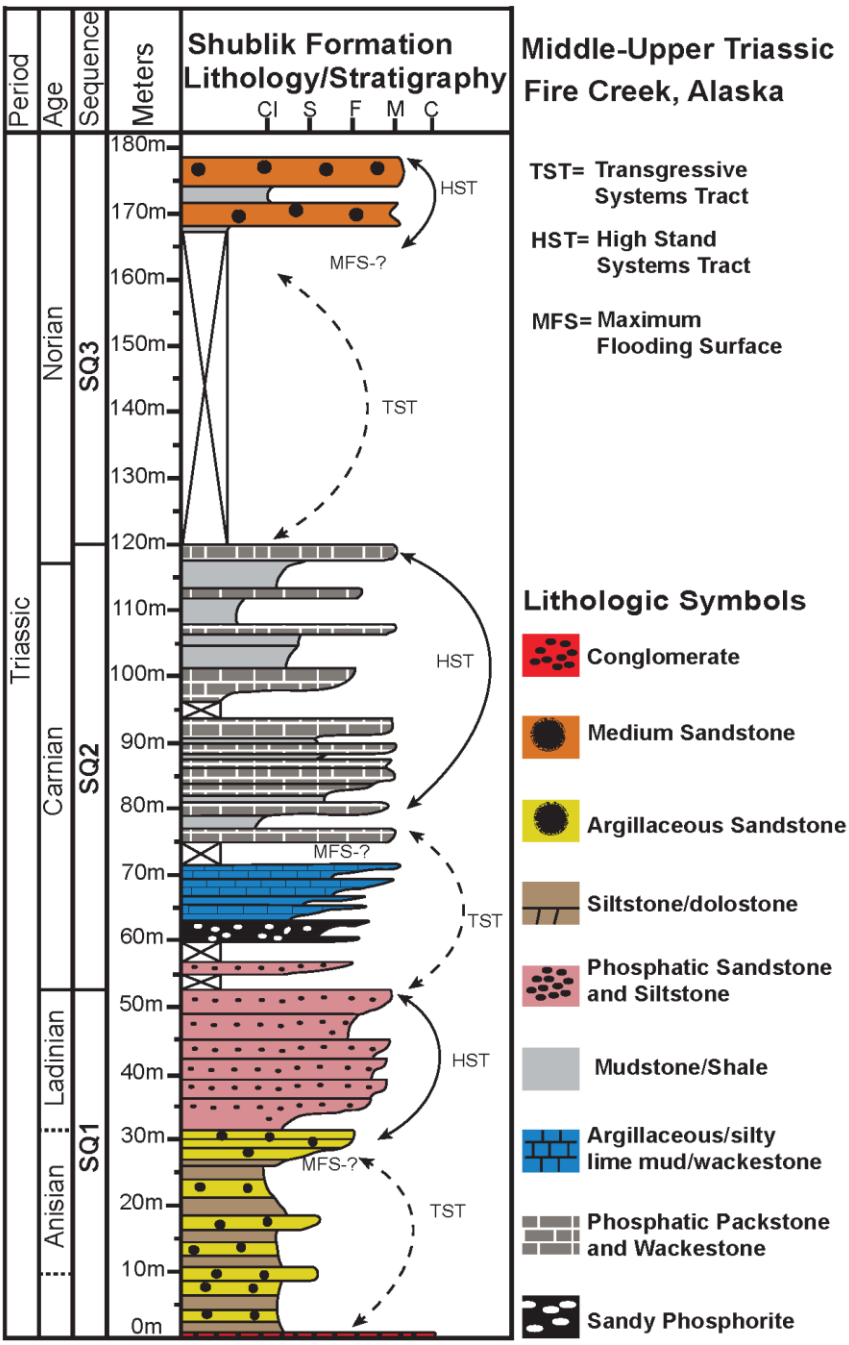


**Fig. 12** Lithostratigraphic diagram of the Triassic Shublik Fm. Exposure located at Fire Creek, in northeastern Alaska. The geologic age, lithostratigraphic units, thickness in meters, lithology, and average grain size are indicated. Diagram shows current sequence stratigraphic interpretation for Upper-Triassic deposits in northern Alaska. Crossed out sections indicate covered intervals (modified from Kelly *et al*., 2007).

The Mudstone to wackestones facies are interbedded with phosphatic fine grained wackestone to packstones. Depositional cycles consist of thinly laminated phosphatic argillaceous mudstones and siltstones grade into black phosphatic bioclastic organic wackestone to packstones. The fissile mudstones grade into more carbonate dominated wackestone to packstone facies within the carbonate and phosphatic progradational facies association (Fig. 8).

Overlying the carbonate and phosphatic progradational facies association at 120 m are thinly bedded siltstones (56.5 m thick) which are then overlain by the Karen Creek Sandstone (Sag River Sandstone equivalent). True stratigraphic thickness measurements of the upper Shublik Fm. are difficult due to a large covered interval and folding at the Fire Creek exposure (Fig. 9). The overlying Karen Creek Sandstone was folded and potential structural thickening of the surrounding formations complicates thickness measurements. The Karen Creek Sandstone is highly burrowed which destroyed any relict sedimentary structures. Outcrop sediments contain abundant phosphate nodules (up to 10 cm), phosphatized shell casts and encrustations, oxidation of pyrite and are capped with a vertically burrowed horizon with penetrations up to 10 cm deep. Abundant phosphate encrusted shell fragments and phosphatic nodules created pristine phosphatic horizons (Föllmi, 1996). The uppermost sequence boundary with the Kingak Shale (~176 m) is abrupt although erosional features from exposure were not observed at the Fire Creek outcrop.

## 4.2 Microfacies

A detailed petrographic inspection of rocks sampled from the phosphatic and carbonate progradational facies association within Kelly *et al*.'s (2007) sequence two at the Fire Creek outcrop was performed. The samples include 38 thin-sections sampled over ~13.5 meters. The HST is primarily comprised of a shelly substrate with *in situ* peloids and phosphatic nodules. The abundant round–ovoid phosphate nodules range from a few millimeters to more than 15 cm long, and consist primarily of isotropic carbonate fluorapatite with minor amounts of calcite and quartz (Detterman, 1970a). Nodules subjected to cannibalistic re-working were deposited in winnowed layers through hydraulic processes, whereas pristine *in situ* nodule deposits precipitated from direct mineralization from the sea water, high P concentration in the sediments, or through bacterially mediated processes (Detterman, 1970a; Goldhammer *et al*., 2010). Sedimentary features such as HCS interbedded with parallel-laminated bedding are documented within sequence one and sequence two at the Fire Creek outcrop suggesting episodic storm processes or transgressive re-working of inner shelf sediments were common during deposition (Kelly *et al*., 2007).

The microfacies described herein contain similar characteristic fossil assemblages, cement, and grain sizes. Important criteria used include bioturbation, detrital quartz content, phosphate or organic content and larger scale nodule precipitation attributed to hardground formation. For the purposes of this study, the microfacies criteria are used in conjunction with trace element geochemical proxies to interpret shifts in the OMZ, primary productivity and terrigenous dilution, respectively. Four microfacies were

interpreted from outcrop and thin-section observations in this study and are outlined below (Fig. 13-16).

### 4.2.1 Phosphatic Bioclastic Organic-Rich Mudstone

The phosphatic bioclastic organic mudstone microfacies is characterized by calcite cemented mudstones with abundant peloidal phosphatic grains and *in situ* nodules up to 15 mm in diameter (10-40%) (Fig. 13). This facies is moderately bioturbated, displays bimodal sorting, and contains disarticulated and macerated thin shelled clams (*Halobia*) (5-25%), echinoid spines (1-10%) and thick shelled bivalves (0-7.5 %). Relict-bedding was destroyed by bioturbation (ichnofabric index 2-3) and samples contain abundant echinoid spines with calcite twinning on cross-sections. Silt-sized particles consist mainly of macerated thin shelled bivalves and detrital quartz (1-20%) grains. This facies is distinguished by moderate bioturbation within a calcareous mudstone matrix consisting predominantly of calcareous fossil fragments, organic material (1-2% Corg) and minor amounts of clays.

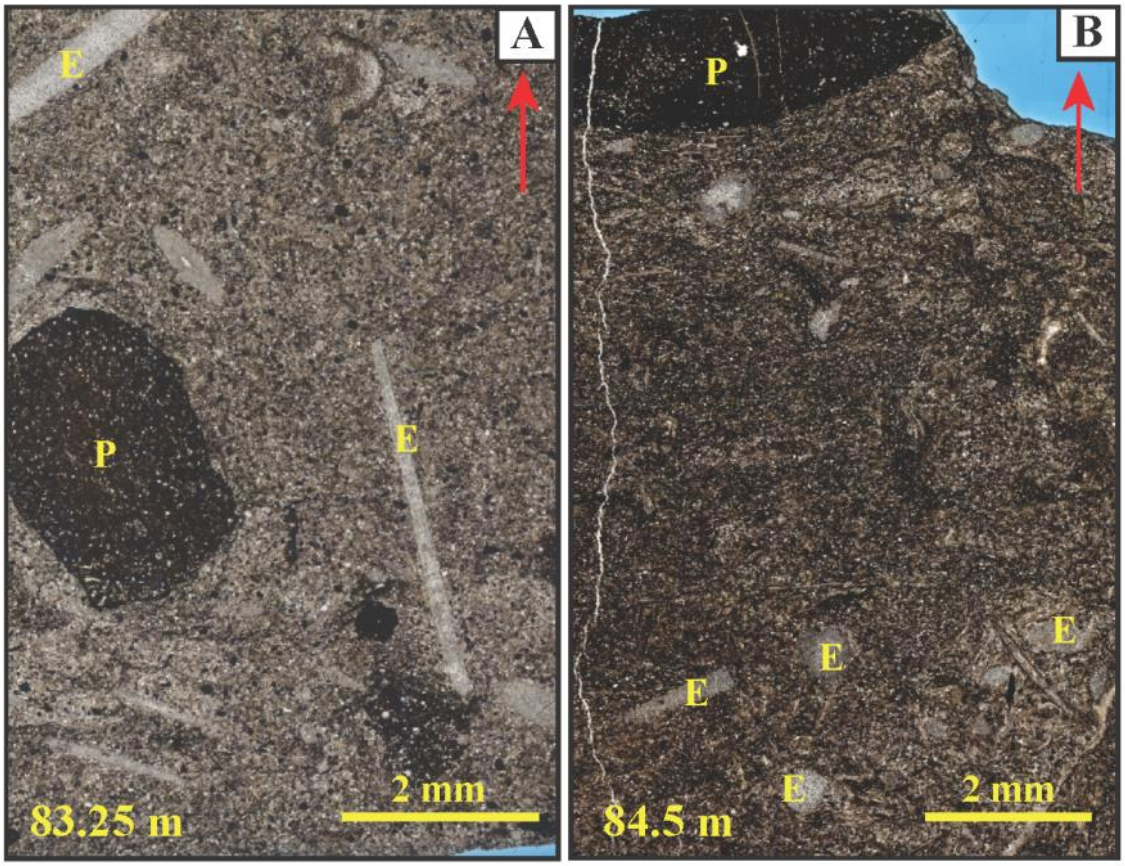


**Fig. 13** Thin section photograph of the Phosphatic Bioclastic Organic Mudstone microfacies. **(A)** Sampled from 83.25 m in section **(B)** Sampled from 84.5 m (see Fig. 12). This facies has abundant isotropic organic material and phosphatic mineralization within a poor to bimodal sorted carbonate matrix. There is moderate bioturbation with *in situ* phosphate nodules up to 15mm. (P) are phosphate nodules and (E) are echinoid spine fragments. Red arrows indicate stratigraphic up.

### 4.2.2 Phosphatic Argillaceous Nodular Wackestone

The phosphatic argillaceous nodular wackestone microfacies is characterized by calcite-cemented wackestones with abundant silt-sized quartz (25-50%) and peloidal phosphatic grains (20-35%) (Fig. 14). It is moderately bioturbated (ichnofabric index 2-

3), well sorted and contains disarticulated and macerated thin shelled clams (*Halobia*) (1-15%), echinoid spines (1-3%) and thick shelled bivalves (0-5%). This facies is distinguished by the abundant, angular, silt-sized, detrital quartz grains and localized concentrations of thick shelled brachiopod fragments. Contacts between phosphatic nodules and matrix are indistinct, except along shell casts, which indicates bioturbation and diagenetic overprint of the matrix (Flügel, 2004).

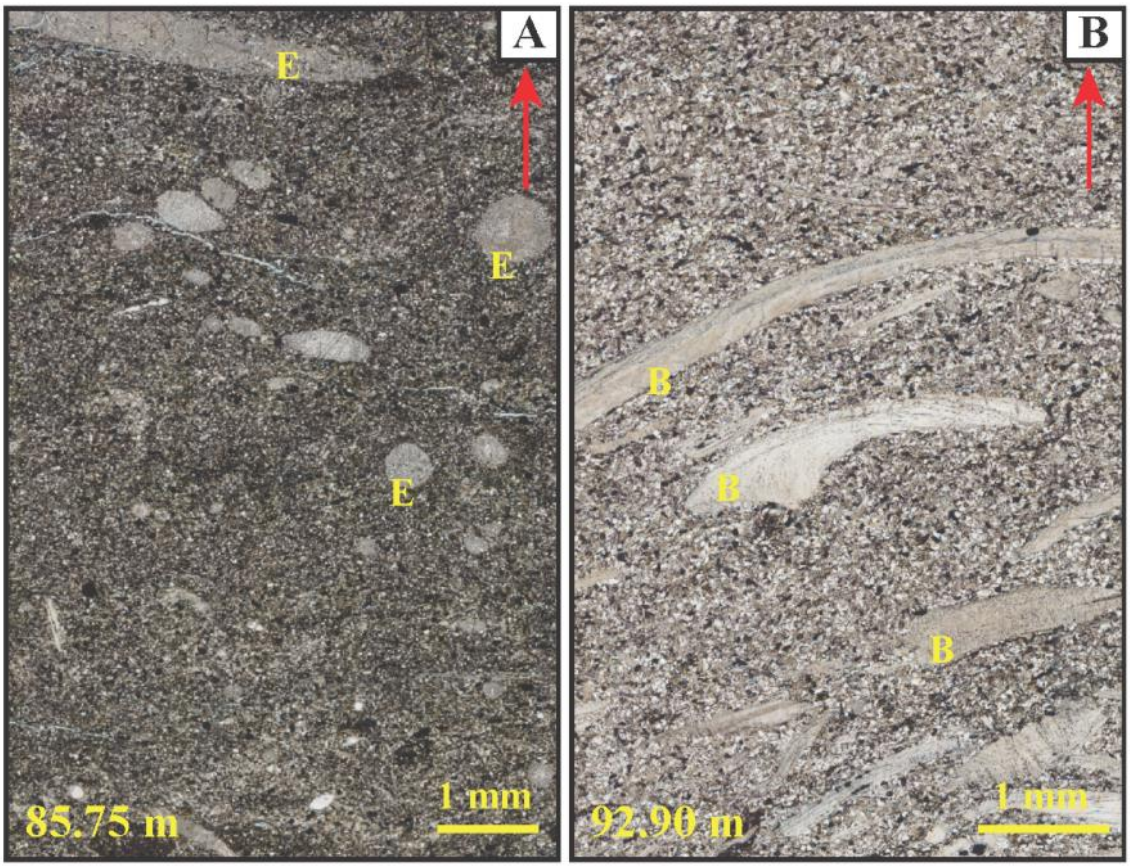


**Fig. 14** Thin section photograph of the Phosphatic Argillaceous Nodular Wackestone facies. **(A)** Sampled from 85.75 m in section while **(B)** was sampled at 92.90 m (see Fig. 13). This facies has abundant isotropic peloidal phosphatic mineralization (small black round grains) within a poor to bimodal sorted carbonate and silt sized angular quartz matrix. There is moderate bioturbation with *in situ* isolated phosphate nodules up to 15mm. Yellow letter (E) indicates echinoid spine fragments and (B) indicates bivalve fragments. Red arrows indicate stratigraphic up.

The peloidal P nodules are ovoid in nature and diagenetically overprint the matrix and grain constituents. The fine bioclastic texture exhibited within the bi-modal matrix contains abundant detrital quartz grains, calcareous fossil fragments, organic material (0.3-1.3 % $C_{org}$) and minor amounts of clay.

### 4.2.3 Phosphatic Peloidal Bioclastic Wacke−Packstone

The phosphatic peloidal bioclastic wacke–packstone microfacies is the most common microfacies documented and is characterized by calcite-cemented wackestones–packstones with abundant peloidal phosphatic grains (25-40%) and *in situ* nodules up to 15 mm in diameter (Fig. 15). The bioclastic nodular texture exhibited within this facies contains abundant, detrital, silt-sized, angular quartz grains (20-35%) and macerated calcite shells with P nodules and organic matter (0.3-1.3 % $C_{org}$). The facies is extensively bioturbated (ichnofabric index 4-5), poorly to well sorted and contains disarticulated and macerated thin shelled clams (*Halobia*) (5-20%), echinoid spines (1-7.5%) and thick shelled bivalves (0-7.5 %). The phosphatic peloidal bioclastic packstone to wackestone facies contains abundant, P diagenetic alteration within burrows and infill within shell fragments. Thick shelled bivalves were replaced with fibrous calcite spar and have a sweeping extinction under cross-polarized light.

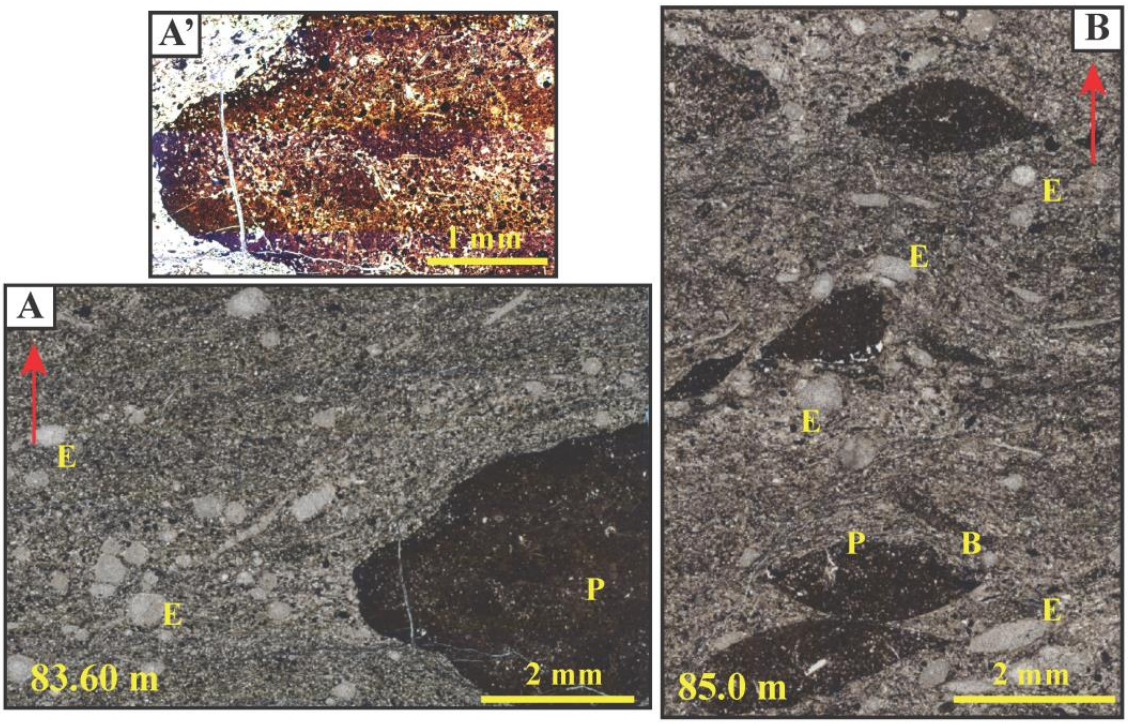


**Fig. 15** Thin section photograph of the Phosphatic Peloidal Bioclastic Packstone microfacies **(A)** Sampled from 83.60 m in section **(B)** Sampled from 85.0 m (see Fig. 12) and **(A')** is a closer view of the large phosphate nodule in the bottom right corner of the 83.60 m sample. Within A' you can relict outlines of the matrix and grain constituents. This facies has abundant isotropic organic material and phosphatic mineralization within a poorly sorted carbonate matrix. There is extensive bioturbation with *in situ* phosphate nodules up to 15mm. Echinoid fragments (E) are highly disarticulated and phosphatic nodules (P) commonly infill bivalve fragments (B). Red arrows indicate stratigraphic up.

### 4.2.4 Phosphatic Bioclastic Packstone

The Phosphatic Bioclastic Packstone microfacies is characterized by fossiliferous calcite-cemented packstones with abundant peloidal phosphate grains up to 500 µm in diameter (15-30%) (Fig. 16). The facies is moderately to extensively bioturbated (ichnofabric index 3-5) and has bimodal sorting, disarticulated and macerated thin shelled clams (*Halobia*) (10-45%), echinoid spines (1-5%) and thick shelled bivalves (0-5 %).

The bioclastic texture of this facies consists of *Halobia* that contain no specific orientation and are largely disintegrated from burrowing organisms. Textural changes within are related to P mineralization within the matrix and vary throughout the facies. There is minimal detrital quartz within the bioclastic matrix (1-15%) which mainly consists of aggregate skeletal grains. This facies contains vertical and horizontal oriented calcite-filled fractures. Fractures are filled with fibrous calcite microspar and vertical oriented fractures are crosscut by subsequent stylolitization and horizontal fractures.

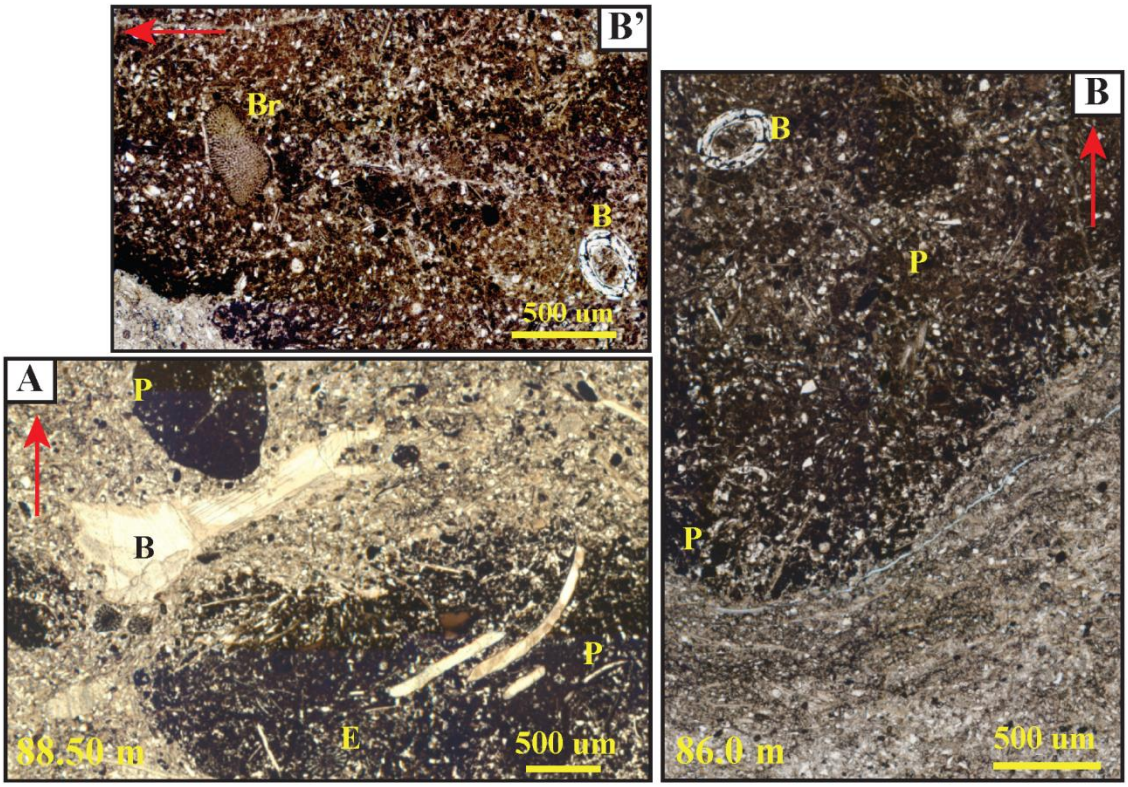


**Fig. 16** Thin section photograph of the Phosphatic Bioclastic Packstone microfacies. **(A)** Sampled from 88.50 m in section **(B)** Sampled from 86.0 m (see Fig. 16). **(B')** Inset within 85.0 m showing P mineralization (brown) around organic material (black) and bryozoan fragment (Br). This facies has abundant isotropic phosphatic mineralization within a poor to bimodal sorted bioclastic matrix. There is extensive bioturbation with *in situ* phosphate nodules (P) up to 15mm in diameter, (E) indicates echinoid spine fragments and (B) indicates bivalve fragments. Red arrows indicate stratigraphic up.

# CHAPTER 5: INTERPRETATION

## 5.1 Revised Sequence Stratigraphy

Previous studies document three depositional sequences within the Shublik Fm. and the adjacent units (supplemental file). The incorporation of Hulm's (1999) and Kelly *et al*.'s (2007) interpretations with recent field observations has led to the interpretation of a fourth depositional sequence, as suggested by Kelly *et al*. (2007) at the Fire Creek outcrop (Fig. 17). A revised sequence stratigraphic interpretation of the Middle-Upper Triassic begins at the base of the Eileen Sandstone, which directly overlies the Ledge Sandstone member of the Ivishak Fm. (Hulm, 1999). Sequence boundaries were picked at sharp contacts where there is an abrupt basinward shift in facies while maximum flooding surfaces were picked at the transition from fining upward to coarsening upward facies. Maximum flooding surfaces were also inferred where the highest gamma ray signature was recognized within each sequence. Sequence boundary interpretations were then propagated from the Fire Creek outcrop exposure using outcrop SGR data to nearby well penetrations and interpreted based on fining upward to coarsening upward patterns in the gamma ray log.

Sequence one generally thins to the west of Fire Creek against the Mikkelsen High, over the Colville High, Fish Creek Platform, and against the Barrow High (Fig. 18). To the southeast of Prudhoe Bay sequence one thickens towards the Fire Creek outcrop to 53.5 m.

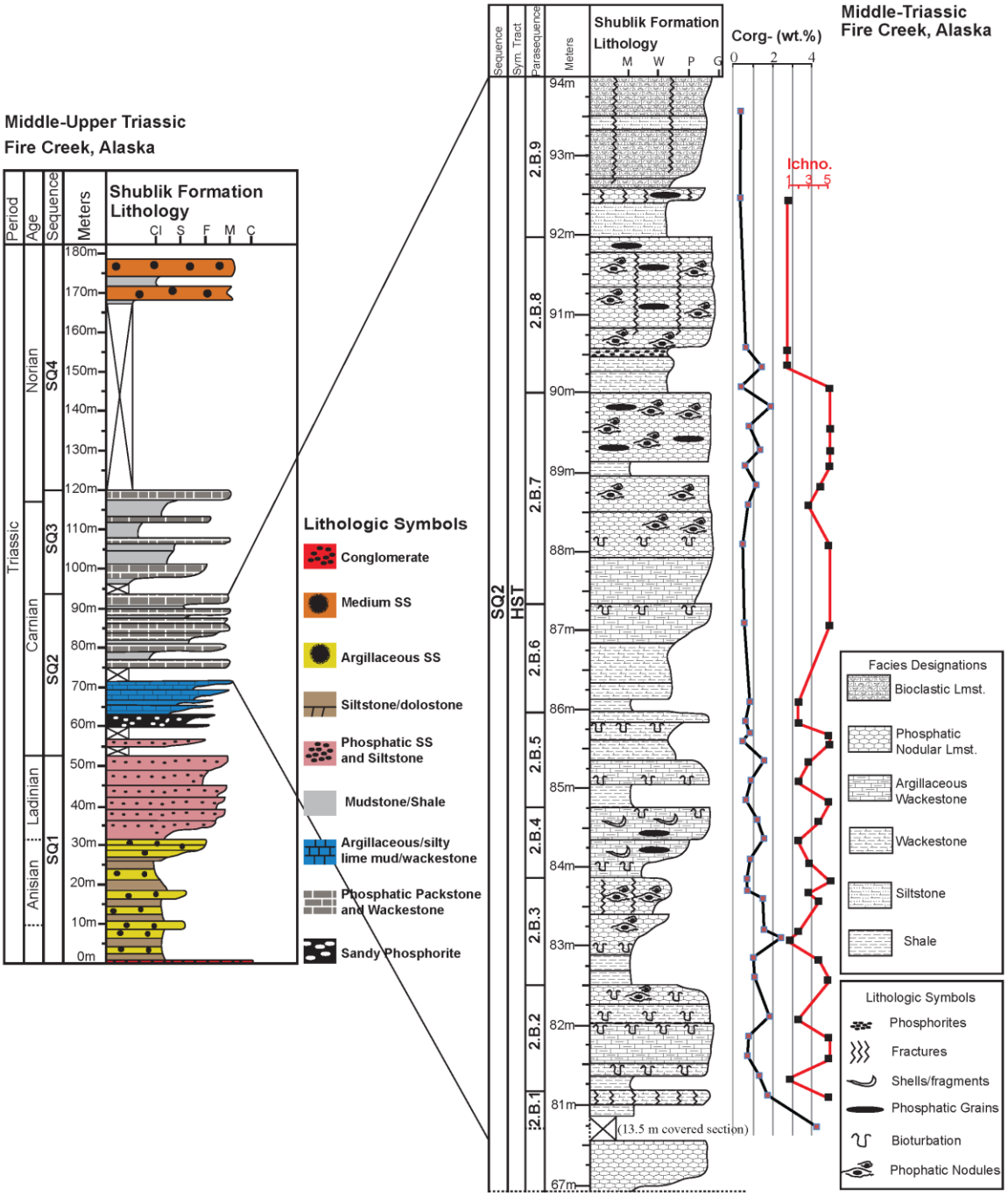


**Fig. 17** Revised lithostratigraphic diagram of the Triassic Shublik Fm. exposed at Fire Creek, northeastern Alaska. The geologic age, lithostratigraphic units, thickness in meters, lithology, and average grain size are indicated. SQ2 was measured with a Jacob's Staff and closely spaced samples were collected during in the summer of 2012. Crossed out sections indicate covered intervals (modified from Kelly *et al*., 2007).

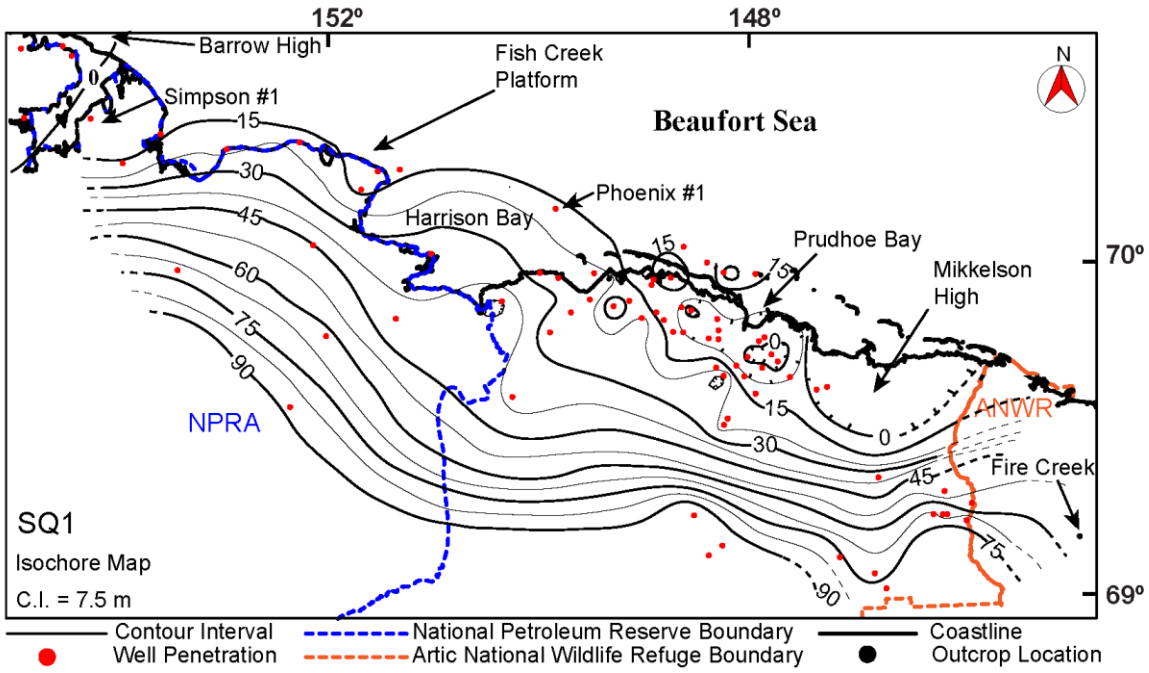


**Fig. 18** Isochore map using well penetrations in northern Alaska of SQ1. Well inclination and stratigraphic dip were not accounted for, while mean log thickness (MLT) was used to delineate contours. Dotted contours indicate areas with no data available to make interpretations.

There is also pronounced thickening within the Harrison Bay embayment fill (~40 m), west of Prudhoe Bay (Fig. 18) and also to the south of Prudhoe Bay. Petrophysical wireline log correlations indicate thickening from proximal positions around Prudhoe Bay (~5-10 m thick) to more distal locations southward, specifically the Bush Fed #1, Kemik #1, and Fin Creek Unit #1 well penetrations with thicknesses of ~90 meters. Provenance for the clastic phosphatic rocks of sequence one is considered to be from the northeast as water depths increase from south–west (Detterman, 1989). The base of the FCS, at the Fire Creek outcrop, is demarcated by a thin conglomerate that marks the basal erosional transgressive lag of sequence one and the uppermost contact with the Ledge Sandstone (Hulm, 1999; Kelly *et al*., 2007). In the Tenneco Phoenix #1 core the base of sequence one is documented at a chert/quartz pebble conglomerate horizon with oxidized

interbedded shales at the top of the Ledge Sandstone (Robison *et al*., 1996; Hulm, 1999). The base of sequence one has yet to have accurate age constraints applied to it and is interpreted to occur during the Smithian Age of the Middle Triassic (Detterman *et al*., 1975).The conglomerate is directly overlain by marginal marine coastal plain tidal bars and re-worked shoreface sands and tidal creeks of the Eileen Sandstone (Robison *et al*., 1996; Hulm, 1999). The FCS transitions into the stratigraphic equivalent Eileen Sandstone to the north and west in the subsurface of northern Alaska until it laps out depositionally near Point Barrow or the "Barrow High" (Parrish *et al*., 2001 a&b). Deposits of the FCS lie at the base of sequence one, which is the uppermost member of the Ivishak Fm. (Detterman *et al*., 1975; Hulm, 1999; Parrish *et al*., 2001 a&b). The FCS was deposited in an inner-shelf environment based on sedimentary features and grain size (Kelly *et al*., 2007; also see Duke *et al*., 1991; Cheel, 1991; Ekdale *et al*., 1984).

The HST within sequence one consists of phosphatic sandstones interbedded with organic fissile silts and shales overlain by bioturbated, phosphatic nodular argillaceous sandstones. The two parasequences within the HST of sequence one shoal upward into winnowed phosphorites that were deposited in a terrigenous dominated, shallow ramp subtidal environment (Hulm, 1999; Kelly *et al*., 2007). The removal of finer-grained sediments, through winnowing processes and redistribution of phosphate nodules, formed phosphorite beds at the crests of the depositional cycles at the Fire Creek exposure (Kelly *et al*., 2007). The phosphorite lag deposits within sequence one indicate current induced winnowing existed on the shelf (Föllmi, 1996). The upper contact of sequence one is defined by fine-grained transgressive facies abruptly overlying a coarse-grained late

highstand facies capping sequence one and is interpreted as a regional flooding surface, thus a sequence boundary.

Kelly *et al*. (2007) interpreted the uppermost contact of their sequence two to be located at 120 m (top Zone B) within the stratigraphic section, whereas results of this study suggest that the uppermost contact of sequence two lies at 94 m (Fig. 17). The difference in interpretation is based on recognition of a flooding surface overlying the massive bioclastic packstone located at 94 m. The abrupt change in lithology from the massive, cliff face-forming, well cemented, interbedded fine-grained sandstones and coquinas to fissile, thin bedded mudstone to wackestones facies indicates a drastic change in depositional environment. This study proposes the breaking out of an additional sequence and subsequent renumbering of the Middle−Upper Triassic deposits in northern Alaska.

Sequence two pinches out against the Mikkelsen High, and thins over the Colville High, Fish Creek Platform, and against the Barrow High (Fig. 19). Sequence two depositionally thins to the south due to sediment starvation in a deeper water setting that was subjected to episodic terrigenous influx due to storm deposition. The sequence is thickest along a linear trend, south of Prudhoe Bay, westward from the Fire Creek outcrop. Basinward thickening of sequence two supports the Kelly (2004) interpretation of carbonate-ramp style deposition where decreased accommodation space during progradation forces terrigenous influxes further basinward (Burchette & Wright, 1992). Temporal fluctuations in carbonate production, linked to high-frequency changes in sea

level, allowed shoaling cycles to accumulate on the prograding flank (Kendall & Schlager, 1981).

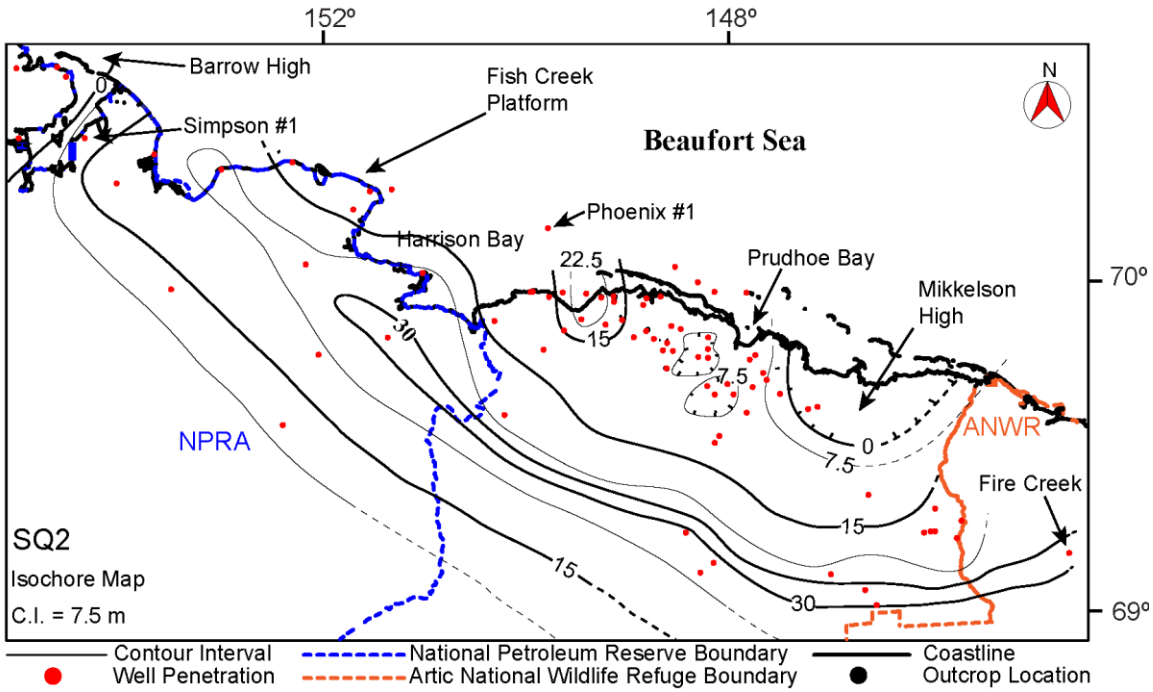


**Fig. 19** Isochore map using well penetrations in northern Alaska of SQ2. Well inclination and stratigraphic dip were not accounted for, while mean log thickness (MLT) was used to delineate contours. Dotted contours indicate areas with no data available to make interpretations.

The lowermost boundary between sequence one and two can be correlated west to nearby industry wells by recognizing the abrupt positive shift in gamma-ray readings (Fig. 20, Fig. 23). A depositional shift from coarse-grained proximal deposits to fine-grained distal sediments within the TST of sequence two is documented at the outcrop and interpreted in the well logs. The TST of sequence two consists of nodular argillaceous mudstones overlain by burrowed phosphatic nodular wackestones to packstones with wavy bedding planes (0.5 m thick beds). The TST is interpreted to have been deposited in the mid–outer ramp depositional environment below storm wave base but subjected to bottom water currents (Kelly *et al.*, 2007) and storm deposition with

sharped-based fining upward beds documented at the outcrop. There is a prominent positive shift in the gamma-ray profile and decreased detrital input at 77 m that is interpreted as the mfs of sequence two. The predominantly carbonate deposition overlying the mfs of sequence two forms a prominent cliff face at the Fire Creek outcrop. The interbedded coarse-grained phosphatic, wackestones to packstones with $C_{org}$ rich phosphatic siltstones to mudstones is capped by coquina beds at 94 m. The oolitic and coquina beds transition to glaucontic sandstones in more proximal areas, respectively (Hulm, 1999; Kelly *et al*., 2007).

A positive shift in gamma-ray profile above 94 m is recognized throughout the basin due to the shift in coarse-grained carbonate to sandstone proximal facies overlain by distally deposited fissile $C_{org}$ rich mudstones. Initial transgression over the coarse-grained burrowed bioclastic packstones deposited $C_{org}$ rich mudstone to wackestone facies that currently lies in a covered section at the Fire Creek outcrop. The $C_{org}$ rich mudstone to wackestone facies were interpreted as fissile, nodular, argillaceous mudstone facies by Kelly *et al*. (2007), and represent the initial transgression of sequence three. Thus, this project subdivide sequence two of Kelly *et al*. (2007) (supplemental file) into two separate sequences for a total of four depositional sequences based on stratal stacking patterns of transgressive to regressive events (Fig. 17). An overview outcrop photo indicates the renumbering and breaking-out of the additional sequence (Fig. 21).

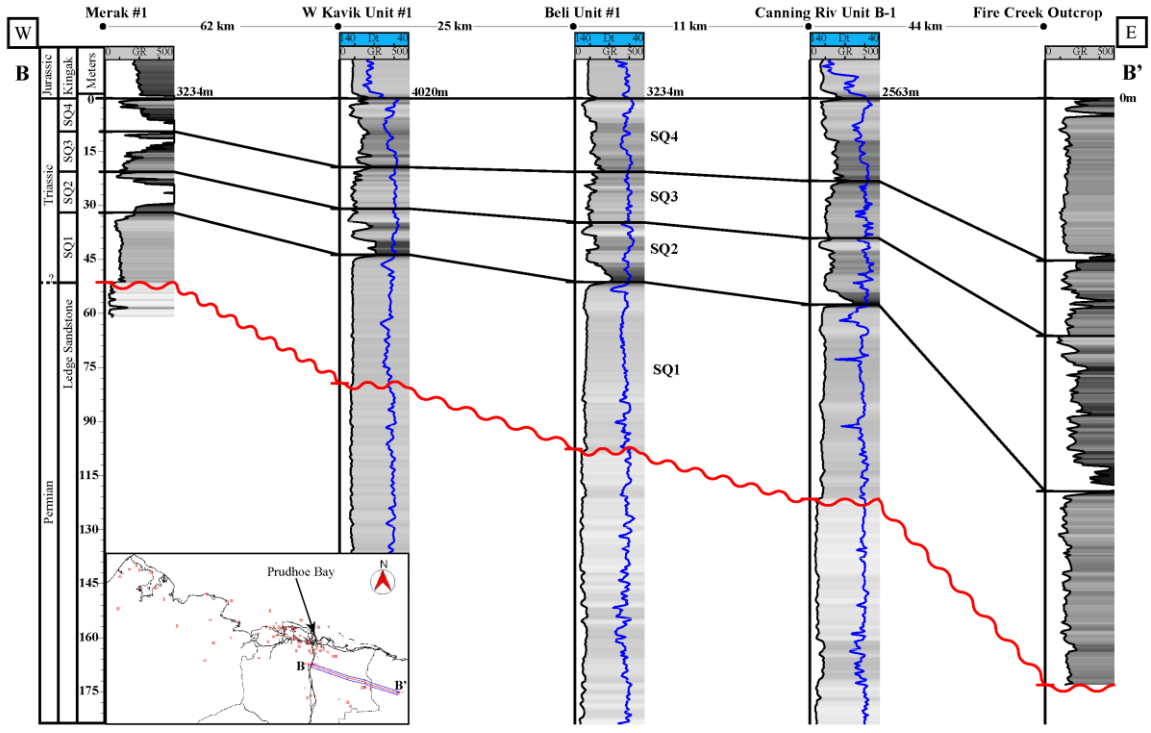


**Fig. 20** Outcrop to subsurface correlation from the east to west. Correlation from the Merak #1 well penetration to spectral gamma-ray data (SGR) measurements documented at the Fire Creek outcrop. Gamma-ray (GR) log profile is from 0-400 API where darker colored shading indicates higher GR. The blue log profile is the sonic log scaled from 140 µs/m on the left to 40 µs/m on the right. The wavy red correlation line indicates the base of sequence one or the top of the Ledge Sandstone, while the straight black lines indicate the tops associated with the four sequences identified. The correlation line is hung from the top of the Sag River Sandstone.

From the Fire Creek exposure west into the subsurface, sequence three is fairly constant in thickness (~15-20 m) but thickens over the Fish Creek Platform (~30 m) and within the north central part of NPRA (~30 m) (Fig. 22, Fig. 24–25).The phosphatic, $C_{org}$ rich rocks within sequence three are interpreted to be deposited in a distal outer-ramp setting,

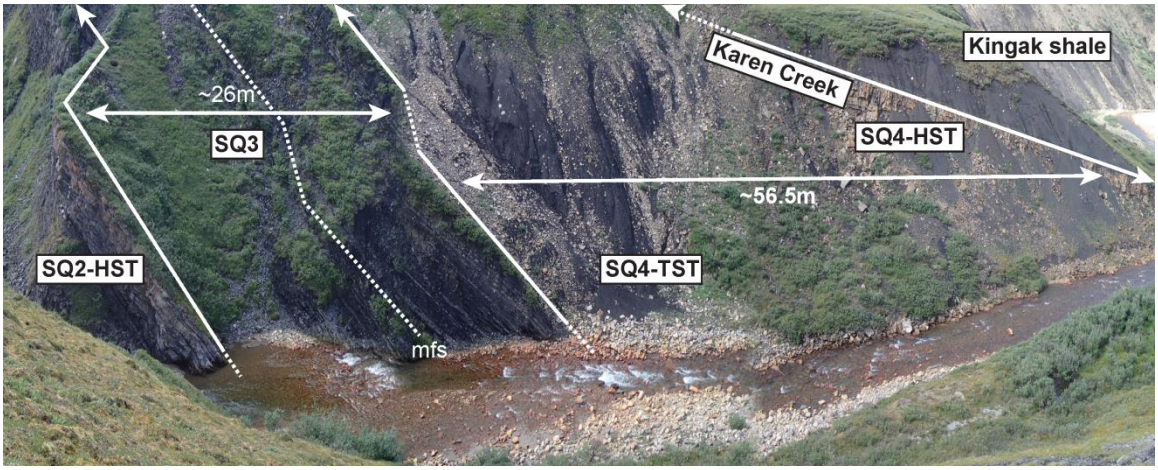


**Fig. 21** Outcrop photograph of upper Shublik Fm. and Karen Creek Sandstone. Dividing sequence two in to two separate sequences required the renumbering of Upper–Middle Triassic deposits in northern Alaska.

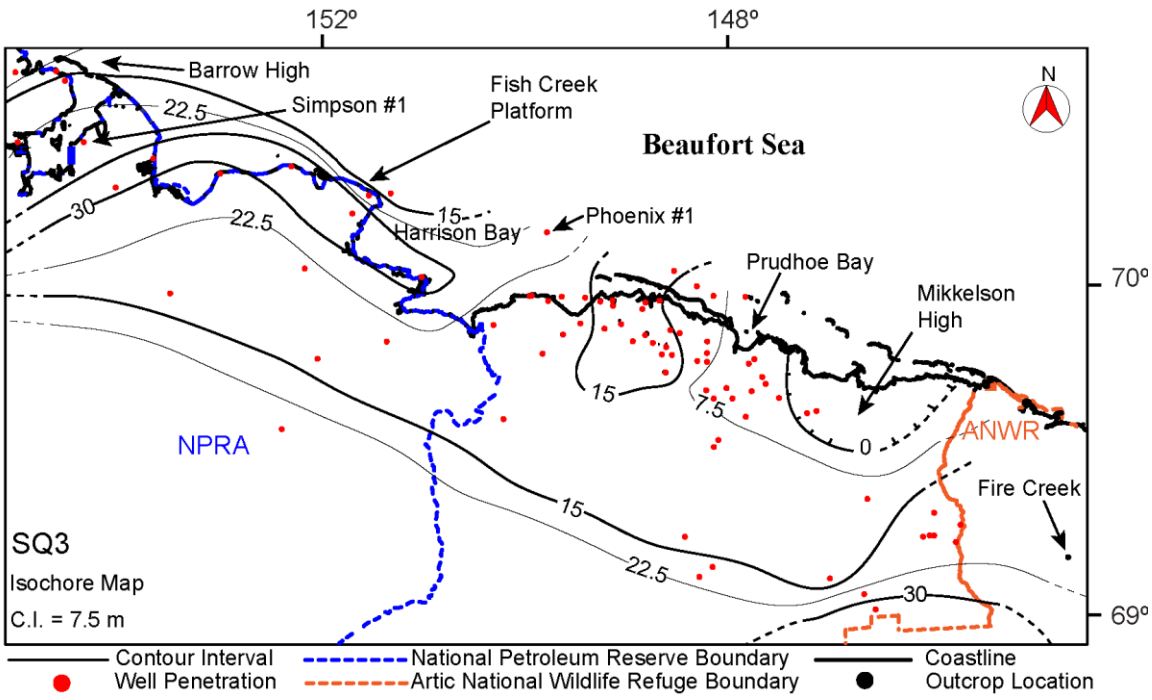


**Fig. 22** Isochore map using well penetrations in northern Alaska of SQ3. Well inclination and stratigraphic dip were not accounted for, while mean log thickness (MLT) was used to delineate contours. Dotted contours indicate areas with no data available to make interpretations.

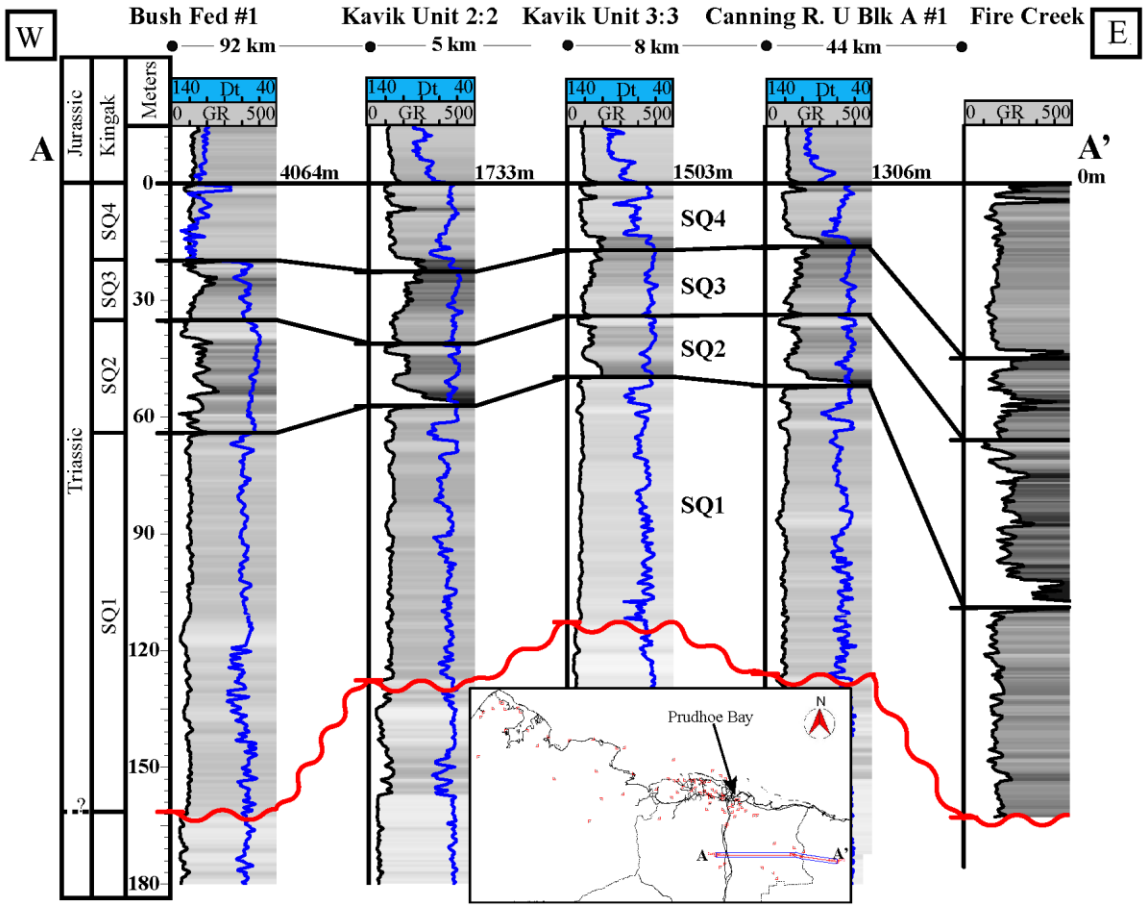


**Fig. 23** Outcrop to subsurface correlation from the east to west. Correlation from the Bush Federal #1 well penetration to spectral gamma-ray data (SGR) measurements documented at the Fire Creek outcrop. Gamma-ray (GR) log profile is from 0-400 API where darker colored shading indicates higher GR. The blue log profile is the sonic log scaled from 140 µs/m on the left to 40 µs/m on the right. The wavy red correlation line indicates the base of sequence one or the top of the Ledge Sandstone, while the straight black lines indicate the tops associated with the four sequences identified. The correlation line is hung from the top of the Sag River Sandstone.

based on thinly bedded (1-15 cm) mudstones and high $C_{org}$ concentrations (anoxic bottom waters). Sequence three is comprised of two progradational parasequences (94-107 m and 107-120 m) with two stratigraphic intervals indicating low oxygen bottom water conditions during initial deepening and associated high bioproductivity which resulted in high $C_{org}$ concentrations. The dysoxic conditions were most likely due to high bio-

productivity at the surface influencing a strong OMZ and phosphogenesis at the sediment-water interface. There are abundant phosphatized marine invertebrates on nearly every parting surface along bedding planes.

There is an increased U content that resulted in a positive shift in the gamma-ray profile at ~109 m and this is interpreted as a condensed section which represents the mfs of sequence three. This peak can be correlated regionally using wire-line well logs

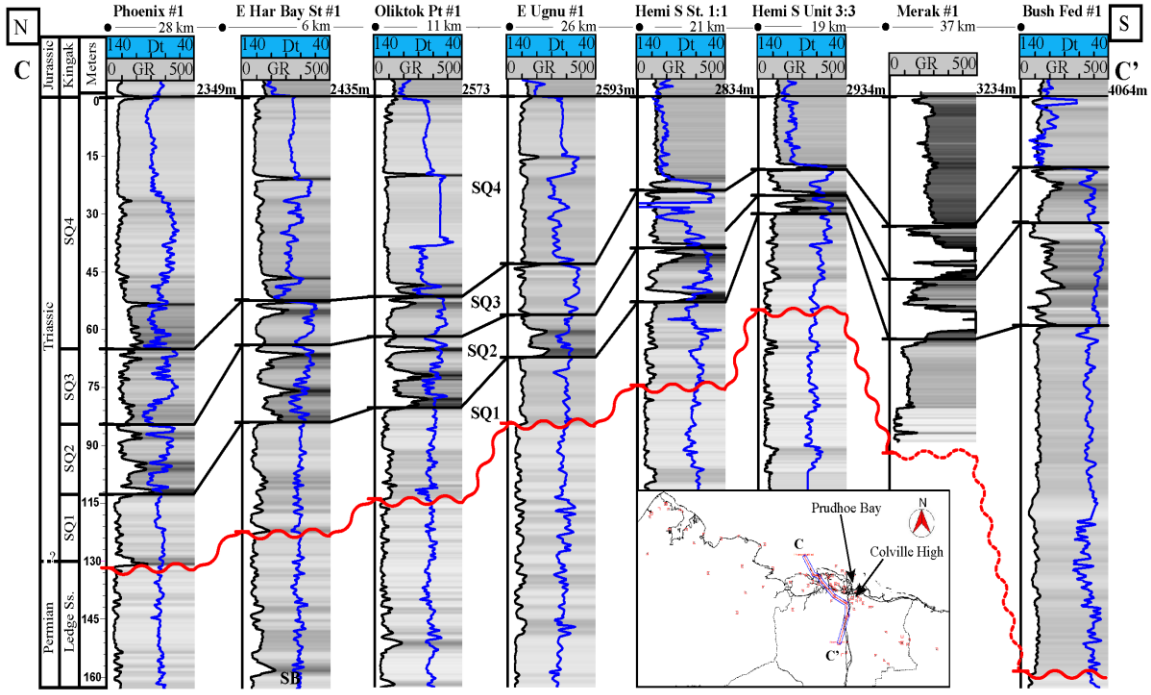


**Fig. 24** North to south well correlation from the Phoenix #1 to the Bush Federal #1 subsurface penetrations. Gamma-ray (GR) log profile is from 0-500 API where darker colored shading indicates higher GR. The blue log profile is the sonic log scaled from 140 µs/m on the left to 40 µs/m on the right. The wavy red correlation line indicates the base of sequence one or the top of the Ledge Sandstone, while the straight black lines indicate the tops associated with the four sequences identified. The correlation line is hung from the top of the Sag River Sandstone.

and is interpreted as the mfs due to the lack of terrigenous input and high-gamma-ray signature. Sequence three is relatively thin and finer grained in comparison to the adjacent sequences. Thin bedded argillaceous carbonates interbedded with $C_{org}$-rich

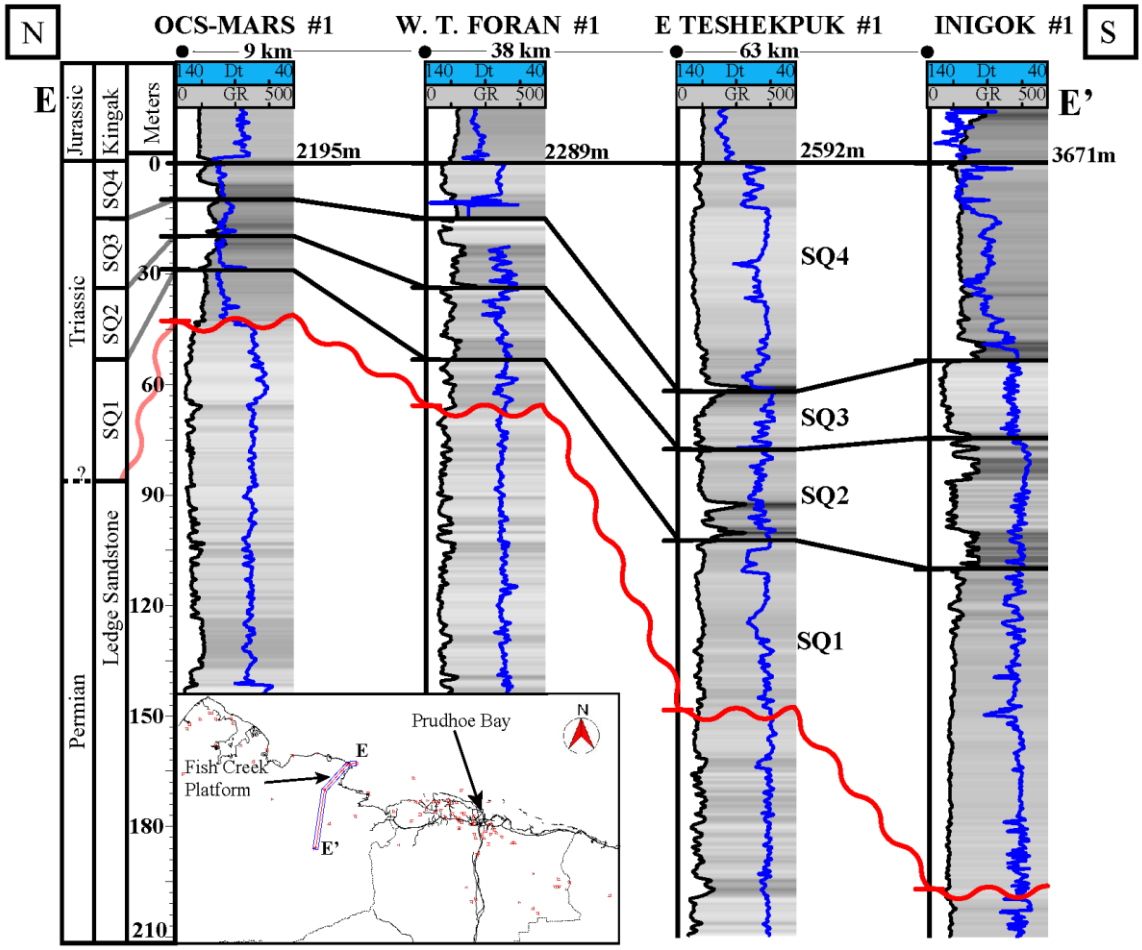


**Fig. 25** North to south well correlation from the offshore Mars #1 to the Bush Inigok #1 subsurface penetrations. Gamma-ray (GR) log profile is from 0-500 API where darker colored shading indicates higher GR. The blue log profile is the sonic log scaled from 140 µs/m on the left to 40 µs/m on the right. The wavy red correlation line indicates the base of sequence one or the top of the Ledge Sandstone, while the straight black lines indicate the tops associated with the four sequences identified. The correlation line is hung from the top of the Sag River Sandstone.

mudstones indicate a deeper water setting. Meter-scale internal scouring surfaces (Fig. 8) within coarse-grained facies suggest bottom current-induced reworking during relative falls in sea level. Thickening over regional highs suggests carbonate production was able to keep pace within the overall transgression, although core evidence wasn't available for this study.

Sequence four was previously interpreted to be the third depositional sequence incorporating the Shublik Fm. and the Karen Creek Sandstone, (Kelly, 2004; Kelly *et al*., 2007) but subdivision of sequence three necessitated renumbering (Fig. 17). Kelly *et al*. (2007) documented the change in grain size at the lowermost boundary of sequence four at 120 m and they also interpreted condensed phosphorites throughout the TST to indicate hiatus periods resulting from an overall transgression. The isochore map (Fig. 26) indicates a depositional thick in the north central part of NPRA (~180m), within the Harrison Bay embayment fill (~60 m), and at Fire Creek (45 m, although unaccounted structural thickening has occurred). Well penetrations in the north central part of NPRA are located in the northern part of the Ikpikpuk Basin and depositional thickening could be related to local subsidence (Fig. 27). In more proximal settings, at the Phoenix #1 well, the TST of sequence four is a highly bioturbated, calcareous mudstone with internal scour surfaces and abundant fossil fragments (Hulm, 1999). The TST at the Fire Creek outcrop lies largely within a thick covered interval that has likely been influenced by tectonic forces. The Sag River Sandstone, in more proximal locations, is a heavily burrowed, fossiliferous, fine-grained sandstone with calcite cement indicative of lower shoreface deposition within three backstepping parasequences (Hulm, 1999). Barnes

(1987) interpreted Sag River Sandstone deposition to have taken place during a regionally significant marine regression on the North Slope.

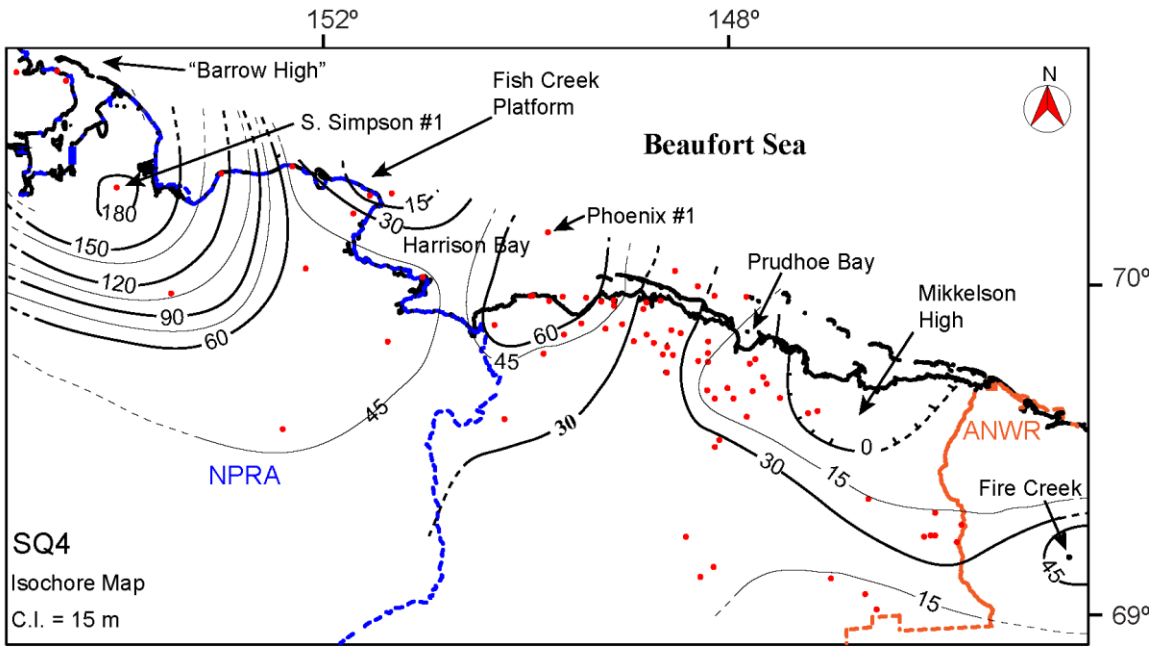


**Fig. 26** Isochore map using well penetrations in northern Alaska of SQ4. Well inclination and stratigraphic dip were not accounted for, while mean log thickness (MLT) was used to delineate contours. Dotted contours indicate areas with no data available to make interpretations.

The uppermost sequence boundary within the Upper Triassic in northeastern Alaska is located at the top of the Karen Creek Sandstone (Sag River Sandstone equivalent) which is overlain by a thick succession of papery black shale comprising the Kingak Fm. (Hulm, 1999; Kelly *et al*., 2007). The transition from Triassic–Jurassic aged rocks occurs at this boundary based on early Jurassic fossil evidence found in the lower Kingak Fm. (Detterman *et al*., 1975).

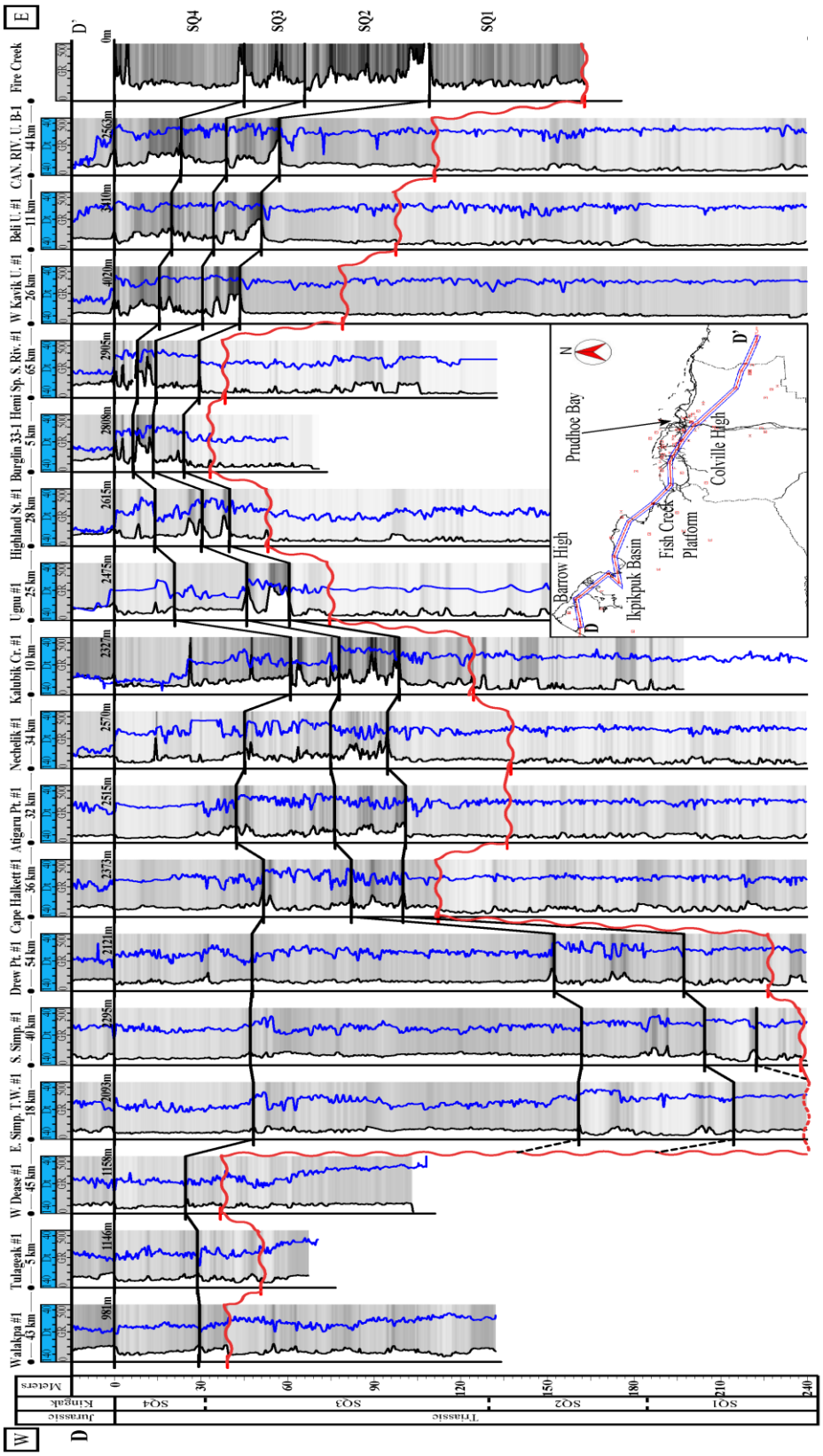


**Fig. 27** West to east well correlation from the Walakpa #1 well to the Fire Creek outcrop exposure. Gamma-ray (GR) log profile is from 0-500 API where darker colored shading indicates higher GR. The blue log profile is the sonic log scaled from 140 µs/m on the left to 40 µs/m on the right. The wavy red correlation line indicates the base of sequence one or the top of the Ledge Sandstone, while the straight black lines indicate the tops associated with the four sequences identified. The correlation line is hung from the top of the Sag River Sandstone.

## 5.2 Geochemical Proxy Trends

The Kelly (2004) major-element dataset was integrated with data from this study to interpret trends in paleoredox, primary production and detrital proxies. Conditions such as upwelling or terrigenous input increase nutrient availability to surface waters, thus increasing the biogenic fraction of marine sedimentation with increased planktonic debris (Piper, 1994). A fraction of bio-available trace nutrients utilized by phytoplankton (e.g. Cu, Ba, Zn and Ni) can become entrained into the sediment along with the organic detritus (Piper & Calvert, 2009) allowing interpretation of bio-productivity. The relative minor–major elemental concentrations of terrigenous material (e.g. Al, Si, K and Ti) record another environmental signal that influences a primary control on $C_{org}$ concentration by governing dilution of the organic material by detrital sediments. These trends are compared with $C_{org}$ concentrations and interpretations are made about Middle−Upper Triassic paleoceanography during deposition of the Shublik Fm. within a sequence stratigraphic context.

Siliciclastic deposition within the Shublik Fm. is pronounced within sequence one and during highstand deposition in the overlying sequences. Kelly *et al*. (2007) interpret that siliciclastic deposition took place in a nearshore or an inner shelf environment. The terrigenous proxies (Fig. 28), along with outcrop observations indicate the primary sediment input during sequence one was detrital quartz (~50–75% $SiO_2$) deposition

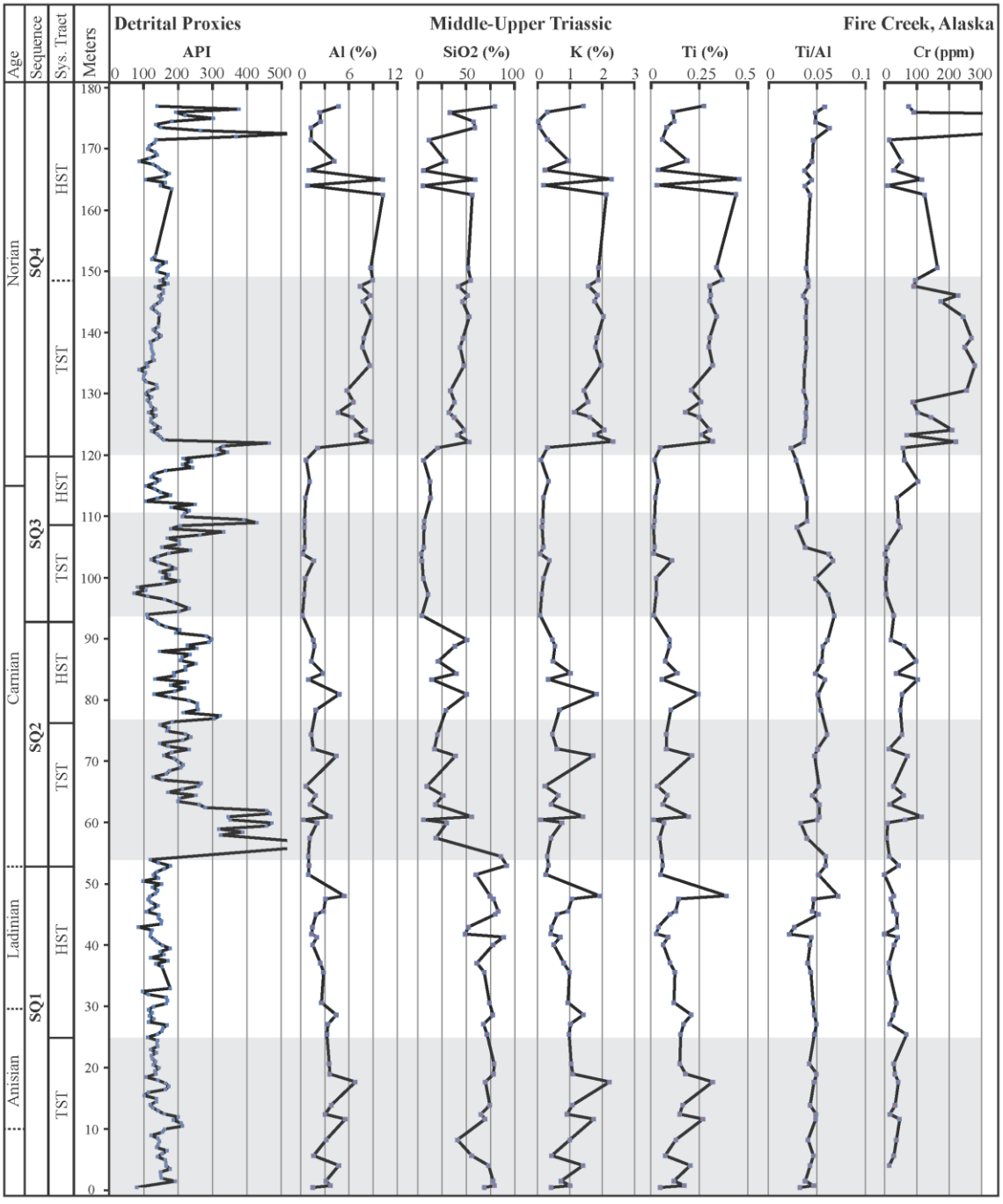


**Fig. 28** Spectral gamma-ray, Al, $SiO_2$, K, Ti, Ti/Al, and Cr data from Kelly (2004) dataset through entire Fire Creek interval. Spectral gamma-ray data converted to American Petroleum Institute gamma-ray units (API) using the following equation API =16*K(%) + 8*U(ppm)+ 4*Th(ppm). Shading reflects the TST within each sequence.

(Kelly, 2004; Kelly *et al.*, 2007). $C_{org}$ levels generally remain below 1 wt. % throughout sequence one with two excursions at 17.5 m (1.2 wt. %) and 37.5 m (1.4 wt. %) (Fig. 28). The lowermost pulse correlates with higher detrital input, specifically K and Ti enrichment where the uppermost pulse does not correlate with detrital, paleoredox or primary production proxies.

There is a distinct shift in the geochemical proxies between sequence one and two at 53.5m which indicates a reduction in detrital input and an increase in primary productivity (Fig. 29) with periodic anoxic bottom waters. Overall these geochemical proxies indicate an abrupt transgressive event where flooding of the HST of sequence one inhibited terrigenous deposition onto the shelf and brought nutrient-rich waters, increasing productivity and thus deposition of $C_{org}$. Trends in trace element proxies indicate primary production and redox conditions co-varied with $C_{org}$ concentrations, except where bioturbation masks the signature. Based on these features it is inferred that sequence two was deposited on a carbonate ramp, specifically within a middle-ramp environment, which agrees with previous interpretations (Kelly *et al*., 2007).

The lower TST (53.5−57 m) of sequence two contains abundant $SiO_2$ while K, Ti and Cr remain near background levels (Fig. 28). Immediately overlying this interval there is a positive shift in the gamma-ray count, increased $C_{org}$ concentration and peaks in U, Mo, V, Ni and P concentrations (Fig. 30). Detrital, bioproductivity and paleoredox trends sink to background levels around 77 m but there is a positive shift in Mo values.

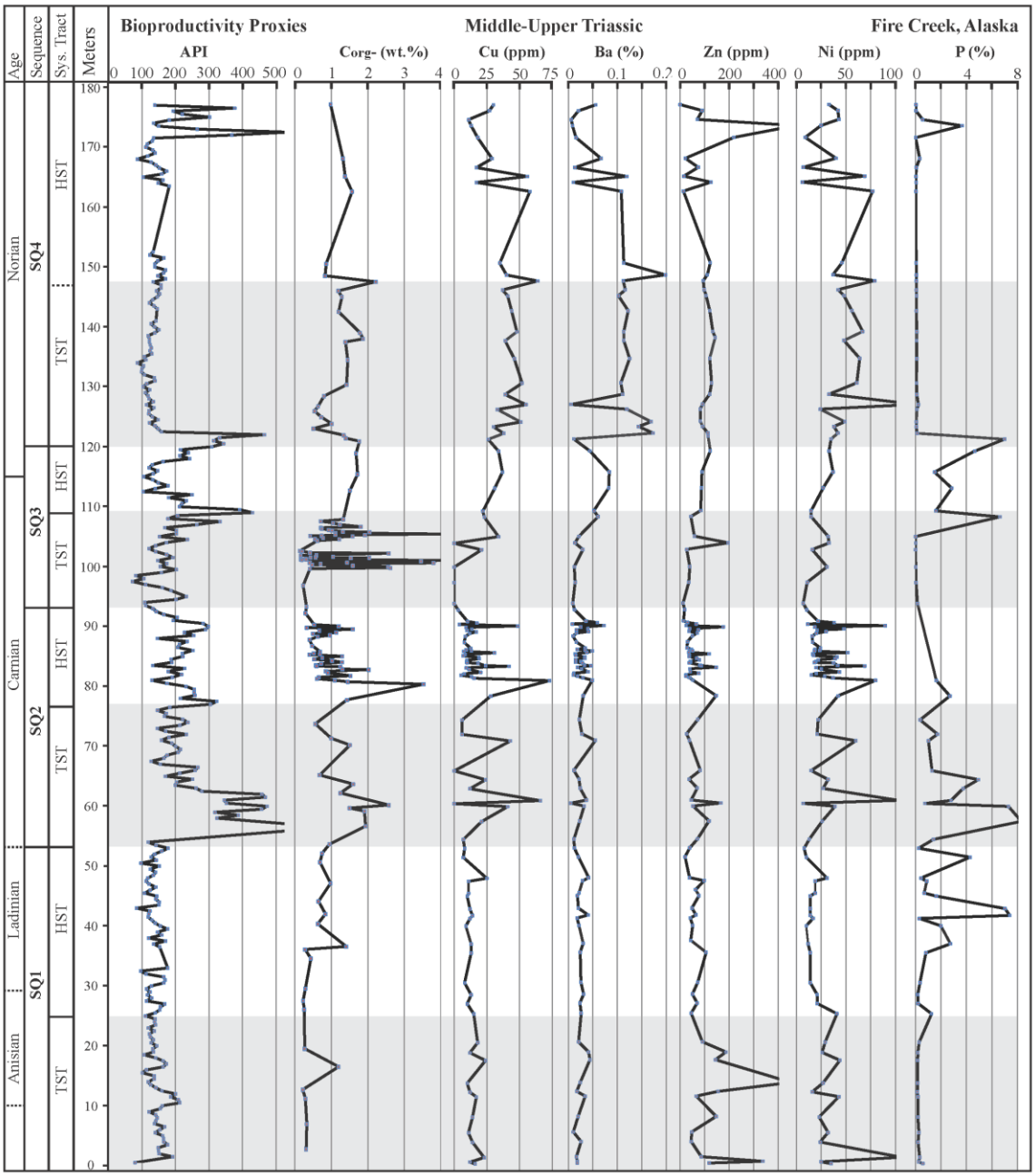


**Fig. 29** Bioproductivity proxies. $C_{org}$ data from 0-81 m, 93-100 m & 108-175 m from Kelly (2004) dataset, while Corg measurements from 81-93 m & 100-108 m are from this study. Cu, Ba, Zn, Ni trace element measurements from 0-81 m and 93-175 m are from Kelly (2004) dataset, while 81-93 m is from this study. P measurements are from Kelly (2004) dataset through entire Fire Creek interval. Spectral gamma-ray data (Kelly, 2004) converted to American Petroleum Institute gamma-ray units (API) using the following equation API =16*K(%) + 8*U(ppm)+ 4*Th (ppm). Shading reflects the TST within each sequence.

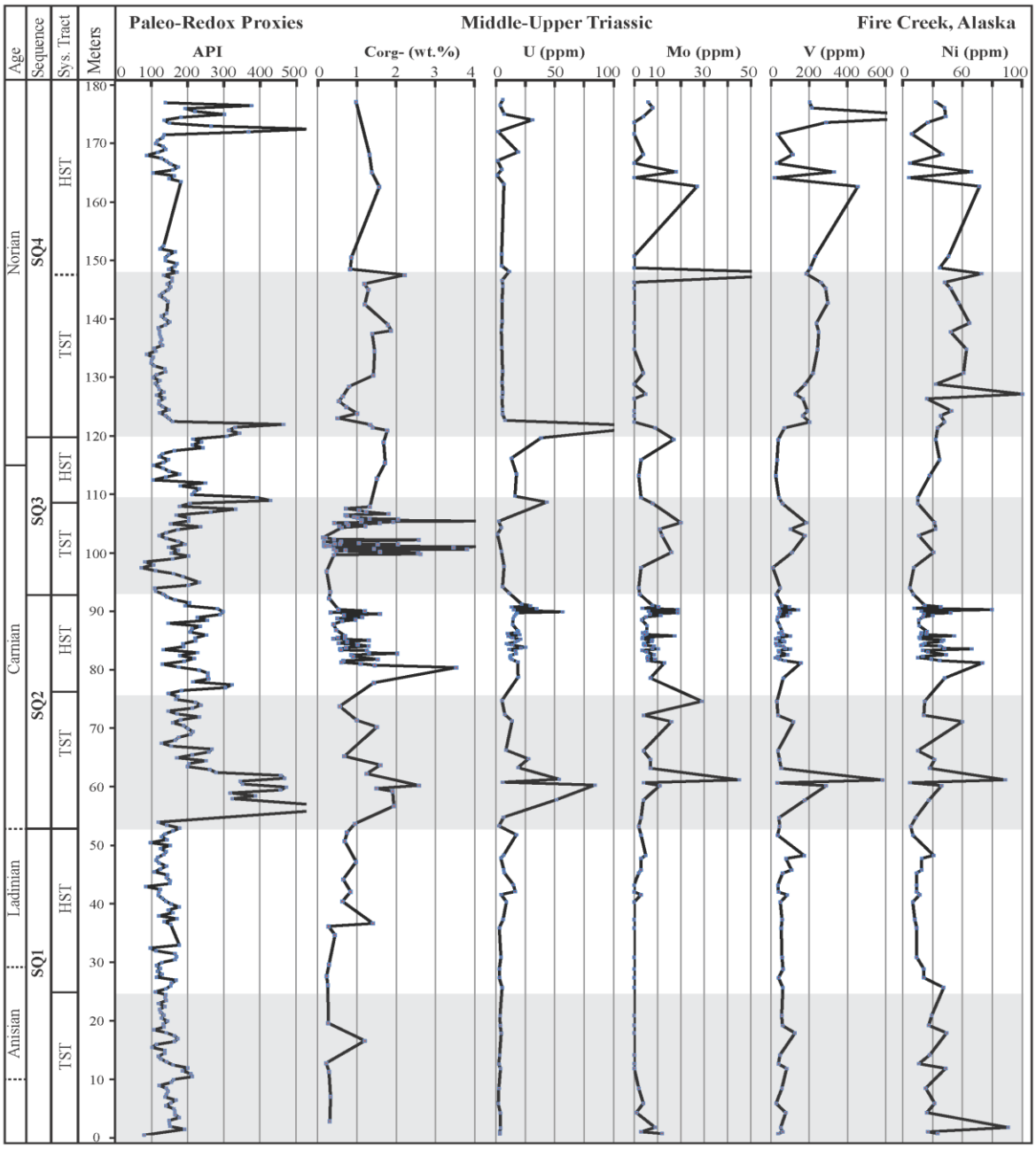


**Fig. 30** Paleredox proxies. $C_{org}$ data from 0-81 m, 93-100 m & 108-175 m from Kelly (2004) dataset, while Corg measurements from 81-93 m & 100-108 m are from this study. U, Mo, V & Ni trace element measurements from 0-81 m and 93-175 m are from Kelly (2004) dataset, while 81-93 m is from this study. Spectral gamma-ray data (Kelly, 2004) converted to American Petroleum Institute gamma-ray units (API) using the following equation API =16*K(%) + 8*U(ppm)+ 4*Th(ppm). Shading reflects the TST within each sequence.

Above 77 meters, within the lower HST, there is a peak in $C_{org}$ concentration that correlates with positive shifts in bioproductivity and detrital proxies.

The HST of sequence two (Fig. 17) was sampled in detail to highlight high-frequency changes in primary production and preservation of $C_{org}$, using elemental proxies within a stratigraphic framework. The elemental proxies are displayed in two chemostratigraphic profiles (paleoredox, Fig. 31 and productivity, Fig. 32) to distinguish trends in elemental enrichment with relation to the ichnofabric index documented from thin-section analyses. The U proxy shows a strong correlation with API units and $C_{org}$ concentration within the HST. Enrichment of U, Mo, V and Ni show similar trends and co-vary with $C_{org}$ values (Fig. 32). The ichnofabric profile indicates increased bioturbation during periods of perceived oxic-conditions. During storm influenced deposition small quantities of dissolved oxygen can be carried onto the shelf promoting bioturbation while still preserving $C_{org}$ (Algeo & Maynard, 2008). The paleoredox sensitive trace element concentrations show decreased concentrations in samples where high ichnofabric indices are observed. Between 89 and 90 m, increased bioturbation indicates a seemingly oxic environment with nodular phosphatic facies that masks the interbedded finer grained lithology (Fig. 32). However, the paleoredox proxies indicate episodic pulses of anoxia shown by co-variation in U, Mo, V, Ni and $C_{org}$ (Fig. 32).

The increased concentration in bio-productivity proxies, indicative of high primary production (Tribovillard *et al.*, 2006), co-varies with paleoredox proxies and $C_{org}$ enrichment. The bio-productivity proxies, plotted within the HST of sequence two,

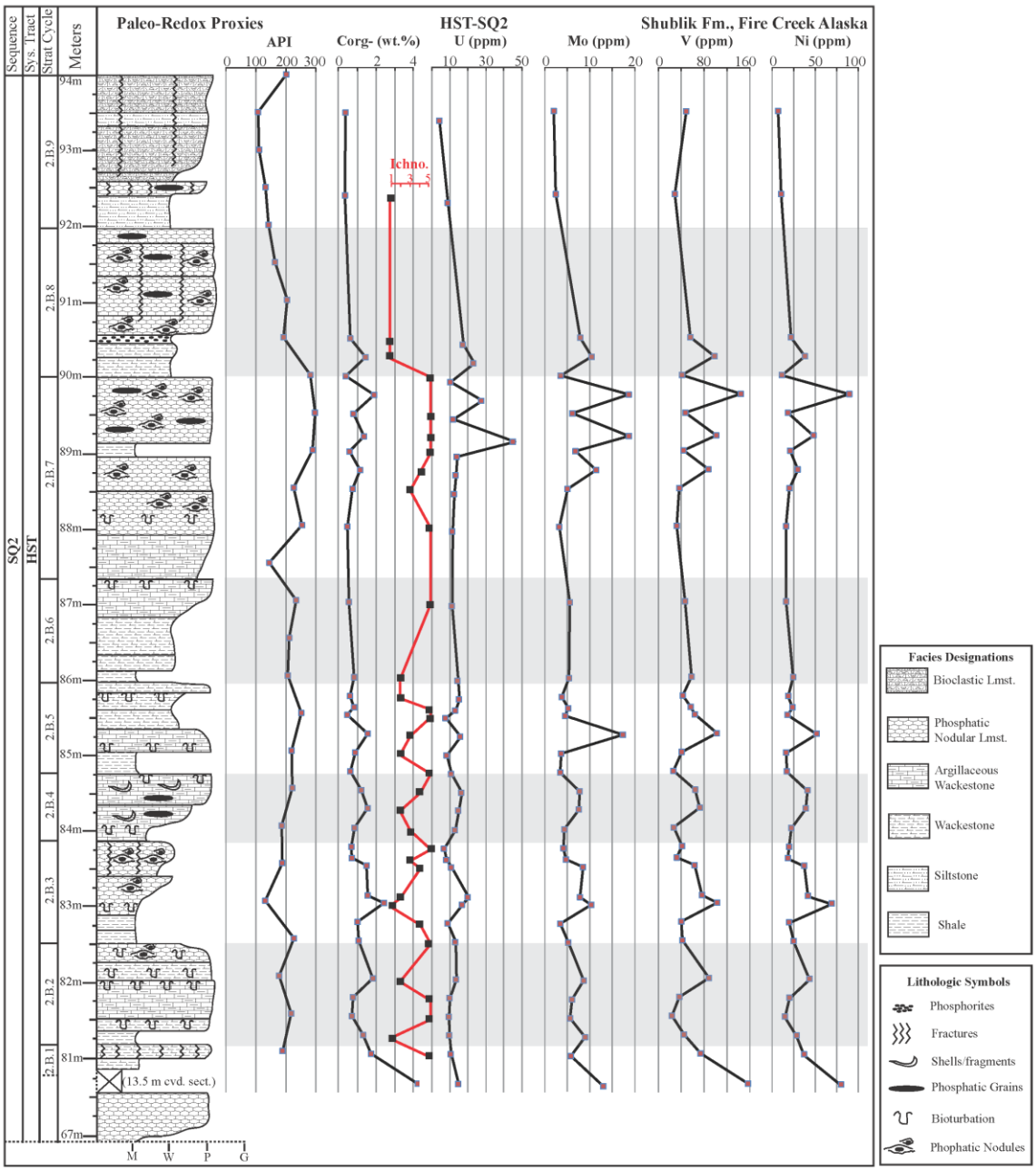


**Fig. 31** Paleoredox proxies within the HST of SQ2. Spectral gamma-ray data (Kelly, 2004) converted to American Petroleum Institute gamma-ray units using the following equation API =16*K(%) + 8*U(ppm)+ 4*Th(ppm). Corg (wt. %) measured on LECO carbon analyzer. U, V, Mo and Ni concentrations (ppm) measured utilizing PANalytical's PROTrace trace element standard suite on a (WD) XRF. Red line indicates Ichnofabric index (Droser & Bottjer, 1986) and shading reflects alternating depositional cycles and is meant to help visualize trends, not infer about cycle deposition or type.

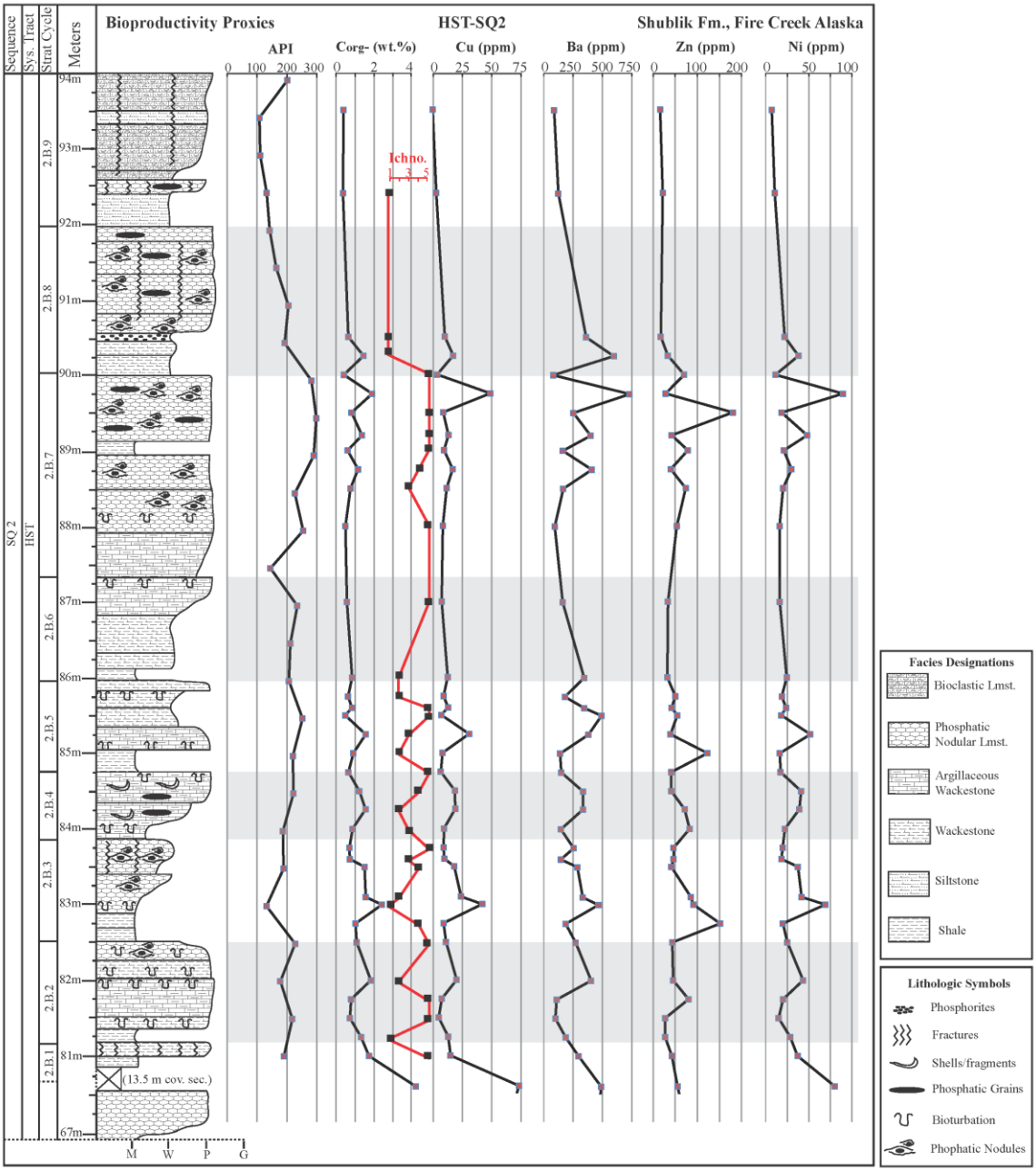


**Fig. 32** Bioproductivity proxies within the HST of SQ2. Spectral gamma-ray data (Kelly, 2004) converted to American Petroleum Institute gamma-ray units using the following equation API =16*K(%) + 8*U(ppm)+ 4*Th(ppm). Corg (wt. %) measured on LECO analyses device. Cu, Ba, Zn and Ni concentrations (ppm) measured utilizing PANalytical's PROTrace trace element standard suite on a (WD) XRF. Red line indicates ichnofabrics (Droser & Bottjer, 1986) and shading reflects depositional cycles.

indicate the same relationship between increased Cu, Ba, Zn and Ni and the $C_{org}$ profile, which also shows an inverse relationship with the ichnofabric indices. Terrigenous pulses occur at 81 m, 84.5 m and 90 m with the most abundant at the top of the HST. This uppermost HST of sequence two contains thin (10-15 cm) fine-grained sandstones interbedded with coquinas capping the sequence. A positive shift in gamma-ray in the upper HST of sequence two, correlates with high bioproductivity, increased paleoredox proxies and a pulse of $SiO_2$ concentrations (Figs. 28-30). Primary production trends within the individual stratigraphic cycles show a general increase during flooding events and subsequent decrease to background levels during progradation when the upwelling is interpreted to move further basinward. The paleoredox and primary-production proxies show an inverse correlation with the ichnofabric indices which is consistent with a productivity–anoxia feedback loop (e.g. Rimmer *et al*., 2004).

Proxy data recorded within sequence three facies indicate increased $C_{org}$ preservation which co-varies with redox-sensitive trace element enrichment, increased bioproductivity (Fig. 29) and low detrital input. The TST contains the highest concentration of $C_{org}$ at the Fire Creek outcrop. The high $C_{org}$ concentrations correlate with positive shifts in paleoredox and bioproductivity trends while detrital trends are at background levels. At the Fire Creek exposure the lowermost spike in gamma-ray readings (~450 API) can be correlated west across northern Alaska and it co-varies with a positive shift in the U and P profile. This peak is located between the TST and the HST of sequence three and is interpreted as the mfs at 109 m. The HST shows subtle increases

in $C_{org}$ that co-vary with increasing bioproductivity trends and background levels for paleoredox and detrital proxies (Figs. 28-30).

The second peak in gamma-ray readings is at 121.5 m within the lower TST of sequence four and it can also be correlated across northern Alaska. This peak co-varies with U and P enrichments within the interval at the base of sequence four. Paleoredox and bioproductivity proxies remain near background levels throughout the TST until ~148 m where there is a positive shift and the proxies show similar trends. Detrital proxies remain near background levels within this interval which is interpreted to be the mfs of sequence four. The lower HST lies within a covered interval while trends within the upper HST indicate major influxes of terrigenous sediment with peaks in $SiO_2$, K, Ti and Cr (168.5 m and ~175 m). The bioproductivity and paleoredox trends co-vary with the terrigenous influxes while the U and $C_{org}$ show weaker correlations. There is a strong positive shift in gamma-ray readings at ~172 m that correlates strongly with high Cr, V, Zn and P enrichments, whereas U concentrations are low. Concentrations of Cr are highest within sequence four with a peak of 2,360 ppm within the Karen Creek Sandstone. The abnormally high peak in Cr corresponds with peaks in V, P and Zn which could be related to the marked enrichment in phosphorites (Tribovillard *et al*., 2006) or a terrigenous source during late highstand deposition as suggested by Kelly *et al*. (2007).

## 5.3 Microfacies Implications

High frequency sequence stratigraphic interpretations of the carbonate, phosphatic progradational facies association developed in this study are combined with previous studies (Hulm, 1999; Kelly *et al*., 2007) to evaluate the Middle−Upper Triassic paleoenvironment, specifically controls that influence the vertical stacking patterns of organic mudstone to bioclastic packstone facies within the Shublik Fm. Petrographic analyses of the silty/argillaceous limestone and phosphatic wackestone/packstone facies deposits indicate predominantly phosphatic wackestones to packstones with phosphatized bivalve, brachiopod shells and phosphatic nodules. Matrix and intraclasts are predominantly bioclastic grains and detrital silt. The high-frequency petrographic investigation of the HST indicates increased burrowing activity when the OMZ had shifted down-dip and oxygen rich waters were present at more proximal positions within the coarsening-upward stratigraphic cycles (Fig. 31-32). Periodic storm deposition was documented at the outcrop where fining-upward cycles are interbedded within the overall coarsening-upward HST of sequence two.

The phosphatic bioclastic organic mudstones commonly represent the basal transgressive beds within the mid- to outer-ramp depositional facies. The organic mudstone to wackestones facies are heavily degraded through bio-erosional processes possibly from clionid sponges, endolithic algae, and echinoids. The bio-erosion produced silt-sized angular clasts and peloids that contribute to the calcareous sediment present on the sea floor (Flügel, 2004). They are typically overlain by burrowed nodular wackestones to packstones capping the individual stratigraphic cycles. Nodule formation

is attributed to in-situ diagenetic replacement of calcite, and often infill molds of marine invertebrate fossils. Nodules range in size from 1 mm−15 cm in diameter and are composed primarily of carbonate fluorapatite as described by Detterman (1970a). Phosphate particles appear dark brown to isotropic under magnification and typically replace matrix, cement and constituent grains. Changes in depositional facies were observed through changes in lithofacies, ichnofabrics and geochemical signatures. The HST of sequence two contains nine coarsening-upward progradational carbonate dominated parasequences deposited within an inner-ramp environment subjected to storm-related influences.

A high frequency sequence stratigraphic approach was used in this study to detail the parasequence stacking patterns in the HST of sequence two within the Shublik Fm. The sedimentary features recorded indicate a complex succession of stratigraphic variability on the meter (depositional parasequence cycle) to decameter (depositional sequence) scale (cf. Goldhammer *et al*., 1990; Elrick *et al*., 1991) that are documented at the Fire Creek exposure of the Shublik Fm. Small-scale fluctuations in relative sea level influenced the OMZ which led to high resolution variability in sedimentary features due to $C_{org}$ detritus, carbonate production, phosphate replacement and bioerosion of the sediments.

The meter–decameter-scale parasequences, recognized at the Fire Creek outcrop, are bounded by marine flooding surfaces. Marine flooding surfaces were interpreted where deposition of fine-grained organic-rich sediments lay directly over coarse-grained proximal facies. Trends in facies stacking patterns were moderated by changes in relative

sea level, climate and water chemistry over a low-angle passive continental margin (Parrish, 1987; Robinson *et al*., 1996; Parrish *et al*., 2001a&b & Kelly *et al*., 2007) on the western coast of Pangea. This study documents four major fluctuations in sea level through the Middle–Upper Triassic deposits in northern Alaska.

# CHAPTER 6: DISCUSSION

## 6.1 Triassic Paleoceanography

The formation of Pangea culminated with the collision of Laurasia and Gondwana and formed a supercontinent that extended from 85° N to 90° S during the Triassic (Dubiel *et al*., 1991 and references within). The late Paleozoic to early Mesozoic Panthalassic Ocean was much wider than the present Pacific Ocean with relatively low sea levels and an extensive landmass disrupting zonal atmospheric circulation (Vail *et al.*, 1977; Dubiel *et al*., 1991; Jewell, 1995). A north–south configuration of Arctic Alaska, as suggested by Lawver *et al*. (2002) would have subjected Arctic Alaska to upwelling conditions from northerly winds and associated Ekman transport in an eastern ocean basin setting during the Triassic (Kelly *et al*., 2007) (Fig. 33). The meridionally influenced, oceanic upwelling setting is the current interpretation for the deposition of glauconitic, phosphatic, and organic-rich facies observed in the Shublik and Otuk Formations (Kelly *et al*., 2007).

The late Paleozoic to early Mesozoic is a highly dynamic period in the Earth's past due to active volcanism from large igneous provinces. The Late Permian was characterized by a harsh hot house climate that was most likely sustained into the Early Triassic (Preto *et al*., 2010). At the Permian–Triassic boundary, active volcanism from the Siberian Traps large igneous province increased atmospheric $CO_2$ levels creating hot house conditions (Renne *et al*., 1995; Lawver *et al*., 2002). Then again at the Triassic–Jurassic boundary the Central Atlantic Magmatic Province (CAMP) generated abundant volcanic gasses, specifically $CO_2$ and $SO_2$, which were introduced into the atmosphere

perturbing Earth's climate (Schaller *et al*., 2011). Isotopic results, presented by Schaller *et al*. (2011), document pedogenic carbonates within the Newark Basin of northeastern North America that suggest atmospheric carbon dioxide levels of ~2,000 ppm before CAMP and ~4,200 ppm after the first volcanic expulsion. The mechanisms

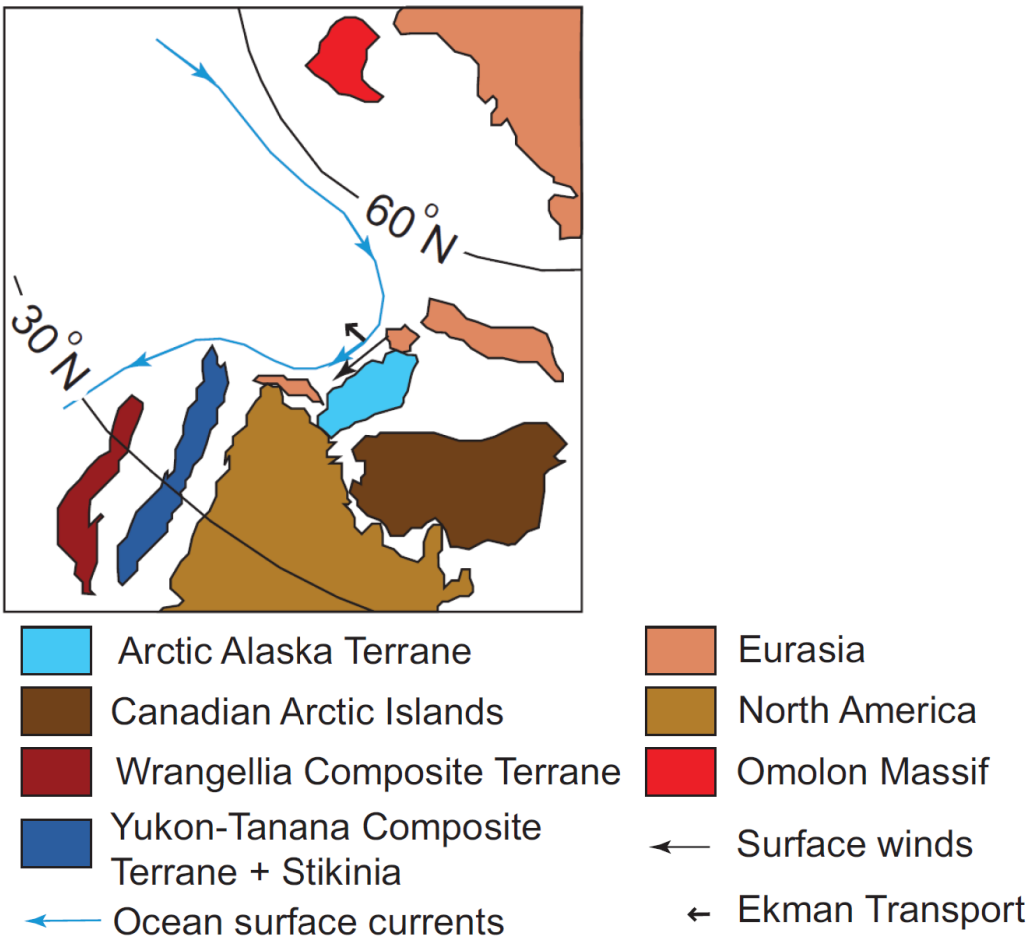


**Fig. 33** Meridional upwelling along the stable west coast of the Arctic Alaska Terrane during the Triassic. Upwelling driven by northerly winds and Ekman transport. Paleogeographic reconstruction after Lawver *et al*. (2002) (modified from Kelly *et al*., 2007).

driving changing seawater chemistry have been argued to revolve around atmospheric carbon dioxide concentrations globally by many authors. Importantly, the shift in high-Mg vs. low-Mg carbonates could be a direct result of plate tectonics and has an adverse effect on marine shell tests as argued by Montañez (2002).

Paleoceanographic studies during the Triassic indicate high levels of atmospheric carbon dioxide derived from large igneous provinces that influenced seawater chemistry and biota. Global circulation models indicate reduced atmospheric circulation due to the lateral extent of Pangaea between the poles (Dubiel *et al*., 1991). The effects of high atmospheric carbon dioxide heavily influenced sea water temperature, pH, carbonate speciation and concentrations, and hypoxia within the water column (Pörtner, 2008). The geochemical, biotic, and facies evidence from the coast of northern Alaska during the Triassic suggest hypoxic conditions on the shelf and periodic oxygenation pulsed onto the shelf, likely caused by storms. The low-oxygen conditions facilitated the bio-mediated precipitation of pristine phosphate nodules and peloids within a carbonate dominated system. The depositional environment was controlled by relative sea-level fluctuations, sediment transport onto the shelf and regional upwelling currents influencing primary productivity and biologic activity at the sediment water interface (Parrish, 1987; Parrish *et al*., 2001 a&b). The primarily low-angle shelf was inundated with nutrient-rich waters, upwelling from deeper in the basin and influencing a strong OMZ that shifted relative to the sea level (Kelly *et al*., 2007).

Outcrop observations of Middle–Upper Triassic sequences at Fire Creek indicate a general shoaling upward from a finer grained shaley or silty facies to a sandy,

phosphatic or carbonate facies resulting from dominant regressive facies trends with abrupt transgressive facies or deepening at the base of sequences (Parrish *et al*., 2001a&b; Kelly *et al*., 2007). There are significant fluctuations within paleoredox, detrital and bioproductivity proxies from the centimeter to decameter scale lithologies throughout the Shublik Fm. The abrupt transgressive facies coincide with the most organic-rich sediments within the Shublik Fm., particularly within sequences two and three. Bottom water conditions were subjected to anoxic conditions during transgressive events while $C_{org}$ preservation was at its highest. Oxygen laden bottom water currents, possibly through storm deposits, were washed onto the shelf during the transgressive re-working of inner shelf sediments, thus the deposition of wackestone to packstone facies interbedded within the organic-rich mudstones. The storm influenced fining-upward packages are prevalent within the fine-grained organic-rich facies deposited during the transgressive events, as well as HCS documented within the coarser-grained interbedded facies (Kelly *et al*., 2007).

The oxygenated bottom-waters deposited during the HST have characteristic sedimentary features such as a high bioturbation index within the coarse grained nodular phosphatic facies while trends in geochemical proxies indicate sufficient oxygenation to limit redox sensitive elemental concentrations. Interbedded within the coarse-grained nodular phosphatic facies are preserved redox sensitive elements indicating anoxic bottom waters were intermittently prevalent during HST deposition as well. This observation is interesting given the highly organic-rich sediments present (0-3.5 wt.%;

Kelly, 2004) during HST deposition within the Shublik Fm. as described by Kelly *et al*. (2007).

### 6.2 Unconventional Petroleum Source Rock Implications

The Ellesmerian mega-sequence contains the most prolific petroleum reservoir and source rocks on the North Slope, including the Ivishak Fm., Shublik Fm., Sag River Sandstone, and Karen Creek Sandstone (Lower–Upper Triassic) (Fig. 3). Source rocks within the Ellesmerian mega-sequence contribute more than 90% of recoverable crude oil and 82 % of recoverable hydrocarbon gasses (Bird, 2001). A rather recent subsurface study by Peters *et al*. (2006) quantifies the oil-prone organic matter within the TST dominated by laminated marls and shales of the lower Shublik Fm. with $C_{org}$ concentrations over 4 wt. % and hydrogen index greater than 600 mg hydrocarbon/g $C_{org}$.

The Fire Creek outcrop is the best exposure of the Shublik Fm. for demonstrating the highly cyclic nature of the unit (Kelly *et al*., 2007). Macro-scale homogeneity of shale plays currently being exploited for hydrocarbons have resulted in the need for micro-scale reservoir characterization and stratigraphic correlation (Ratcliffe *et al.*, 2012). In order to better create a sequence stratigraphic framework within homogenous unconventional prospects continual data points through well penetrations and geochemical investigations are needed. This study takes a "first look" approach at correlating a heterogeneous unconventional prospect in the subsurface using petrographic, geochemical and wire-line well log data. Homogeneous shale reservoirs are currently investigated using micro–macro-scale inorganic whole rock analyses to create

regional chemostratigraphic correlations, model bulk mineralogy, understand $C_{org}$ distribution and paleoredox conditions, and estimate relative rock brittleness (Wright & Ratcliffe, 2010; Ratcliffe *et al.*, 2012).

The Shublik Fm. is not a homogenous unconventional prospect and consists of complicated rhythmically interbedded clay–quartz–carbonate and phosphate-rich facies associations. The unit is a proven source interval with several $C_{org}$ rich (1–6.3 wt. %, Bird, 1994; Peters *et al*., 2006) zones that would be optimal for unconventional exploration. There are several basin-wide flooding events: one within sequence two, one within sequence three, and another event during the initial flooding of sequence four, that contain $C_{org}$ rich facies up to 4 wt. % (Kelly, 2004). This makes the Shublik Fm. a world class unconventional target. The transgressive facies contain the highest concentrations of $C_{org}$ within the Shublik Fm. while the HST deposits contain slightly lower but significant amounts of organic carbon. The transgressive facies are generally carbonate mudstones to wackestones interbedded with coarser grained wackestones to packstones. The organic-rich units within the HST facies are also mudstone to wackestone facies interbedded with predominantly coarse-grained proximal sediments.

The transgressive events within sequence two and three coincide with high gamma-ray peaks (~250 API) which are areally extensive and appear to be restricted when onlapping basement structures across northern Alaska. The initial transgression overlying sequence one contains a highly $C_{org}$ rich facies with measurements up to 2–3 wt. % (Kelly, 2004). This regional flooding event is recognized basin wide using gamma-ray well logs and $C_{org}$ measurements and at the same stratigraphic interval within the

Phoenix #1 well shows values greater than 10 wt. % $C_{org}$ (cf. Kupecz, 1995; Robinson *et al*., 1996). The organic-rich sediments within the TST of sequence two generally thin over the Colville High near Prudhoe Bay and thicken to the south and east to ~10-15 meters. To the west of the Colville high the organic-rich rocks of sequence two thicken again off the flanks of the Fish Creek platform and within the northern part of the Ikpikpuk Basin. Trends in the gamma-ray profile within the TST of sequence three show two ~5-10 meter thick intervals with potentially high $C_{org}$ values. The lateral and vertical heterogeneity within the Shublik Fm. should be taken into consideration while evaluating the unconventional potential within a prospective area. The heterogeneous and cyclic nature of these rocks will undoubtedly prove difficult to interpret laterally and vertically until more data points are gathered and this complex formation is explored in better detail.

Using these newly devised concepts involving trace element geochemical proxies, one purpose of this study was to understand the paleoenvironmental influences that relate to the accumulation and preservation of $C_{org}$. The lithological record within a marine environment is influenced by paleobathymetry, energy regime and bio-geochemical cycles during sedimentation recorded at or near the sediment-water interface. The three controls on $C_{org}$ accumulation and preservation within marine sediments are: 1) preservation of $C_{org}$ in a static situation where stagnant waters promote anoxic conditions and degradation is low; 2) high primary productivity in a dynamic setting where organic accumulation outpaces degradation regardless of oxidizing conditions; and 3) adsorption of $C_{org}$ on to mineral surfaces, specifically the interlayers within smectite clay particles,

within the depositional environment (Pederson & Calvert 1990,1991; Ransom *et al*., 1998; Kennedy *et al*., 2002; Rullkotter, 2006).

The sequence stratigraphic interpretation within this study and within previous studies utilized several well penetration measurements and cores in the subsurface. Correlation across northern Alaska will require future work applying a consistent sequence stratigraphic nomenclature to the Middle–Upper Triassic deposits. The A–D zonal nomenclature adopted from the Prudhoe Bay area correlated on the well log response is based upon recognition of major marine flooding events. Subsequent regional sequence stratigraphic interpretations divide the zonal subdivisions into different packages which can lead to further lateral misinterpretation of the unit (supplemental file). The major marine flooding events outlined within the zonal nomenclature do not identify all of the organic-rich horizons, which is where the sequence stratigraphic approach is necessary to identify the lateral extent of genetically related organic-rich facies. Thus, the products of a thorough high-resolution sequence stratigraphic architecture help define the major genetically related packages and quantify the lateral extent of organic-rich rock distribution. Using the methods utilized by Ratcliff *et al*. (2012) or Wright and Ratcliffe (2010) to understand the mineralogy and clay type will aid in determining the degree of composite layering (carbonate–silica–clay matrices) within or around the desired completion zone.

# CHAPTER 7: CONCLUSIONS

- The recognition of transgressive flooding surfaces, where condensation or reworking occurred, and cyclical stacking patterns of the lithofacies were the keys to establishing the sequence stratigraphic architecture within the Shublik Fm. The interpretation has led to the addition of a fourth depositional sequence within the Middle-Upper Triassic sediments in northern Alaska. Within this context, the transgressive surface located above the coarse-grained facies deposited within the HST of sequence two is recognized as a flooding event and a sequence boundary. Gamma-ray and $C_{org}$ measurements from outcrop aided in this objective and are recommended for regional sequence-stratigraphic studies that provide data about the lateral extent of organic-rich facies within the Shublik Fm.
- Four Shublik Fm. microfacies have been recognized within the phosphatic and carbonate progradational facies association from the Fire Creek outcrop in northern Alaska. Increased bioturbation (ichnofabric index 3-5) removed relict sedimentary features and resulted in decreased $C_{org}$ within the facies (0.3 $C_{org}$ wt. %). Facies with decreased bioturbation (ichnofabric index 2-3) contained higher amounts of precipitated P, $C_{org}$ (2.0 $C_{org}$ wt. %) and, enriched paleoredox proxies. Samples with decreased enrichment in paleoredox sensitive elements also had lower ichnofabric indices and less $C_{org}$ enrichment. The driving mechanisms that influenced environmental changes during the Middle–Late Triassic in Arctic Alaska include but are not limited to relative changes in sea-level and prominent

basement structures (Hulm, 1999) within a marine environment subjected to upwelling conditions.

- The sequence-stratigraphic framework reveals that transgressive events within SQ2 and SQ3 resulted in relatively low-energy deep-water environments, far from terrigenous source areas that lay to the northeast. By contrast, the more interbedded character and abundance of reworked phosphatic sediments with silt-sized detrital quartz and, coarse grained bioclastic intraclasts within the HST facies of each sequence, provides evidence for repeated fluctuations in water depth in a shallower, well oxygenated marine environment. Cyclic stacking patterns reveal that changes in depositional facies were related to fluctuations in OMZ position on the shelf. Changes in relative sea-level influenced the location of primary productivity and bottom-water redox conditions which influenced sedimentary facies patterns.
- Within SQ3 of the Shublik Fm. there is a series of two very high gamma-ray peaks indicating long periods with low rates of sedimentation (e.g. condensed sections) within relatively low-energy deep-water conditions. These events are characterized by high-primary productivity, increases in paleoredox and primary productivity proxies and high $C_{org}$. These peaks, interpreted as flooding events, compliment the proposed sea-level increase during the Carnian as defined by Kelly *et al*. (2007). The high gamma-ray counts in transgressive deposits within the Shublik Fm. are related to high $C_{org}$ at the Fire Creek outcrop and within the Phoenix # 1 well. The Shublik Fm. generally contains high gamma-ray readings

although heterogeneity within the unit and the dilution and preservation of $C_{org}$ must be taken into consideration while mapping the organic-rich facies.

- Successful exploitation of the Shublik Fm. in northern Alaska will be especially difficult due to many factors including the limited drilling season, environmental conditions, and freezing temperatures. Understanding this shale resource play will require a thorough understanding of how $C_{org}$ dilution and preservation within the facies shifts changes within a sequence stratigraphic context. As the formation is explored, tying core information to well log responses and utilizing multiple geochemical measurement points will enable future studies to better constrain the depositional environment.

**Table 1**. Trace and major elemental concentration. Data at measured from stratigraphic intervals documented at the Fire Creek outcrop in northern Alaska. High frequency sampling measurments within the HST of SQ2 (81-94m) are intergrated into the Kelly (2004) dataset.

| | PALEOREDOX | | | | BIO-PRODUCTIVITY | | | | DETRITAL | | | | | |
|---|---|---|---|---|---|---|---|---|---|---|---|---|---|---|
| Meters | U | Mo | V | Ni | Cu | Ba | Zn | P (%) | Al (%) | SiO2 (%) | K (%) | Ti % | Ti/Al | Cr |
| 177.5 | 4.7 | 6 | 203 | 33 | 30 | 559 | 90 | 0.0 | 4.7 | 79.7 | 1.4 | 0.3 | 0.06 | 75 |
| 176.5 | 2.8 | 8 | 215 | 42 | 27 | 205 | 70 | 0.0 | 2.4 | 33.2 | 0.3 | 0.1 | 0.05 | 91 |
| 175 | 5.6 | 4 | 899 | 43 | 11 | 59 | 472 | 0.6 | 2.5 | 57.8 | 0.0 | 0.1 | 0.05 | 2360 |
| 174 | 24.9 | 0 | 289 | 25 | 13 | 84 | 219 | 3.7 | 1.3 | 58.9 | 0.1 | 0.1 | 0.06 | 621 |
| 172 | 1.5 | 0 | 35 | 9 | 18 | 155 | 21 | 0.0 | 1.3 | 11.6 | 0.3 | 0.1 | 0.05 | 15 |
| 168.5 | 15.1 | 4 | 115 | 40 | 29 | 670 | 74 | 0.3 | 4.2 | 29.1 | 1.0 | 0.2 | 0.05 | 53 |
| 167 | 1.1 | 0 | 30 | 7 | 17 | 130 | 15 | 0.1 | 1.0 | 5.8 | 0.2 | 0.0 | 0.04 | 29 |
| 165.5 | 4 | 18 | 330 | 69 | 56 | 1190 | 126 | 0.0 | 10.2 | 59.6 | 2.3 | 0.5 | 0.04 | 116 |
| 164.5 | 0.7 | 0 | 19 | 6 | 17 | 100 | 13 | 0.1 | 0.9 | 5.5 | 0.2 | 0.0 | 0.04 | 10 |
| 163 | 5.4 | 27 | 454 | 77 | 58 | 1080 | 123 | 0.0 | 10.2 | 56.2 | 2.1 | 0.4 | 0.04 | 124 |
| 151 | 3.9 | 0 | 232 | 46 | 35 | 1130 | 111 | 0.1 | 8.7 | 51.9 | 1.9 | 0.3 | 0.04 | 164 |
| 149 | 3.8 | 0 | 207 | 37 | 40 | 1980 | 94 | 0.1 | 8.9 | 54.7 | 1.9 | 0.4 | 0.04 | 96 |
| 148 | 9 | 80 | 185 | 79 | 64 | 1120 | 98 | 0.1 | 7.4 | 42.0 | 1.6 | 0.3 | 0.04 | 91 |
| 146.5 | 4.2 | 0 | 262 | 42 | 37 | 1160 | 106 | 0.1 | 8.6 | 51.7 | 1.9 | 0.3 | 0.04 | 228 |
| 145.5 | 4.7 | 0 | 286 | 48 | 41 | 1020 | 121 | 0.1 | 7.7 | 46.2 | 1.8 | 0.3 | 0.04 | 174 |
| 143 | 4.1 | 0 | 297 | 56 | 44 | 1220 | 133 | 0.1 | 8.8 | 53.2 | 2.0 | 0.3 | 0.04 | 243 |
| 139.5 | 4.3 | 0 | 238 | 67 | 48 | 1130 | 143 | 0.1 | 7.8 | 46.6 | 1.8 | 0.3 | 0.04 | 269 |
| 138 | 3.7 | 0 | 250 | 48 | 39 | 1130 | 121 | 0.1 | 7.7 | 43.8 | 1.8 | 0.3 | 0.04 | 248 |
| 135 | 4 | 0 | 244 | 64 | 46 | 1250 | 128 | 0.1 | 8.6 | 47.8 | 2.0 | 0.3 | 0.04 | 279 |
| 130.9 | 4.5 | 4 | 220 | 61 | 52 | 1070 | 121 | 0.1 | 5.8 | 33.8 | 1.4 | 0.2 | 0.04 | 254 |
| 129 | 4.2 | 0 | 179 | 33 | 39 | 1110 | 91 | 0.1 | 6.6 | 37.9 | 1.6 | 0.3 | 0.04 | 88 |
| 127.3 | 4.6 | 5 | 128 | 120 | 55 | 54 | 82 | 0.2 | 4.7 | 32.1 | 1.1 | 0.2 | 0.04 | 103 |
| 126.5 | 4.3 | 0 | 168 | 24 | 33 | 1190 | 82 | 0.1 | 6.4 | 37.7 | 1.6 | 0.3 | 0.04 | 144 |
| 124.4 | 4.4 | 0 | 191 | 49 | 51 | 1690 | 91 | 0.1 | 8.1 | 48.6 | 2.1 | 0.3 | 0.04 | 210 |
| 123.6 | 4.5 | 0 | 167 | 38 | 30 | 1430 | 113 | 0.1 | 6.9 | 40.9 | 1.8 | 0.3 | 0.04 | 69 |
| 122.5 | 6.2 | 0 | 203 | 42 | 38 | 1730 | 114 | 0.1 | 8.8 | 53.2 | 2.3 | 0.3 | 0.04 | 221 |
| 121.5 | 108 | 9 | 71 | 35 | 26 | 111 | 123 | 7.0 | 2.1 | 20.3 | 0.3 | 0.1 | 0.02 | 58 |
| 119.5 | 30.7 | 17 | 39 | 33 | 34 | 437 | 89 | 4.7 | 0.7 | 6.2 | 0.1 | 0.0 | 0.03 | 62 |
| 116 | 10.5 | 3 | 33 | 37 | 37 | 834 | 87 | 1.5 | 1.1 | 12.7 | 0.3 | 0.0 | 0.04 | 104 |
| 113.3 | 14 | 2 | 26 | 27 | 31 | 822 | 84 | 2.9 | 0.6 | 13.2 | 0.2 | 0.0 | 0.04 | 39 |
| 109.5 | 12.9 | 3 | 43 | 15 | 22 | 519 | 44 | 1.6 | 0.5 | 6.8 | 0.2 | 0.0 | 0.04 | 43 |
| 108.5 | 34.6 | 8 | 61 | 15 | 23 | 607 | 58 | 6.6 | 0.5 | 6.5 | 0.1 | 0.0 | 0.03 | 49 |
| 105.2 | 1.9 | 20 | 185 | 32 | 34 | 215 | 196 | 0.0 | 0.5 | 6.2 | 0.2 | 0.0 | 0.04 | 9 |
| 104.1 | 3.7 | 11 | 103 | 33 | 0 | 133 | 27 | 0.0 | 0.3 | 3.7 | 0.1 | 0.0 | 0.06 | 2 |
| 103 | 1 | 12 | 178 | 16 | 21 | 295 | 39 | 0.0 | 1.6 | 4.4 | 0.4 | 0.1 | 0.07 | 9 |
| 100.1 | 3.7 | 16 | 111 | 31 | 0 | 121 | 35 | 0.0 | 0.6 | 5.8 | 0.2 | 0.0 | 0.05 | 4 |
| 97.5 | 5.5 | 3 | 11 | 11 | 0 | 137 | 12 | 0.0 | 0.5 | 10.7 | 0.1 | 0.0 | 0.06 | 5 |
| 94 | 4.5 | 2 | 49 | 7 | 0 | 89 | 18 | 0.2 | 0.3 | 4.4 | 0.1 | 0.0 | 0.07 | 29 |

**Table 2**. Trace and major elemental concentration. Data at measured from stratigraphic intervals documented at the Fire Creek outcrop in northern Alaska. High frequency sampling measurments within the HST of SQ2 (81-94m) are intergrated into the Kelly (2004) dataset.

| | PALEOREDOX | | | | BIO-PRODUCTIVITY | | | | DETRITAL | | | | | |
|---|---|---|---|---|---|---|---|---|---|---|---|---|---|---|
| Meters | U | Mo | V | Ni | Cu | Ba | Zn | P (%) | Al (%) | SiO2 (%) | K (%) | Ti % | Ti/Al | Cr |
| 92.9 | 9 | 2 | 29 | 11 | 3 | 125 | 14 | -- | -- | -- | -- | -- | -- | -- |
| 91 | 18 | 8 | 56 | 22 | 10 | 360 | 30 | -- | -- | -- | -- | -- | -- | -- |
| 90.75 | 23 | 10 | 98 | 38 | 17 | 594 | 66 | -- | -- | -- | -- | -- | -- | -- |
| 90.5 | 11 | 4 | 42 | 11 | 4 | 83 | 24 | -- | -- | -- | -- | -- | -- | -- |
| 90.25 | 28 | 19 | 144 | 90 | 49 | 727 | 176 | -- | -- | -- | -- | -- | -- | -- |
| 90 | 12 | 6 | 47 | 19 | 9 | 252 | 38 | -- | 1.6 | 50.9 | 0.5 | 0.1 | 0.06 | 20 |
| 89.7 | 45 | 19 | 101 | 48 | 13 | 398 | 75 | -- | -- | -- | -- | -- | -- | -- |
| 89.5 | 14 | 7 | 44 | 21 | 10 | 163 | 36 | -- | -- | -- | -- | -- | -- | -- |
| 89.25 | 13 | 11 | 88 | 30 | 17 | 409 | 70 | -- | -- | -- | -- | -- | -- | -- |
| 89 | 13 | 5 | 37 | 20 | 12 | 167 | 50 | -- | 1.7 | 38.4 | 0.5 | 0.1 | 0.06 | 61 |
| 88.5 | 12 | 3 | 32 | 16 | 9 | 95 | 30 | -- | -- | -- | -- | -- | -- | -- |
| 87.5 | 11 | 6 | 47 | 16 | 8 | 162 | 28 | -- | -- | -- | -- | -- | -- | -- |
| 86.5 | 15 | 5 | 58 | 24 | 13 | 343 | 47 | -- | 1.4 | 21.1 | 0.5 | 0.1 | 0.06 | 98 |
| 86.25 | 15 | 4 | 43 | 19 | 9 | 180 | 38 | -- | -- | -- | -- | -- | -- | -- |
| 86.1 | 13 | 5 | 56 | 24 | 13 | 345 | 51 | -- | -- | -- | -- | -- | -- | -- |
| 86 | 8 | 5 | 64 | 18 | 7 | 490 | 35 | -- | -- | -- | -- | -- | -- | -- |
| 85.75 | 16 | 17 | 102 | 52 | 31 | 379 | 119 | -- | -- | -- | -- | -- | -- | -- |
| 85.5 | 9 | 4 | 41 | 16 | 8 | 139 | 37 | -- | -- | -- | -- | -- | -- | -- |
| 85.25 | 11 | 3 | 27 | 17 | 7 | 150 | 37 | -- | -- | -- | -- | -- | -- | -- |
| 85 | 17 | 8 | 64 | 41 | 19 | 334 | 67 | -- | -- | -- | -- | -- | -- | -- |
| 84.76 | 15 | 8 | 73 | 39 | 19 | 333 | 78 | -- | -- | -- | -- | -- | -- | -- |
| 84.5 | 13 | 4 | 27 | 22 | 10 | 147 | 42 | -- | 2.8 | 40.0 | 1.0 | 0.1 | 0.05 | 36 |
| 84.25 | 7 | 4 | 42 | 20 | 9 | 254 | 42 | -- | -- | -- | -- | -- | -- | -- |
| 84.1 | 8 | 5 | 32 | 18 | 10 | 146 | 37 | -- | -- | -- | -- | -- | -- | -- |
| 84 | 11 | 9 | 64 | 37 | 18 | 285 | 81 | -- | -- | -- | -- | -- | -- | -- |
| 83.6 | 20 | 8 | 77 | 42 | 24 | 332 | 87 | -- | -- | -- | -- | -- | -- | -- |
| 83.5 | 17 | 10 | 103 | 69 | 42 | 464 | 148 | -- | 1.0 | 14.5 | 0.3 | 0.1 | 0.06 | 103 |
| 83.25 | 9 | 3 | 40 | 20 | 9 | 187 | 39 | -- | -- | -- | -- | -- | -- | -- |
| 83 | 13 | 5 | 42 | 25 | 11 | 272 | 41 | -- | -- | -- | -- | -- | -- | -- |
| 82.5 | 14 | 9 | 89 | 43 | 20 | 402 | 76 | -- | -- | -- | -- | -- | -- | -- |
| 82.25 | 10 | 6 | 37 | 20 | 8 | 111 | 23 | -- | -- | -- | -- | -- | -- | -- |
| 82 | 10 | 6 | 24 | 15 | 5 | 100 | 23 | -- | -- | -- | -- | -- | -- | -- |
| 81.75 | 10 | 9 | 45 | 28 | 13 | 187 | 39 | -- | -- | -- | -- | -- | -- | -- |
| 81.5 | 11 | 6 | 74 | 37 | 15 | 297 | 51 | -- | -- | -- | -- | -- | -- | -- |
| 81.1 | 15 | 13 | 157 | 80 | 73 | 488 | 147 | 1.6 | 4.8 | 50.5 | 1.8 | 0.2 | 0.05 | 55 |
| 78.5 | 15 | 7 | 65 | 42 | 28 | 303 | 72 | 2.7 | 1.9 | 29.1 | 0.7 | 0.1 | 0.05 | 49 |
| 74.5 | 4 | 29 | 32 | 22 | 6 | 221 | 26 | 0.4 | 1.3 | 20.4 | 0.5 | 0.1 | 0.06 | 55 |
| 72.1 | 6 | 4 | 38 | 21 | 6 | 276 | 38 | 1.7 | 1.6 | 17.2 | 0.6 | 0.1 | 0.05 | 14 |
| 71 | 11 | 16 | 119 | 60 | 43 | 551 | 82 | 1.0 | 4.5 | 39.0 | 1.7 | 0.2 | 0.05 | 71 |

**Table 3**. Trace and major elemental concentration. Data at measured from stratigraphic intervals documented at the Fire Creek outcrop in northern Alaska. High frequency sampling measurments within the HST of SQ2 (81-94m) are intergrated into the Kelly (2004) dataset.

| | PALEOREDOX | | | | BIO-PRODUCTIVITY | | | | DETRITAL | | | | | |
|---|---|---|---|---|---|---|---|---|---|---|---|---|---|---|
| Meters | U | Mo | V | Ni | Cu | Ba | Zn | P (%) | Al (%) | SiO2 (%) | K (%) | Ti % | Ti/Al | Cr |
| 66 | 7 | 4 | 37 | 15 | 0 | 112 | 36 | 1.3 | 0.7 | 9.5 | 0.2 | 0.0 | 0.05 | 28 |
| 64.5 | 22 | 7 | 46 | 32 | 24 | 219 | 70 | 4.9 | 1.9 | 26.3 | 0.7 | 0.1 | 0.05 | 60 |
| 63 | 15 | 7 | 54 | 27 | 12 | 240 | 45 | 3.7 | 1.2 | 18.1 | 0.4 | 0.1 | 0.05 | 16 |
| 61 | 43 | 45 | 582 | 103 | 66 | 371 | 166 | 2.8 | 3.7 | 55.8 | 1.4 | 0.2 | 0.05 | 115 |
| 60.5 | 5 | 4 | 34 | 7 | 0 | 48 | 52 | 0.7 | 0.3 | 5.8 | 0.1 | 0.0 | 0.05 | 64 |
| 60 | 67 | 11 | 288 | 39 | 41 | 321 | 118 | 7.3 | 2.1 | 30.0 | 0.8 | 0.1 | 0.03 | 10 |
| 57.5 | 41 | 4 | 176 | 26 | 21 | 230 | 71 | 8.3 | 1.2 | 18.8 | 0.4 | 0.0 | 0.04 | 7 |
| 54.5 | 5 | 3 | 43 | 13 | 7 | 115 | 39 | 1.4 | 1.0 | 85.8 | 0.3 | 0.1 | 0.06 | 15 |
| 53 | 2 | 2 | 46 | 8 | 8 | 120 | 20 | 0.2 | 1.1 | 91.7 | 0.3 | 0.1 | 0.06 | 44 |
| 51.5 | 14 | 3 | 36 | 10 | 7 | 204 | 38 | 4.3 | 1.0 | 60.1 | 0.3 | 0.1 | 0.05 | 0 |
| 48 | 5 | 5 | 175 | 31 | 25 | 414 | 98 | 0.4 | 5.4 | 74.6 | 1.9 | 0.4 | 0.07 | 29 |
| 47.5 | 3 | 3 | 79 | 19 | 11 | 289 | 63 | 0.9 | 3.1 | 78.2 | 1.1 | 0.1 | 0.05 | 20 |
| 45.5 | 5 | 3 | 109 | 19 | 11 | 219 | 77 | 0.7 | 2.9 | 82.9 | 1.0 | 0.1 | 0.05 | 29 |
| 45 | 6 | 2 | 62 | 14 | 10 | 184 | 48 | 1.6 | 1.9 | 80.1 | 0.6 | 0.1 | 0.05 | 38 |
| 42.9 | 12 | 0 | 37 | 14 | 12 | 204 | 65 | 7.0 | 1.5 | 52.2 | 0.4 | 0.0 | 0.03 | 39 |
| 41.75 | 13 | 0 | 41 | 14 | 14 | 406 | 41 | 7.4 | 1.4 | 48.9 | 0.4 | 0.0 | 0.02 | 0 |
| 41.25 | 4 | 3 | 86 | 17 | 12 | 177 | 51 | 0.3 | 2.0 | 88.6 | 0.7 | 0.1 | 0.04 | 41 |
| 40 | 7 | 0 | 50 | 10 | 9 | 216 | 43 | 2.0 | 1.5 | 77.7 | 0.5 | 0.1 | 0.04 | 30 |
| 37 | 5 | 0 | 59 | 12 | 13 | 301 | 106 | 2.7 | 2.5 | 61.0 | 0.8 | 0.1 | 0.04 | 14 |
| 35.5 | 2 | 0 | 55 | 14 | 13 | 242 | 72 | 0.8 | 2.9 | 68.6 | 1.0 | 0.1 | 0.04 | 15 |
| 30.5 | 3 | 0 | 59 | 14 | 8 | 255 | 50 | 0.4 | 2.6 | 74.0 | 0.9 | 0.1 | 0.05 | 37 |
| 28.5 | 2 | 0 | 64 | 21 | 13 | 310 | 69 | 0.2 | 4.4 | 77.6 | 1.4 | 0.2 | 0.05 | 27 |
| 27 | 2 | 0 | 41 | 21 | 10 | 236 | 45 | 0.2 | 3.4 | 67.9 | 1.0 | 0.2 | 0.05 | 16 |
| 25.3 | 4 | 0 | 63 | 41 | 15 | 261 | 91 | 1.3 | 3.3 | 71.5 | 1.0 | 0.2 | 0.05 | 68 |
| 20.5 | 3 | 0 | 57 | 29 | 18 | 208 | 187 | 0.3 | 3.5 | 78.7 | 1.0 | 0.2 | 0.04 | 29 |
| 18.8 | 3 | 0 | 61 | 26 | 12 | 414 | 144 | 0.2 | 3.6 | 78.2 | 1.1 | 0.2 | 0.05 | 32 |
| 17.5 | 4 | 0 | 126 | 44 | 24 | 440 | 452 | 0.2 | 6.8 | 69.8 | 2.2 | 0.3 | 0.05 | 43 |
| 13.7 | 3 | 0 | 48 | 27 | 10 | 241 | 155 | 0.2 | 3.8 | 74.3 | 1.1 | 0.2 | 0.04 | 33 |
| 12.2 | 2 | 0 | 40 | 16 | 12 | 172 | 66 | 0.1 | 3.1 | 65.1 | 0.9 | 0.2 | 0.05 | 17 |
| 11.4 | 3 | 0 | 83 | 43 | 17 | 343 | 147 | 0.2 | 5.5 | 69.6 | 1.7 | 0.3 | 0.05 | 47 |
| 8 | 2 | 2 | 58 | 23 | 14 | 199 | 47 | 0.2 | 3.2 | 40.9 | 1.0 | 0.1 | 0.04 | 37 |
| 5.4 | 2 | 4 | 28 | 32 | 11 | 99 | 45 | 0.3 | 1.6 | 55.7 | 0.4 | 0.1 | 0.05 | 29 |
| 3.8 | 3 | 1 | 78 | 24 | 14 | 258 | 86 | 0.2 | 4.8 | 73.1 | 1.4 | 0.2 | 0.04 | 15 |
| 1.25 | 3 | 9 | 52 | 106 | 23 | 164 | 337 | 0.3 | 3.2 | 77.8 | 0.7 | 0.1 | 0.04 | -- |
| 0.5 | 3 | 3 | 62 | 25 | 12 | 181 | 118 | 0.2 | 3.7 | 79.1 | 1.0 | 0.2 | 0.05 | -- |
| 0.2 | 3 | 12 | 39 | 35 | 16 | 180 | 41 | 0.6 | 1.5 | 68.8 | 0.4 | 0.1 | 0.03 | -- |

**Table 4.** Corg- measurements. Concentrations measured in wt. % using LECO analyses instrument.
Table integrates Corg- measurements from Kelly (2004) dataset. Meters indicate stratigraphic height within section.

| Meters | Corg- | Meters | Corg- | Meters | Corg- | Meters | Corg- | Meters | Corg- | Meters | Corg- | Meters | Corg- | Meters | Corg- |
|---|---|---|---|---|---|---|---|---|---|---|---|---|---|---|---|
| 177.5 | 1.0 | 123.6 | 0.5 | 105.97 | 1.1 | 101.91 | 0.3 | 91.0 | 0.5 | 84.5 | 0.7 | 63.0 | 1.3 | 13.7 | 0.2 |
| 168.5 | 1.3 | 122.5 | 1.3 | 105.90 | 1.9 | 101.87 | 0.3 | 90.8 | 1.2 | 84.3 | 0.6 | 61.0 | 2.6 | 12.2 | 0.3 |
| 165.5 | 1.4 | 122.0 | 1.4 | 105.80 | 0.7 | 101.87 | 0.3 | 90.5 | 0.3 | 84.1 | 0.6 | 60.5 | 1.5 | 8.0 | 0.3 |
| 163.0 | 1.6 | 121.5 | 1.8 | 105.75 | 0.4 | 101.86 | 0.2 | 90.3 | 1.6 | 84.0 | 1.3 | 60.0 | 1.9 | 3.8 | 0.3 |
| 151.0 | 0.9 | 119.5 | 1.7 | 105.70 | 1.6 | 101.85 | 0.3 | 90.0 | 0.7 | 83.6 | 1.3 | 57.5 | 1.9 | | |
| 149.0 | 0.8 | 116.0 | 1.7 | 105.40 | 0.8 | 101.80 | 0.2 | 89.7 | 1.1 | 83.5 | 2.0 | 54.5 | 1.0 | | |
| 148.0 | 2.2 | 113.3 | 1.5 | 105.25 | 0.6 | 101.70 | 4.1 | 89.5 | 0.5 | 83.3 | 0.9 | 53.0 | 0.8 | | |
| 146.5 | 1.2 | 108.50 | 1.3 | 105.20 | 1.2 | 101.55 | 3.5 | 89.3 | 1.0 | 83.0 | 0.9 | 51.5 | 0.7 | | |
| 145.5 | 1.3 | 108.20 | 0.7 | 104.95 | 0.6 | 101.35 | 1.4 | 89.0 | 0.6 | 82.5 | 1.5 | 48.0 | 1.0 | | |
| 143.0 | 1.2 | 107.90 | 1.1 | 103.25 | 0.1 | 101.30 | 0.4 | 88.5 | 0.4 | 82.3 | 0.7 | 45.0 | 0.7 | | |
| 139.5 | 1.8 | 107.63 | 1.2 | 103.20 | 0.2 | 101.25 | 3.8 | 87.5 | 0.5 | 82.0 | 0.6 | 42.9 | 0.8 | | |
| 138.5 | 1.9 | 107.28 | 1.8 | 102.95 | 0.4 | 101.10 | 0.7 | 86.5 | 0.7 | 81.8 | 1.1 | 41.3 | 0.6 | | |
| 138.0 | 1.4 | 107.10 | 0.7 | 102.87 | 2.6 | 100.95 | 0.5 | 86.3 | 0.5 | 81.5 | 1.5 | 37.5 | 1.4 | | |
| 135.0 | 1.5 | 106.95 | 0.7 | 102.55 | 0.6 | 100.81 | 1.6 | 86.1 | 0.7 | 81.1 | 3.5 | 37.0 | 0.3 | | |
| 130.9 | 1.4 | 106.75 | 0.9 | 102.53 | 0.2 | 100.65 | 2.6 | 86.0 | 0.4 | 78.5 | 1.4 | 35.5 | 0.4 | | |
| 129.0 | 0.8 | 106.65 | 1.0 | 102.30 | 1.1 | 100.45 | 2.6 | 85.8 | 1.3 | 74.5 | 0.6 | 30.5 | 0.3 | | |
| 127.3 | 0.6 | 106.47 | 1.3 | 102.20 | 0.6 | 100.30 | 0.4 | 85.5 | 0.8 | 72.1 | 1.0 | 28.5 | 0.2 | | |
| 126.5 | 0.5 | 106.37 | 2.1 | 102.15 | 0.4 | 97.50 | 0.2 | 85.3 | 0.5 | 71.0 | 1.5 | 27.0 | 0.3 | | |
| 125.5 | 0.7 | 106.25 | 1.1 | 102.13 | 2.0 | 94.00 | 0.3 | 85.0 | 1.0 | 66.0 | 0.7 | 20.5 | 0.3 | | |
| 124.4 | 1.0 | 106.05 | 4.2 | 102.10 | 1.5 | 92.9 | 0.3 | 84.8 | 1.3 | 64.5 | 1.6 | 17.5 | 1.2 | | |

# REFERENCES

Algeo, T. J. and Lyons, T. W., 2006, Mo–total organic carbon covariation in modern anoxic marine environments: Implications for analysis of paleoredox and paleohydrographic conditions: Paleoceanography, v. 21, no. 1.

Algeo, T.J. and Maynard, J.B., 2008, Trace-metal co-variation as a guide to water-mass conditions in ancient anoxic marine environments: Geosphere, v. 4, p. 872-887.

Algeo, T.J. and Rowe, H., 2012, Paleoceanographic applications of trace-metal concentration data: Chemical Geology 324-325, p. 6-18.

Baccelle, L. and Bosellini, A., 1965, Diagrammi per Ia stima visiva della composizione percentuale nelle rocche sedimentarie.- Annali deii' Universita di Ferrara (Nuova Serie), Sezione 9, Scienze geologiche e paleontologiche, v. 1, no. 3, p. 59- 62.

Barnes, D.A., 1987, Reservoir quality in the Sag River Formation, Prudhoe Bay Field, Alaska, *in* Tailleur, I.L., and Weimer, P., eds., 2001, Alaskan North Slope geology: Field Trip Guidebook, Pacific Section SEPM and Alaska Geological Society, v. 50, p. 85–94.

Baturin, G.N., 1982, Phosphorites on the sea floor: origin, composition, and distribution: Developments in Sedimentology 33: New York, NY, Elsevier, p. 343.

Berner, R. A., Ruttenberg, K. C., Ingall, E. D., and Rao, J. L.,1993, The nature of phosphorus burial in modern marine sediments: Interactions of C, N, P and S Biogeochemical Cycles and Global Change, v. 14, p. 365-378.

Bird, K.J., 1982, Rock-unit reports of 228 wells drilled on the North Slope, Alaska: U.S. Geological Survey Open File Report 82-278, p. 105.

Bird, K.J., and Bader, J.W., 1987, Regional geologic setting and history of petroleum exploration, in Bird, K.J., and Magoon, L.B., eds., Petroleum geology of the northern part of the Arctic National Wildlife Refuge, northeastern Alaska: U.S. Geological Survey Bulletin 1778, p. 17–25.

Bird, K.J. and Molenaar, C.M., 1987, Petroleum geology of the northern part of the Arctic National Wildlife Refuge, northeastern Alaska: U.S. Geological Survey Bulletin 1778, p. 37-59.

Bird, K.J., 1994, Ellesmerian(!) petroleum system, North Slope of Alaska, U.S.A. *in* Magoon, L. and Dow, W., The petroleum system-from source to trap: AAPG Memoir, v. 60, p. 339-358.

Bird, K. J., 2001, Alaska: A twenty-first-century petroleum province *in* Downey, M. W. Threet, J. C. and Morgan, W. A., Petroleum provinces of the twenty-first century: AAPG Memoir, v. 74, p. 137–165.

Bodnar, D.A., 1984, Stratigraphy, age, depositional environments, and hydrocarbon source rock evaluation of the Otuk formation, north-central Brooks Range, Alaska: Master's Thesis, University of Alaska Fairbanks, Fairbanks, Alaska.

Briet, G.N., and R.B. Wanty, 1991, Vanadium accumulation in carbonaceous rocks; a review of geochemical controls during deposition and diagenesis: Chemical Geology, v. 91, p. 83-97.

Burchette, T. P., and Wright, V. P., 1992, Carbonate ramp depositional systems: Sedimentary Geology, v. 79(1), p. 3-57.

Calvert, S.E. and Pedersen, T.F., 1993, Geochemistry of Recent oxic and anoxic marine sediments: Implications for the geological record: Marine Geology 113, p. 67-88.

Calvert, S.E., Bustin, R.M. and Ingal, E.D., 1996, Influence of water column anoxia and sediment supply on the burial and preservation of organic carbon in marine shales: Geochimica et Cosmochimica Acta, v. 60, p. 1577-1593.

Catuneanu, O., Abreu, V.; Bhattacharya, J. P., Blum, M. D., Dalrymple, R. W., Eriksson, P. G.,Fielding, C. R., Fisher, W. L., Galloway, W. E., Gibling, M. R., Giles, K. A., Holbrook, J. M., Jordan, R., Kendall, C. G. St.C., Macurda, B., Martinsen, O. J.,Miall, A. D., Neal, J. E., Nummedal, D., Pomar, L., Posamentier, H. W., Pratt, B. R., Sarg, J. F., Shanley, K. W., Steel, R. J., Strasser, A.,Tucker, M. E., and Winker, C., 2009, Towards the Standardization of Sequence Stratigraphy: Papers in the Earth and Atmospheric Sciences, Paper 238.

Cheel, R.J., 1991, Grain fabric in hummocky cross-stratified storm beds: genetic implications: Journal of Sedimentary Petrology, v. 61, p. 102–110.

Chapman, R.M., Detterman, R.L. and Mangus, M.D., 1964, Geology of the Killik-Etivluk Rivers region, Alaska: U.S. Geological Survey Professional Paper 303-F, p. 325-407.

Decker, P., 2011, http://dog.dnr.alaska.gov/ResourceEvaluation/Documents/Shale_Well_Data_Sampler/NAK_Shale_Resource_Plays_AGS_20110915.pdf: Source-Reservoired Oil Resources, Alaska North Slope, Alaska Geological Society.

Detterman, R.L., 1970a, Sedimentary history of the Sadlerochit and Shublik formations in northeastern Alaska *in* Adkinson W.L. and Brosge,M.M., Proceedings of the geological seminar on the North Slope of Alaska: Pacific Section AAPG, p. 1-13.

Detterman, R.L., Reiser, H.N., Brosge', W.P. and Dutro Jr., J.T., 1975, Post-Carboniferous stratigraphy, northeastern Alaska: U.S. Geological Survey Professional Paper 886, p. 46.

Detterman, R.L., 1989, Triassic phosphate deposits, north-eastern Alaska, USA *in* Notholt, A. J., Sheldon, R. P. and Davidson, D. F., Phosphate deposits of the world: Phosphate rock resources, Cambridge University Press, v. 2, p. 14-17.

Dingus, A.S., 1984, Paleoenvironmental reconstruction of the Shublik Formation on the North Slope of Alaska: Master's Thesis, University of California, Berkeley,California, p. 108.

Dubiel, R.F., Parrish, J.T., Parrish. J.M. and Good, S.C., 1991, The Pangaean Megamonsoon- Evidence from the Upper Triassic Chinle Formation, Colorado Plateau: PALAIOS, v. 6, no. 4, p. 347-370.

Duke, W. L., Arnott, R. W. C., and Cheel, R. J.,1991, Shelf sandstones and hummocky cross-stratification: new insights on a stormy debate: Geology, v. 19, no. 6, p. 625-628.

Dunham, R. J., 1962, Classification of carbonate rocks according to depositional texture: AAPG Memoir, v. 1, p. 108-121.

Droser, M.L., Bottjer, D.J., 1986, A semiquantitative field classification of ichnofabrics: Journal of Sedimentary Research, v. 56, no. 4, p. 558–559.

Ekdale, A. A., Bromley, R. G., and Pemberton, S. G., 1984, Ichnology: Trace Fossils in Sedimentology and Stratigraphy: SEPM Short Course, no. 15.

Elrick, M., Read, J.F., Coruh, C., 199l, Short-term paleoelimatic fluctuations expressed in Lower Mississippian ramp-slope deposits, southwestern Montana: Geology, v. 19, p. 799-802.

Embry III, A. F. and Klovan, J. E., 1971, A Late Devonian reef tract on northeastern Banks Island, NWT. Bulletin of Canadian Petroleum Geology, v. 19, no. 4, p. 730-781.

Embry, A.F., 1988, Triassic sea-level changes; evidence from the Canadian Arctic Archipelago, in Wilgus, C.K., Hastings, B.S., Ross, C.A., Posamentier, H., Van Wagoner, J., and Kendall, C.G.St.C., eds., Sea level Changes; an Integrated Approach: Tulsa, Oklahoma, SEPM Special Publication, v. 42, p. 249–259.

Embry, A.F., 1997, Global sequence boundaries of the Triassic and their recognition in the Western Canada Sedimentary Basin. Bulletin Canadian Petroleum Geology, v. 45, p. 415-433.

Flügel, E., 2004, Microfacies of carbonate rocks: analysis, interpretation and application: Springer Verlag.

Föllmi, K.B. and Grimm, K.A., 1990, Doomed pioneers: gravity- flow deposition and bioturbation in marine oxygen-deficient environments: Geology, v.18, p.1069-1072.

Föllmi, K.B., Garrison, R.E. and Grimm, K.A., 1991, Stratification in phosphatic sediments: Illustrations from the Neogene of Central California *in* Einsele, G., Rieken W. and Seilacher, A., Cycles and Events: Stratigraphy, Springer, Berlin, p. 492-507.

Föllmi, K. B., 1996, The phosphorus cycle, phosphogenesis and marine phosphate-rich deposits. Earth-Science Reviews, v. 40, no. 1, p. 55-124.

Galloway, W.E., 1989, Genetic stratigraphic sequences in basin analysis I: Architecture and genesis of flooding-surface bounded depositional units: AAPG Bulletin, v. 73, p. 125-142.

Garrison, R. E. and Douglas, R. G., 1981, The Monterey Formation and related siliceous rocks of California: Pacific Section SEPM, p. 327.

Goldhammer, R.K., Dunn, P.A. and Hardie, L. A., 1990, Depositional cycles, composite sea-level changes, cycle stacking patterns, and the hierarchy of stratigraphie forcing: Examples from Alpine Triassic platform carbonates: Geological Society of America Bulletin, v. 102, p. 535-562.

Goldhammer, T., Brüchert, V., Ferdelman1, T.G. and Zabe, M., 2010, Microbial sequestration of phosphorus in anoxic upwelling sediments: Nature Geoscience Letters, August , v. 3, p. 557-561.

Gryc, G., 1988, Geology and exploration of the National Petroleum Reserve in Alaska, 1974 to 1982: USGS Professional Paper 1399, p. 940.

Haq, B.U., Hardenbol, J., and Vail, P.R., 1988, Mesozoic and Cenozoic chronostratigraphy and eustatic cycles, in Wilgus, C.K., Hastings, B.S., Ross, C.A., Posamentier, H.W., Van Wagoner, J., and Kendall, C.G. St. C., Sea- level changes; An integrated approach: SEPM Special Publication 42, p. 72–108.

Hendrix, M.S. and Byers, C.W., 2000, Stratigraphy and sedimentology of the Permian strata, Uinta Mountains, Utah: Allostratigraphic controls on the accumulation of economic phosphate *in* Glenn, C.R., Marine Authigenesis: From Global to Microbial: SEPM Special Publication 64, p. 1-19.

Hildred, G. V., Ratcliffe, K. T., Wright, A. M., Zaitlin, B. A., and Wray, D. S., 2010, Chemostratigraphic Applications to Low-Accommodation Fluvial Incised-Valley Settings: An Example from the Lower Mannville Formation of Alberta, Canada: Journal of Sedimentary Research, v. 80, no. 11, p. 1032-1045.

Houseknecht, D.W. and Bird, K.J., 2004, Oil and Gas Resources of the Arctic Alaska Petroleum Province: U.S. Geological Survey Professional Paper 1732–A.

Houseknecht, D.W., Bader, J.W. and Bird, K.J., 2012b, Thermal maturation history of Arctic Alaska and southern Canada basin *in* N.B. Harris and K.E. Peters, Thermal History Analysis of Sedimentary Basins: Methods and Applications, SEPM Special Publication, in press.

Hubbard, R. J., Edrich, S.P., and Rattey, R.P., 1987, Geologic evolution and hydrocarbon habitat of the ‘‘Arctic Alaska microplate’’: Marine and Petroleum Geology, v. 4, p. 2- 34.

Hulm, E.J., 1999, Subsurface facies architecture and sequence stratigraphy of the Eileen Sandstone, Shublik Formation, and Sag River Sandstone, Arctic Alaska: Master’s Thesis, University of Alaska Fairbanks, Fairbanks, Alaska.

Ingall, E. D. and Jahnke, R., 1994, Evidence for enhanced phosphorus regeneration from marine sediments overlain by oxygen depleted waters: Geochim. Cosmochim. Acta, v. 58, p. 2571−2575.

Ingall, E.D., 2010, Phosphorus Burial: Nature Geoscience, v. 3, p. 521-522.

Isaacs, C.M., Bird, K.J., Medrano, M., Keller, M.A., Piper, D.Z. and Gautier, D.L., 1995, Preliminary report on major and minor elements in cores from the Triassic Shublik Formation, Jurassic and Cretaceous Kingak Shale, and Cretaceous pebble shale unit, Hue Shale, and Torok Formation, North Slope, Alaska: U.S. Geological Survey, Open-File Report 95-236, p. 6.

Jewell, P.W., 1995, Geologic consequences of globe-encircling equatorial currents: Geology, v. 23, no. 2, p. 117-120.

Jones, H.P. and Speers, R.G., 1976, Permo-Triassic reservoirs of Prudhoe Bay field, North Slope, Alaska, *in* Braunstein, J., North American Oil and Gas Fields: AAPG Memoir, v. 24, p. 23-50.

Jones, B. and Manning, D.A.C., 1994, Comparison of geochemical indices used for the interpretation of paleoredox conditions in ancient mudstone: Chemical Geology, v. 111, p. 111-129.

Kelly, L.N., 2004, High Resolution sequence stratigraphy and geochemistry of middle and Upper Triassic sedimentary rocks, northeast and central Brooks Range, Alaska: Master's Thesis, University of Alaska Fairbanks, Fairbanks, Alaska, p. 224.

Kelly, L.N., Whalen, M.T., McRoberts, C.A., Hopkin, E. and Tomsich, C.S., 2007, Sequence stratigraphy and geochemistry of the upper Lower through Upper Triassic of Northern Alaska: Implications for paleoredox history, source rock accumulation and Paleoceanography: Division of Geological and Geophysical Surveys, Alaska, Report of Investigations, 2007-1.

Kendall, C.G. and Schlager, W., 1981, Carbonates and Relative Changes in Sea Level *in* Cita, M.B. and Ryan, W.B.F., Carbonate Platforms of the Passive-Type Continental Margins, Present and Past: Marine Geology, v. 44, p. 181−212.

Kennedy, M.J., Pevear, D.R. and Hill, R.J., 2002, Mineral Surface Control of Organic Carbon in Black Shale: Science, v. 295, p. 657- 660.

Kupecz, J.A., 1995, Depositional Setting, Sequence Stratigraphy, Diagenesis, and Reservoir Potential of a Mixed-lithology, Upwelling Deposit, Upper Triassic Shublik Formation, Prudhoe Bay, Alaska: AAPG Bulletin, v. 79, p. 1301-1319.

Lawver, L.A., Grantz, A., and Gahagan, L.M., 2002, Plate kinematic evolution of the present Arctic region since the Ordovician, in Miller, E.L., Grantz, A., and Klemperer, S.L., eds., Tectonic Evolution of the Bering Shelf–Chukchi Sea–Arctic Margin and Adjacent Landmasses: Geological Society of America Special Paper 360, p. 333–358.

Leffingwell, E., 1919, The Canning River region, northern Alaska: U.S. Geological Survey Professional Paper 109, p. 251.

Loutit, T.S., Hardenbol, J., Vail, P.R., 1988, Condensed Sections: The Key to Age determination and Correlation of Continental Margin Sequences: Sea-Level Changes-An Integrated Approach, SEPM Special Publication, no. 42., p. 183-213.

Magoon L. B. and Claypool G. E., 1983, Petroleum geochemistry of the North Slope of Alaska: Time and degree of thermal maturity *in* Wiley, J., Advances in Organic Geochemistry, p. 28-38.

Magoon, L.B. and Bird, K.J., 1988, Evaluation of petroleum source rocks in the National Petroleum Reserve in Alaska using organic-carbon content, hydrocarbon content, visual kerogen, and vitrinite reflectance data *in* Gryc, George, ed., Geology and Exploration of the National Petroleum Reserve in Alaska, 1974–1982: U.S. Geological Survey Professional Paper 1399, p. 381-450.

McKelvey, V.E., Williams, J.S., Sheldon, R.P., Cressman, E.R., Cheney, T.M. and Swanson, R.W., 1967, The Phosphoria, Park City, and Shedhorn Formations in Western Phosphate Field *in* Hale, L.A., Anatomy of the Western Phosphate Field: Salt Lake City, Intermountain Association of Geologists, Fifteenth Annual Field Conference, p. 15-34.

Mitchum, R.M. Jr., Vail, P.R. and Thompson, S., 1977, Seismic stratigraphy and global changes of sea level, part 2: the depositional sequence as a basic unit for stratigraphic analysis *in* Payton, C.W., Seismic Stratigraphic Applications to Hydrocarbon Exploration, AAPG Memoirs, v. 26, p. 53-62.

Mitchum, R.M. and Van Wagoner, J.C., 1991, High-frequency sequences and their stacking patterns: sequence-stratigraphic evidence of high-frequency eustatic cycles: Sedimentary Geology, v. 70, p. 131-160.

Montañez, I. P., 2002, Biological skeletal carbonate records changes in major-ion chemistry of paleo-oceans. Proceedings of the National Academy of Sciences, v. 99, no. 25, p. 15852-15854.

Moore, T. E., Wallace, W. K., Bird, K. J., Karl, S. M., Mull, C. G. and Dillon, J. T., 1994, Geology of northern Alaska, *in* Plafker G. and Berg, H. C., The geology of Alaska: Boulder, Colorado, Geological Society of America, The geology of North America, v. G-1, p. 49-140.

Notholt, A.J.G. and Jarvis, I., 1990, Phosphate Research and Development: Geological Society of London Special Publication, v. 52, p. 61-86.

Osleger, D. and Read, J., 1991, Eustacy and Cycle Stacking Patterns of Meter-Scale Carbonate Cycles, Late Cambrian, U.S.A.: Journal of Sedimentary Petrology, v. 61, No.7, p. 1225-1252.

Parrish, J.T., 1982, Upwelling and petroleum source beds, with reference to the Paleozoic: AAPG Bulletin 66, p. 750-774.

Parrish, J.T., 1987, Lithology, geochemistry, and depositional environment of the Triassic Shublik Formation, northern Alaska *in* Tailleur, I.L. and Weimer, P. , Alaskan North Slope geology: Field Trip Guidebook – SEPM, Pacific Section, Special Publication 50, p. 391-396.

Parrish, J.T., Droser, M.L. and Bottjer, D.J., 2001a, A Triassic upwelling Zone: the Shublik Formation, Arctic Alaska, U.S.A.: Journal of Sedimentary Research 71, p. 272-285.

Parrish, J.T., Whalen, M.T. and Hulm, E.J., 2001b, Shublik Formation lithofacies, environments, and sequence stratigraphy, Arctic Alaska, U.S.A. *in* Houseknecht, D.W., Petroleum Plays and Systems in the National Petroleum Reserve-Alaska: SEPM Core Workshop, no. 21, p. 89-110.

Pearce, T.J., Wray, D., Ratclife, K., Wright, D.K., Moscariello, A., 2005, Chemostratigraphy of the Upper Carboniferous Schooner Formation, southern North Sea *in* Carboniferous hydrocarbon geology: the southern North Sea and surrounding onshore areas, edited by J. D. Collinson, D. J. Evans, D. W. Holliday, N. S. Jones:Yorkshire Geological Society, v. 7, p. 147–164

Pedersen, T.F. and Calvert, S.E., 1990, Anoxia versus productivity: What controls the formation of organic carbon-rich sediments and sedimentary rocks?: AAPG Bulletin 74, p. 454-466.

Pedersen, T.F. and Calvert, S.E., 1991, Anoxia versus productivity: What controls the formation of organic carbon-rich sediments and sedimentary rocks?: AAPG Bulletin, v. 75, p. 500-501.

Peters, K. E., Magoon, L.B., Bird, K.J., Valin, Z.C. and Keller, M.A., 2006, North Slope, Alaska: Source rock distribution, richness, thermal maturity, and petroleum charge: AAPG Bulletin, v. 90, p. 261-292.

Piper, D.Z., 1994, Seawater as the source of minor elements in black shales, phosphorites and other sedimentary rocks: Chemical Geology, v. 114, p. 95-114.

Piper, D.Z. and Calvert, S.E., 2009, A marine biogeochemical perspective on black shale Deposition: Earth-Science Reviews, v. 95, p. 63-96.

Pörtner, H. O., 2008, Ecosystem effects of ocean acidification in times of ocean warming: a physiologist's view: Mar Ecol Prog Ser, v. 373, p. 203-217.

Posamentier, H.W., and Allen, G.P., 1999, Siliciclastic Sequence Stratigraphy—Concepts and Applications: Society of Economic Paleontologists and Mineralogists, Concepts in Sedimentology and Paleontology v.7, p. 210.

Quinby-Hunt, M.S., and P. Wilde, 1996, Chemical depositional environments of calcic marine black shales: Economic Geology, v. 91, p. 4-13.

Ransom, B., Kim, D., Kastner, M. and Wainwright, S., 1998, Organic matter preservation on continental slopes: Importance of mineralogy and surface area: Geochim. Cosmochim. Acta 62, p. 1329-1345.

Ratcliffe, K.T., Martin, J., Pearce, J., Hughes, A.D., Lawton, D.E., Wray, D.S. and Bessa, F., 2006, A regional chemostratigraphically-defined correlation framework for the late Triassic TAG-I Formation in Blocks 402 and 405a, Algeria: Petroleum Geoscience, v. 12, p. 3-12.

Ratcliffe, K.T., Wright, A.M. and Schmidt, K., 2012, Application of inorganic whole-rock geochemistry to shale resource plays: an emample from the Eagle Ford Shale Formation, Texas: The sedimentary Record (SEPM), v. 10, no. 2, p. 4-9.

Read, J.F., 1985, Carbonate Platform Facies Models: The American Association of Petroleum Geologists v. 69, no. 1, p. 1-21.

Renne, P. R., 1995, Excess $^{40}$Ar in biotite and hornblende from the Norils'k 1 intrusion: Implications for the age of the Siberian traps: Earth and Planetary Science Letters, v. 131, p. 165–176.

Riehle, J.R., Fleming, M.D., Molnia, B.F., Dover, J.H., Kelley, J.S., Miller, M.L., Nokleberg, W.J., Plafker, G., and Till, A.B., 1997, Digital shaded-relief image of Alaska: Reston, VA, U.S. Geological Survey, Miscellaneous investigation series Map I-2585.

Rimmer, S.M., Thompson, J.A., Goodnight, S.A. and Robl, T.L., 2004, Multiple controls on the preservation of organic matter in Devonian-Mississippian marine black shales: geochemical and petrographic evidence: Palaeogeography Palaeoclimatology Palaeoecology, v. 215, p. 125-154

Robison, V.D., Liro, L.M., Robinson, C.R., Dawson, W.C. and Russo, J.W., 1996, Integrated geochemistry, organic petrology, and sequence stratigraphy of the Triassic Shublik Formation, Tenneco Phoenix # 1 well, North Slope, Alaska, U.S.A.: Organic Geochemistry, v. 24, no. 2, p. 257-272.

Rullkotter, J., 2006, Organic matter: The driving force for early diagenesis. *in* Schulz, H.D. and Zabel, M.: Marine Geochemistry, p. 125-168.

Schaller, M. F., Wright, J. D., and Kent, D. V., 2011, Atmospheric pCO2 perturbations associated with the Central Atlantic Magmatic Province. Science, v. 331, no. 6023, p. 1404-1409.

Shields, G., and P. Stille, 2001, Diagenetic constraints on the use of cerium anomalies as paleoseawater redox proxies: an isotopic and REE study of Cambrian Phosporites: Chemical Geology, v. 175, p. 29-48.

Sholokovitz, E.R., W.M. Landing, and B.L. Lewis, 1994, Ocean particle chemistry: the fractionation of rare earth elements between suspended particles in seawater: Geochimica et Cosmochimica Acta, v. 58, p. 1567-1579.

Tailleur, I.L., 1964, Rich oil shale from northern Alaska: U.S. Geological Survey Professional Paper 475-D, p. D131-D133.

Thiede J. and Suess, E., 1983, Sedimentary Record of Ancient Coastal Upwelling: Episodes, no. 2, p. 15-18.

Tourtelot, H.A. and Tailleur, I.L., 1971, The Shublik Formation and adjacent stratigraphy in northeast Alaska; Description, minor elements, depositional environments and diagenesis: U.S. Geological Survey Open-File Report 71-284, p. 62.

Tribovillard, N., Algeo, T.J., Lyons, T. and Riboulleau, A., 2006, Trace metals as paleoredox and paleoproductivity proxies: An update: Chemical Geology 232, p. 12-32.

Tribovillard, N., Algeo, T.J., Baudin, F. and Riboulleau, A., 2012, Analysis of marine environmental conditions based on molybdenum–uranium covariation: Applications to Mesozoic paleoceanography: Chemical Geology, v. 324-325, p. 46-58.

Van der Weijden, C.H., 2002. Pitfalls of normalization of marine geochemical data using a common divisor: Marine Geology, v. 184, p. 167-187.

Vail, P.R., Mitchum Jr., R.M. and Thompson III, S., 1977, Seismic stratigraphy and global changes of sea level; Part 4, Global cycles of relative changes of sea level, *in* Payton, C.E., ed., Seismic stratigraphy; applications to hydrocarbon exploration: AAPG Memoir, v. 26, p. 83-97.

Van Wagoner, J. C., Posamentier, H. W., Mitchum, R. M. J., Vail, P. R., Sarg, J. F., Loutit, T. S., and Hardenbol, J., 1988, An overview of the fundamentals of sequence stratigraphy and key definitions: Exxon Production Research Company, Houston, Tx.

Wright, A., and Ratcliffe, K., 2010, Application of Inorganic Whole Rock Geochemistry to Shale Resource Plays *in* Canadian Unconventional Resources and International Petroleum Conference.